NASA Contractor Report **181849**

SUPERPLASTIC FORMING AND DIFFUSION BONDING OF RAPIDLY SOLIDIFIED, DISPERSION STRENGTHENED ALUMINUM ALLOYS FOR ELEVATED TEMPERATURE STRUCTURAL APPLICATIONS

E.Y. Ting and J.R. Kennedy

Corporate Research Center
Grumman Aerospace Corporation
A02-26
Bethpage, New York 11714

CONTRACT NAS1-18533
September 1989

National Aeronautics and
Space Administration

Langley Research Center
Hampton, Virginia 23665-5225

NASA Contractor Report **181849**

SUPERPLASTIC FORMING AND DIFFUSION BONDING OF RAPIDLY SOLIDIFIED, DISPERSION STRENGTHENED ALUMINUM ALLOYS FOR ELEVATED TEMPERATURE STRUCTURAL APPLICATIONS

E.Y. Ting and J.R. Kennedy

Corporate Research Center
Grumman Aerospace Corporation
A02-26
Bethpage, New York 11714

CONTRACT NAS1-18533
September 1989

NASA
National Aeronautics and
Space Administration

Langley Research Center
Hampton, Virginia 23665-5225

REPORT RE-772

SUPERPLASTIC FORMING AND DIFFUSION BONDING OF RAPIDLY SOLIDIFIED, DISPERSION STRENGTHENED ALUMINUM ALLOYS FOR ELEVATED TEMPERATURE STRUCTURAL APPLICATIONS

SEPTEMBER 1989

by

E.Y. Ting
and
J.R. Kennedy

Grumman Corporate Research Center
Bethpage, New York 11714-3580

Final Report on
Contract NAS1-18533

for

National Aeronautics and Space Administration
Langley Research Center
Hampton, VA 23665-5225

NASA Contractor Report 181849

Approved by: Richard DeIasi
Richard DeIasi, Director
Corporate Research Center

PREFACE

This technical report covers the work performed under Contract NAS1-18533. This research is being funded by the Langley Research Center of the National Aeronautics and Space Administration (NASA), Hampton, VA. The program is being conducted under the technical direction of Mr. Dick Royster of the Metallic Materials Branch in the Materials Division of the NASA Langley Research Center.

The work presented here was performed during the period November 1987 to December 1988 by Grumman Corporation (Bethpage, NY) and the Allied-Signal Corporation (Morristown, NJ).

The materials fabrication, base-line mechanical property evaluation, and microstructural characterization were performed by the Alloy Development group of the Metals and Ceramics Laboratory within the Corporate Technology section of Allied-Signal Inc. The evaluation of superplasticity, diffusion bonding and additional mechanical properties were performed by the Structural Materials group of the Corporate Research Center, Corporate Technology, Grumman Corporation.

Program Principal Investigator: Dr. E.Y. Ting
Grumman Corporate Research Center
A02-26
Bethpage, New York 11714

Grumman Principal Investigator: Dr. E.Y. Ting
Grumman Co-investigators: Mr. J. Kennedy

Allied-Signal Principal Investigator: Dr. P.S. Gilman
Allied-Signal Co-investigators: Dr. M.S. Zedalis, D.J. Skinner, and Dr. J.M. Peltier

Contributors (Allied-Signal): M. Rodriguez, J. Gleason, C. Calderone , A. Testa, and D. Timan

Contributors (Grumman): Dr. J. Papazian, Dr. P. Adler, W. Poit , T. Williams Jr., and J. Havranek

THIS PAGE INTENTIONALLY LEFT BLANK

CONTENTS

CONTENTS (cont'd)

ILLUSTRATIONS

ILLUSTRATIONS

ILLUSTRATIONS

ILLUSTRATIONS

ILLUSTRATIONS

ILLUSTRATIONS

Tables

THIS PAGE INTENTIONALLY LEFT BLANK

1. INTRODUCTION

High strength, high temperature, lightweight structural materials are critical to the aerospace industry. Although conventional aluminum alloys have excellent strength-to-weight ratios at temperatures up to 180°C (356°F), structural applications at higher temperatures must rely on heavier titanium alloys. However, advanced dispersion-strengthened aluminum alloys could operate at temperatures up to 400°C (752°F) while still retaining useful properties. Produced by rapid solidification, these high temperature aluminum (HTA) alloys can effectively replace titanium alloys and reduce structural weight of advanced engines and aerospace vehicles. Weight can be further reduced through innovative design of efficient multi-sheet structures using advanced forming and joining methods such as superplastic forming and diffusion bonding (SPF/DB). These methods, used either individually or in a combined process, are advantageous manufacturing techniques for multisheet structures.[1-3] SPF/DB technology has already been successfully demonstrated using titanium alloys and is currently being developed for other alloy systems, such as aluminum alloys.

By virtue of the ultra-fine grain microstructure imparted to the HTA alloys during rapid solidification, similarities exist between them and conventional aluminum alloys that can be superplastically formed and diffusion bonded. The beneficial influence of small grain size on SPF has been clearly established and, recently, the dependence of diffusion bonding on grain size for an aluminum alloy has also been demonstrated.[4] The current work was undertaken to determine if superplastic forming and diffusion bonding techniques could be applied to dispersion strengthened Al-Fe-V-Si alloys. The effects of dispersoid volume fraction, dispersoid size, elevated temperature exposure, deformation rate, and bonding pressure on alloy behavior related to superplastic forming and diffusion bonding were characterized. The microstructure and mechanical properties were also evaluated.

THIS PAGE INTENTIONALLY LEFT BLANK

2. BACKGROUND

2.1 HIGH TEMPERATURE ALUMINUM (HTA) ALLOYS

Aluminum alloys are attractive for weight-critical aerospace structural applications because of their high strength, low density, and ease of fabrication. High strength is achieved in conventional aluminum alloys through alloying and subsequent heat treatment to generate a fine distribution of strengthening precipitates within the microstructure. Conventional high-strength aluminum alloys are limited to a maximum service temperature of less than 180°C (356°F) because of the limited thermal stability of the strengthening precipitates. At elevated temperatures, coarsening or dissolution of the strengthening phase results in rapid strength loss. During the past decade considerable attention has been devoted to the development of HTA alloys capable of competing with high temperature materials, such as titanium alloys, on a specific strength and stiffness basis up to 375°C (700°F). The nearly twofold increase of the useful temperature range of aluminum alloys has been achieved using newly developed rapid solidification technology. The HTA alloys are strengthened by fine dispersoid particles that are formed from a supersaturated alloy condition generated during rapid solidification. These dispersoid particles have significantly more thermal stability than the precipitates found in conventional age-hardening aluminum alloys. Given the low density of aluminum alloys in general, HTA alloys show remarkable specific properties at temperature up to 400°C (752°F). The resulting stiffness of the HTA alloys is also increased because the dispersoids are of greater modulus than pure aluminum. The application of these new HTA alloys could extend the temperature limit to which aluminum alloys are used and, thereby, result in major weight savings.

Al-Fe-V-Si Alloys. Dispersion strengthened alloys derive their strength from the interaction of insoluble particles and dislocations. Thermal stability of the strengthening phase requires that the strengthening particles have low solubility and diffusivity in aluminum, and a spherical or polygonal morphology to reduce interface stress. Furthermore, some degree of interfacial coherency is desired between the dispersoid and the matrix to reduce interface energy to lessen the driving force for coarsening. The implementation of these requirements will reduce the growth kinetics at elevated temperatures. Several alloy systems have emerged that report substantial improvements in the elevated temperature strength of aluminum by the application of these ideas. Most of these systems are based on Al-Fe or Al-Cr systems with the addition of ternary and/or quaternary elements to provide additional binary strengthening dispersoids;[5,6] to stabilize the existing binary intermetallics;[7] or to formulate ternary and/or quarternary intermetallics with a more symmetrical lattice.[8,9] The Al-Fe-V-Si system of alloys can thus be categorized in the latter classification, whereby the quarternary additions of V to Al_8Fe_2 Si alloys stabilizes the cubic Al_{13} $(Fe,V)_3$ Si phase over the hexagonal Al_8Fe_2Si and monoclinic Al_3Fe phases that would normally form in the absence of these additions. This cubic phase can, in general terms, be stabilized with most other body-centered cubic (BCC) elements.[10,11]

Dispersoid Phase. The intermetallic that strengthens the Al-Fe-V-Si alloys has a general composition close to $Al_{13}(Fe,V)_3Si$. The characteristics of this intermetallic phase within the Al-Fe-V-Si alloy system has been reported[12] and will only be briefly discussed here.

The silicide dispersoid structure is BCC,(Im3, 138 atoms/unit cell). [13] The atomic structure of this intermetallic can be described as: empty (Fe+V) icosahedra (i.e., with an unoccupied

center) situated at the sites of a BCC lattice; they are all parallel and each icosahedron is connected to its eight neighbors along their three-fold axes parallel to the <111> direction. The connecting atoms form a slightly distorted octahedron. Each of these (Fe+V) icosahedra contains an empty (Al+Si) icosahedron of the same orientation and these are connected through chains of three slightly distorted (Al+Si) octahedra sharing their triangular faces (Fig. 1). However, only five of the possible eight neighboring icosahedra are connected with these octahedra chains. The remaining (Al+Si) atoms occupy positions primarily on the cube faces while still maintaining the BCC symmetry. Based upon TEM analysis, it is thought that the silicide phase and the aluminum matrix have low interface energy due to ledge formation and a high atomic coincidence. This greatly improves the coarsening resistance of the silicide phase.

The silicide phase is not a line compound; while the number of (Fe+V) atoms remain the same, the Fe:V ratio can vary slightly. The Al:Si ratio can also be altered to some extent. The composition variation for this silicide phase may be represented by the following: $Al_{12.0-14.0}(Fe,V)_3 Si_{0.9-1.2}$. These compositional variations can be controlled because the nominal Fe:V and Al:Si ratios formulated in the alloy composition are carried through to the silicide phase in the consolidated material. In addition, these effects have so far not proven to be as significant as the effects of volume fraction dispersoid, grain size, and particle size distribution.

The modulus of the silicide dispersoid phase has been estimated to be 150 GPa [13]. The thermal expansion coefficient for the silicide has been extrapolated to a relatively low value of 11.6×10^{-6} m/m/K .

2.2 SUPERPLASTIC FORMING (SPF)

Superplastic materials exhibit stable plastic deformation behavior in tension at elevated temperatures typically over half that of the melting point. They can be deformed to very large strains at low stresses prior to failure. Using SPF, complex shapes can be fabricated in a more direct and less costly manner than conventional fabrication techniques used for non-superplastic materials[14]. For example, the fabrication of thin-sheet structures can be achieved through a simple cost-effective blow-forming method similar to those used in the thermoplastics industry.

Superplastic Behavior. The phenomena of superplasticity is made possible by the stabilization of inhomogeneous deformation (commonly termed necking) through a highly rate-sensitive deformation yield stress. This rate-sensitive yield stress is typically characterized by the simplified relationship[15]

$$\sigma = k\dot{\varepsilon}^m \qquad (1)$$

where σ is the applied stress, $\dot{\varepsilon}$ is the strain rate, and k and m are constants. The strain-rate sensitivity index, m, is a measure of the extent of deformation stabilization derived from strain rate effect. Both constants are functions of temperature and material. As can be seen in Eq. (1), any local increase in strain rate due to localized deformation results in an increased flow stress, thus stabilizing the inhomogeneous deformation. Values of m typically in excess of 0.4 correspond to superplastic deformation. In addition to temperature, the value of m for a material is often found to be a function of strain rate. For most superplastic materials, a maximum value of m exists at the optimum strain rate for SPF. A recent review of superplasticity has been performed by Padmanabhan.[16]

Other Contributions to Deformation Stability. In addition to a high strain rate sensitivity, deformation stability can also be achieved through a high strain hardening coefficient. The most commonly used equation to describe the stress-strain behavior is [17]

$$\sigma = k\,\varepsilon^{n} \tag{2}$$

where k is a constant, ε is the total plastic strain, and n is a constant that depends on material and temperature. At low temperatures, strain hardening occurs during initial straining and provides sufficient stability for cold forming applications of many common engineering alloys.

In some alloys that exhibit strain rate sensitivity, the combined effects of strain rate and strain hardening can delay the onset of deformation instability.[18,19] At the elevated temperatures associated with SPF, strain based effects are typically associated with some microstructural change such as grain growth or recrystallization. The combined effects of strain and strain rate can be expressed as

$$\sigma = k\,\varepsilon^{n}\,\dot{\varepsilon}^{m} \tag{3}$$

Equation (3) only approximates the final relationship between stress, strain, and strain rate on an empirical basis. It makes no determination as to the mechanisms involved except that there is a strain or strain rate sensitivity. Since plastic stability can arise from both strain and strain rate effects, microstructural evidence is needed to determine which mechanism is in effect.

Microstructural Requirement. The mechanism responsible for superplasticity is generally recognized to be grain boundary deformation (sliding[20] or core/mantle flow[21,22]) with diffusional accommodation. The rate limiting step is the diffusional transport of atoms away from the stressed region and is mainly controlled by the grain size of the material. Thus, a basic microstructural requirement for superplasticity in Al alloys is a stable, fine grain size at elevated temperatures. In addition, the ability of the grain boundary to freely deform without separation under tensile loads is also required. As discussed for Eq. (1), the influence of temperature and strain rate are expected to have significant influence on the deformation behavior of a superplastic material. Maximum superplasticity is typically achieved at an optimum strain rate where the m value is maximized. For a given temperature, the optimum strain rate typically increases as the grain size is decreased. The Eq.

$$\dot{\varepsilon}^{*} \propto \frac{1}{L^{c}} \tag{4}$$

with $\dot{\varepsilon}^{*}$ equal to the optimum strain rate, L is the grain size and c equal to 2 has been proposed to relate grain size to optimum strain rate.[23,24] It is possible that given a submicron grain size, the optimum strain rate for superplastic deformation can be significantly increased.

Grain size can be stabilized in superplastic aluminum alloys using a distribution of fine second phase particles such as the Al_3Zr particles used in commercial Al SPF alloys. These particles pin grain or subgrain boundaries and prevent rapid grain growth. Furthermore, the matrix must also be free of large inhomogeneous particles that can nucleate grain boundary cavitation. At the other extreme, due to the existence of a high volume fraction of large "second

phase particles" in certain composite materials, internal stress plasticity has been observed. Differences in expansion coefficients between the matrix and second phase constituents can generate high internal stresses during thermal cycling. This internal stress has been shown to create a superplastic-like behavior in SiC-reinforced metal matrix composite and high ductility can be achieved in these normally low ductility materials. [25,26]

Because superplasticity is mainly achieved through grain boundary deformation and diffusional transport, superplastically deformed materials show little or no evidence of dislocation generation. The grain morphology encountered after SPF is typically of an equiaxed fine grain. With long duration exposure to SPF conditions, superplastic alloys may show an increase in grain size due to grain growth. For alloys which do not undergo dynamic recrystallization, the initial microstructure often gives an indication of the alloy's potential for superplasticity behavior.

2.3 DIFFUSION BONDING (DB)

The use of DB in conjunction with superplastic forming (SPF/DB) to produce integral near-net shapes of titanium alloys has been very successful. The SPF/DB of aluminum alloys has been severely impeded because of aluminum's stable surface oxide, which is a tenacious diffusion barrier(4-6). Unlike titanium, which have oxides that easily dissolve in the metal during heating, aluminum and its alloys form oxides that do not dissolve.

Typically, aluminum has been "solid state" bonded by methods that rely upon considerable mechanical deformation (up to 60% reduction in thickness) under high stress (up to 40,000 psi) to bring the surfaces together and to rupture the surface oxide barrier. In general, such high-stress methods are not compatible with the constraints imposed by SPF technology. For example, practical limitations set by production equipment dictate that SPF gas pressures probably should be limited to 1000 psi and, perhaps, should be much lower. Therefore, the development of a low pressure DB technique combined with superplastic forming could significantly advance the design of advanced structures. To this end, various approaches have been developed for low pressure bonding of aluminum alloys. For example, one approach relies upon the use of diffusion brazing with a variety of interlayers, such as Cu, Zn, and Al-Si, which serve as melting point depressants.[27,28] The liquid phase that forms during bonding helps to displace the surface oxide that allows a bond to form between the substrate metals. However, additional interfaces can increase the oxide content at the bond line and can also lead to the formation of undesirable intermetallic compounds and brittle bonds. Another approach, developed at the Grumman Research Center, depends upon proper surface cleaning combined with the use of a highly-plastic surface layer to induce localized surface deformation during bonding to disrupt the oxide layer; thus, leading to intimate metal-to-metal contact and diffusion.

Research has shown that it is possible to produce high-strength diffusion bonds in aluminum alloy. [29,4] High-strength bonds with grain boundary-like interfaces have been produced by bonding superplastic 7475 Al alloy at the superplastic forming temperature (516°C (960°F)) using very low pressures (≤0.7 MPa (100 psia)) without diffusion aids or intermediate materials. In general, the strength of bonds in the as-bonded and heat treated conditions are comparable to those of the base metal. Results indicate that shear strength is time and pressure dependent and that a minimum pressure-time condition must be satisfied to attain high strength bonds. More

importantly, it has been identified that grain size has a major effect on bond strength. Fine grained superplastic alloys were found to bond significantly better than coarse grain alloys. Transmission electron microscopic observations of high-strength bonds revealed that the bond interface was barely discernible, looked essentially like a normal grain boundary, and did not contain obvious continuous layers or films of oxide. These results are of major significance because they demonstrate that DB is greatly improved in alloys that have characteristic fine-grained microstructures usually associated with superplasticity. The data lead to the conclusion that improved DB is made possible by enhanced localized surface deformation caused by a fine-grained superplastic microstructure that leads to extensive oxide film disruption.

THIS PAGE INTENTIONALLY LEFT BLANK

3. PROGRAM PLAN

The objective of this work was to investigate the SPF and DB characteristics of dispersion strengthened HTA alloys based upon the Al-Fe-V-Si alloy system and to evaluate the effect of such processing conditions on microstructure and mechanical properties. The results reported here represent work performed during the period from November 1987 to March 1989 at the Grumman Corporate Research Center (Bethpage, NY) and the Allied-Signal Corporate Technology Center (Morristown, NJ).

3.1 ALLOY SELECTION

The strength of a dispersion strengthened alloy depends on the extent to which the motion of dislocations can be retarded within the matrix through dislocation-particle interaction. Thus, alloy strength is strongly determined by the volume fraction, size, and distribution of the strengthening dispersoid phase. In order to evaluate the SPF and DB characteristics of the HTA alloys, four alloy compositions and three dispersoid conditions were selected for examination. The alloy dispersoid volume fractions were 8, 16, 27, and 36 volume percent. The size and spacing of the dispersoids were controlled by extrusion and rolling at different temperatures.

3.2 MECHANICAL PROPERTIES DETERMINATION

Room and elevated temperature tensile properties, fracture toughness, and fatigue crack growth rate testing were performed to establish base-line data. The properties of extruded and sheet conditions, before and after exposure to typical service temperatures, were characterized. Since fabrication using SPF or DB will likely require exposure to temperatures above 500°C (932°F), properties after short-term high temperature exposure at these temperatures also were determined. These data will help determine the possible manufacturing and application parameters for the alloys.

3.3 SUPERPLASTIC EVALUATION

In the Al-Fe-V-Si alloys characterized by an ultra-fine and stable grain size, it was anticipated that strain rate sensitivity might be encountered. Evaluation for superplastic behavior was first performed at elevated temperatures at strain rates between $1x10^{-6}$ and $1x10^{-3}$ s^{-1}. In addition, an investigation was conducted to determine if internal stress superplasticity could be generated by rapid temperature cycling. Finally, deformation behavior under high (> $1x10^{-3}$ s^{-1}) strain rates were evaluated.

3.4 DIFFUSION BONDING EVALUATION

Because of the ultra-fine grain size of the rapidly solidified alloys, it was anticipated that diffusion bonding of these alloys might be enhanced. Since likelihood of successful diffusion bonding increases with temperature, the stability of the strengthening dispersoids must also be considered. This was characterized by both microstructural and mechanical properties determination. The anticipated difficulty in DB of dispersion strengthened alloys was the coarsening of the dispersoid. Diffusion bonding of the HTA alloys to another aluminum alloy system at a lower temperature was also investigated to evaluate bonding at temperatures that will not coarsen

the dispersoids. The DB behavior of dissimilar couples between 7475 aluminum alloy, a high-strength precipitation hardened alloy, and the high temperature dispersion strengthened HTA alloys was evaluated. This might offer a novel opportunity to produce hybrid structures.

4. EXPERIMENTAL PROCEDURES

4.1 ALLOYS

Alloy Production. The four alloys, FVS0301, FVS0611, FVS0812, and FVS1212 were rapidly solidified using planar flow casting and ribbon comminution technology developed at Allied-Signal. The alloys were produced representing 8,16,27, and 36 volume percent of silicide dispersoids, respectively. The alloys were solidified at cooling rates in excess of $10^6 K\ s^{-1}$ using the planar flow casting technique. Ribbon approximately 5 cm wide and 25 μm in thickness were produced. The ribbons were then comminuted into -60 mesh (<250 μm) powder prior to being vacuum hot pressed into 11.5 cm (4.5 in.) diameter billets. Three 11 cm (4.3 in.) diameter vacuum hot pressed billets approximately 3.2 kg (7.0 lb) each were made for each alloy. The billets were extruded at the RMI extrusion plant (Ashtabula, OH) to 1.0 x 5.5 cm (0.4 x 2.2 in.) cross-section bars at 385°C (725°F) except for the 1212 alloy which was extruded at 427°C (800°F).

The extrusions were sectioned for baseline mechanical property testing. The remaining portions of the extrusions were cut into 12.5 cm lengths for hot rolling on a 15.0 cm diameter Stannett rolling mill. Graphite lubrication was used for rolling. To modify the final sheet microstructure, the cut sections from each alloy were rolled at 300, 400, and 500°C (572, 752, and 932°F). Rolling was performed in the extrusion direction until the 5.5 cm dimension was approximately 12.5 cm. Subsequently, the pieces were cross rolled to a final gauge of 2.0 mm. The pieces were deformed approximately 15% per pass and were reheated after each pass to keep the temperature as constant as possible in the extrusion direction. Baseline tensile data as well as microstructural characteristics were determined for the sheet conditions.

Alloy Designation. The alloy name assigned to each of the Al-Fe-V-Si alloys by Allied-Signal represents the approximate amount of alloying elements in each composition. The FVS identifies the iron (Fe), vanadium (V), and silicon (Si) components; the digit(s) representing the approximate weight percent (rounded to an integer) of Fe, V, and Si in the alloy respectively. In further references to the alloy sheets, the temperature at which the sheet was rolled will be added to its identification. For example, FVS1212/500 will denote the FVS1212 (approximately 12 w% Fe, 1 w% V, and 2 w% Si alloy) rolled at 500°C (932°F).

4.2 MICROSTRUCTURE EXAMINATION

Light microscopy samples were mechanically polished to a one micron finish and etched in Keller's reagent prior to examination on a Lietz Ultraphot II (Allied-Signal) or a Leitz MM6 metallograph (Grumman). Transmission electron microscopy (TEM) foils were mechanically thinned and electropolished in a 20% HNO_3- 80% CH_3OH solution at -40°C (233K). TEM microscopy was performed on a Philips EM400T microscope. Scanning electron microscopy with energy dispersive x-ray and wavelength dispersive spectrography (SEM/EDX/WDS) analysis was performed on a Jeol 840 (Allied-Signal) or an Amray 1000 scanning electron microscope (Grumman). Grain size was measured using the Heyn intercept method.[30] Values of mean dispersoid radius, $\bar{r}$, were determined from measurements made on approximately 200 silicide particles.

A General Electric XRD-5 X ray unit was employed in conjunction with a Huber texture

goniometer, a Siemens rate meter, and a scintillation counter for pole figure measurements. X-ray intensity data were obtained for (111) planes of aluminum and fed directly into a computer to construct pole figures demonstrating equal value contours.

4.3 MECHANICAL TEST

Tensile Test. Mechanical tests were performed on samples of extruded bar and rolled sheet. Tensile testing was performed according to ASTM Specification E8, B557, and E21. Fatigue crack growth tests followed ASTM Standard E647. Fracture toughness tests were according to ASTM E399, B645, B646, and E561.

Tensile tests were performed on an Instron model 1125 screw-driven machine. Elevated temperature tests were performed within an Instron box oven mounted to the test machine. Each specimen was allowed to stabilize for at least 20 min. after reaching test temperature before starting the test. Temperature accuracy was to ±2°C (±4°F). All tests were at a crosshead speed of .011 mm/s (4.2×10^{-4}/s), resulting in a "nominal" strain rate (based upon the initial gauge length) of $5.56 \times 10^{-4}\ s^{-1}$. A computer was used to collect data and calculate results. Tensile test data was plotted as load vs. crosshead displacement and the yield strength, ultimate tensile strength, and tensile elongation were calculated. The yield strength was determined by drawing a tangent to the load-displacement curve at its steepest point, then drawing a parallel line corresponding to 0.2% plastic strain; the load at which this offset line intersected the load-displacement curve was divided by the initial cross-sectional area of the specimen to arrive at the 0.2% offset yield strength. The ultimate tensile strength (engineering tensile strength) is defined as the maximum load during the test divided by the initial cross-sectional area. The elongation was calculated by dividing the plastic displacement at fracture from the load-displacement curve by the initial gauge length. The reduction-in-area was calculated by direct measurement of the failed specimen.

Tensile tests of the high-temperature aluminum extrusions were carried out in the longitudinal direction (extrusion direction) at 25°, 149, 232, and 316°C (77, 300, 450, and 600°F). A small number of FVS0812 specimens were tested transverse to the extrusion direction at room temperature. Tests were run using cylindrical specimens 4.75 mm (0.188 in.) in diameter with a gauge length of 1.9 cm (0.75 in.), in accordance with the suggestion of ASTM E8 (gauge length is four times the gauge diameter).

Room temperature tensile tests of sheet alloys were performed on flat specimens with a gauge length of 1.9 cm (0.75 in.), a gauge width of 9.5 mm (0.375 in.), and thickness equal to that of the rolled sheet, 1.8-2.4 mm (0.070-0.095 in.). Samples were oriented transverse to the rolling direction, but parallel to the extrusion direction, since the sheet had been cross-rolled.

Thermal Stability. To evaluate the thermal stability of the base alloys, tensile specimens machined from the extrusion were exposed for 120 h at 399°C (750°F). Additional specimens of extruded FVS0812 were exposed for 504 h at 400°C (750°F), and for 120 h at 455°C (850°F) and 510°C (950°F). The tensile tests were carried out without removing the oxide layer, if any, from the surface of the specimens.

The stability of the sheet material subjected to exposure temperatures representative of hot SPF or DB processing was measured using specimens exposed to selected temperatures and times. Exposure at 500°C (932°F) and 600°C (1112°F) of 1 and 4 h were performed. Tests were

performed in the uniaxial SPF test system.

Fatigue Crack Growth. Fatigue crack growth testing of extruded FVS0611 and FVS0812 was performed at room temperature on an MTS servohydraulic testing machine. The tests were carried out on standard compact tension fracture mechanics specimens with a width of 40 mm (1.575 in.). A fatigue precrack was grown from the starter notch to 20% of the specimen width under decreasing ΔK, at 10 Hz and with a stress ratio R (minimum stress divided by the maximum stress) of 0.1. Crack length was monitored during fatigue precracking and cracking by a compliance technique, measuring the crack opening displacement with a clip-on extensometer. Crack lengths were calculated from compliance, and stress intensity from crack length, according to equations presented in ASTM E399 and E561. Fatigue crack growth testing was performed with the crack between 20% and 45% of the specimen width, at 10 Hz and R=0.1, under increasing ΔK. Crack growth rates were calculated from a moving least squares fit of crack length vs. cycle number.

Fracture Toughness. Following fatigue crack growth rate measurements, each specimen was used for fracture toughness testing. The crack was opened at constant rate until fracture, and toughness values were calculated from the plot of load vs. crack opening. According to E399 and B645, the provisional fracture toughness Kq was calculated; no Kq value was found to represent the "valid" plane strain fracture toughness K1c. According to E561, the plane stress fracture toughness Kc was determined from the crack resistance R-curve. This value is equivalent to measurements made on wide center-cracked panels of sheet materials.

Other Tests. Superficial hardness was measured using a Rockwell Hardness Tester on the "R_b" scale. Electrical conductivity was measured using an eddy current method with a Verimet M4900 conductivity meter. Conductivity was measured in terms of true International Annealed Copper Standard (IACS), percent conductivity.

4.4 SPF EVALUATION

Superplasticity behavior was evaluated using uniaxial tests at selected temperatures and strain rates. An Instron model TM uniaxial test frame modified with a computer controlled variable speed drive and a rapid heating, four-element elliptical quartz lamp furnace were used. The SPF test specimen geometry had a gauge section of 1.27 cm (0.500 in.) and a shoulder radius of 1.59 mm (0.0625 in.) between the gauge and the grip regions. Specimen thickness was that of the as-rolled sheet. Strain rates tested ranged from a low of approximately $10^{-6}\,s^{-1}$ to a high of $8.5\,s^{-1}$. Most tests at strain rates below $10^{-3}\,s^{-1}$ were performed using constant true strain rate (i.e., grip velocity increased as specimen elongated). Tests at higher strain rates were performed using constant engineering strain rate (constant grip velocity) due to the inability of the data acquisition system to sample as a sufficiently fast rate. Using constant grip velocity, the actual strain rate changes as the sample elongates, but as most of the Al-Fe-V-Si alloys showed low elongation and as this work's objective was to characterized basic deformation behavior, the magnitude of this error was acceptable. The load generated during testing was recorded by the control computer (HP9836 with HP3497 data acquisition unit) or by a strip chart recorder (Instron Model TM). The highest strain rate tests, at strain rates of $8.5\,s^{-1}$, were performed at the University of California, Davis in a constant strain rate servo-hydraulic machine. Elongation after failure was determined by measurement of the final reassembled sample length.

Mechanical properties after elevated temperature exposure were estimated by testing samples exposed to isothermal soaks. The effect of applied stress during exposure was not considered and a first level approximation of mechanical properties was obtained. The sample geometry used was that of the SPF specimen design.

4.5 DB EVALUATION

Diffusion bonding experiments were conducted on the Al-Fe-V-Si alloys in the as-rolled condition in two different fixtures (one for low pressure and one for high pressure bonding). Both fixtures permitted simultaneous argon gas pressurization at one side of the specimen and vacuum (pressure ≈ $1x10^{-3}$ torr) at the other side. The DB specimens used for shear testing consisted of a pair of 2.0 mm (0.079 in.) thick rectangular blanks, approximately 17 mm (0.669 in.) wide and 30 mm (1.18 in.) long. The blanks were prepared for bonding by manual abrasion using successively finer SiC grinding papers of 240, 320, 400, and 600 grit. Ultrasonic rinsing in a high-purity solvent, such as acetone, and in distilled water followed. The rinsed surfaces were then air dried with clean filtered air. Immediately prior to diffusion bonding, the dried surfaces were abraded by metallic brushing.

Bonds were made between similar dispersion strengthened alloys and dissimilar couples between 7475 aluminum alloy and selected dispersion strengthened alloys. Fine-grained, superplastic 7475 aluminum alloy sheet (2.0 mm) was used to produce dissimilar bonds with the dispersion strengthened alloys. The composition of the 7475 alloy (Schedule E, WE6 condition) was reported as follows (wt%) : 5.7 Zn, 2.3 Mg, 1.6 Cu, 0.12 Fe, 0.22 Cr, 0.1 Si, 0.06 Mn, and 0.06 Ti. Bonding was conducted in a furnace using selected combinations of temperature ranging from 500-625°C (932-1157°F), pressure ranging from 100-1000 psia (0.7-7 MPa), and time from1-20 h. After heating, the bonding fixture was removed from the furnace and cooled in air to room temperature. Selected dissimilar bonded (7475/Al-Fe-V-Si) specimens were heat treated to the T6 condition by solution treating at 482°C (899°F) for 1 h, water quenching, and then aging at 121°C (250°F) for 24 h.

The shear strength of diffusion bonds were determined by testing lap-shear specimens machined from the bonded blanks. The shear strength of unbonded base metal alloys after thermal exposure conditions also were determined in a similar manner. The shear specimens were tensile loaded at a crosshead speed of 0.008 mm/s (3.15×10^{-4} in./s) at room temperature. A minimum of three tests to failure were usually conducted for each condition. Microhardness across the bonded region was determined with a Knoop diamond indentor with a 25 g load.

5. RESULTS AND DISCUSSION I : ALLOY CHARACTERISTICS

5.1 ALLOY COMPOSITION

Chemical analyses of the alloys indicated nominal compositions very close to target compositions as shown in Table 1.

Three compacts were prepared for each alloy. The compact identification along with the total quantity of sheet produced is given in Table 2.

The surface quality and overall flatness of the sheet produced varied due to the use of a small rolling mill. (Commercial production on a large mill produces excellent surface quality and flatness.)

5.2 ALLOY MICROSTRUCTURE

Grain size. The average grain size (corresponding to a mean intercept length) for the extrusions and sheets is listed in Table 3.

A typical TEM micrograph of the alloys after extrusion is shown in Fig. 2 and 3 for the largest and smallest grain size condition. Typically, the ultra-fine grain size is found to systematically decrease with increasing dispersoid volume fraction. This is in agreement with conventional dispersion strengthened alloys. Grain size ranged from 1.25 μm for alloy FVS0301 containing approximately 8 vol.% silicide phase to about 0.3 μm for alloy FVS1212 containing approximately 36 vol. % silicide phase.

The grain size after hot rolling was not significantly different from that of the extrusion. The small change in grain size after rolling suggest that the dispersoids are very effective at pinning grain boundaries. Even at the lowest volume fraction investigated, no significant grain growth occurred after rolling at 500°C (932°F).

For both extrusion and sheet, distinct grain boundaries can not be resolved under optical observation, however, the flow pattern arising from the prior powder boundaries may be observed. Light micrographs of the sheet samples of the alloys are shown in Fig. 4 to 15. TEM micrographs of these same sheet samples are shown in Fig. 16 to 27.

Dispersoids. Average dispersoid size for extrusion and sheet is listed in Table 4. The dispersoids consisted of fine $Al_{13}(Fe,V)_3Si$ particles.

In the as-extruded condition, the microstructure consists of under 50 nm dispersoids within an ultra-fine grained matrix. Dispersoid size is observed to be independent of dispersoid volume fraction. Dispersoids, especially in the higher volume fraction alloys tended to be positioned at grain and/or subgrain boundaries. In all samples, average dispersoid particle size was very similar. The slightly larger average particle size noted for alloy FVS1212 is likely to be due to the higher extrusion temperature of 427°C (800°F) versus 385°C (725°F) used for the other alloys.

In the sheet condition, the dispersoid size was found to generally increase due to rolling. However, as can be seen from Table 4, the statistics involved with particle size determination were not able to accurately resolve the actual average size but did allow the determination of approximate sizes before and after hot rolling. It can be only qualitatively concluded that rolling increased dispersoid size most notably in low dispersoid volume fraction alloys. An increase in dispersoid size will ultimately reduce mechanical strength due to reduced dislocation interaction.

The maximum dispersoid size achieved after rolling was approximately less than 100 μm for all but one condition. Isothermal coarsening rates previously measured for these dispersoids at temperatures less than 500°C (932°F) suggest very low growth rates for the dispersoids . However, it has been reported that the imposition of an applied stress during compression creep testing significantly increase the growth kinetics of the dispersoids.[31]

The size distributions for silicide particles in extruded and rolled alloys are shown using histograms in Fig. 28 to 35. In general, the shape of all distributions appear to display a log normal characteristic. However, the distributions in the rolled sheet appear to display a slightly broader range of particle size. The longer trails may be an indication that particles associated with grain and/or subgrain boundaries coarsen at a faster rate than particles dispersed within the grains.

Texture. The effect of hot rolling on texture in sheet samples were investigated for alloys FVS0301 and FVS0611 rolled at 400°C (753°F) and FVS0812 and FVS1212 rolled at 300°C (572°F) . The X-ray (111) pole figure are shown in Fig. 36. All of the alloys exhibited only a weak fcc texture versus conventional ingot Al base alloys following similar thermomechanical processing. Furthermore, the degree of texture appears to increase as the volume fraction of dispersoid particles is decreased.

5.3 ALLOY MECHANICAL PROPERTIES

Tensile Tests. The mechanical properties of the extrusions and sheets were measured at room temperature and elevated temperatures at Grumman and Allied-Signal using different specimen designs. Tests at elevated temperatures were performed to determine "as-received" strengths for comparison to post processing strength.

The tensile properties of the extruded alloys are summarized in Table 5 and shown in Fig. 37. The variation in properties as a function of temperature and dispersoid volume fraction is clearly shown. A steady decrease in the strengths of the alloys with increasing temperature can be observed with a minimum in elongation at intermediate temperatures (150°C (302°F)). This has been attributed to solute drag.[12] The increased strength and reduced ductility with increasing dispersoid content can also be clearly seen.

The average of three transverse tensile tests of extruded FVS0812 at room temperature showed a yield of 374 MPa (54.3 ksi), an ultimate tensile strength (UTS) of 443 MPa (64.3 ksi), an elongation of 14.1% and a reduction in area of 32%. Orientation appears to have very little effect on the strengths, although ductilities in the longitudinal direction are significantly higher than in the transverse direction.

The effect of rolling temperature on room temperature tensile behavior is summarized in Table 6. Tensile properties are similar in the extrusions and in the sheet rolled at the lowest temperature, with possibly a slight increase in yield strength due to additional dispersoid precipitation at 300°C (572°F). As the rolling temperature is increased, the strengths decrease and elongation increases, as shown in Fig. 38. The rolled sheet exhibits the same trends of increasing strength and decreasing elongation with increasing dispersoid content as were found in the parent extrusions. The observed lower than normal elongation in the FVS0611/400 sample occurred due to delamination of the specimen, followed by premature fracture; this can probably be traced to local defects within the microstructure generated by improper powder handling or rolling proce-

dures. The potential for low shear strength in powder metallurgy based alloys is commonly associated with contamination of the powder phase and the alinement of these contaminants during rolling.

The tensile strength and elongation of the Al-Fe-V-Si sheets at 200 and 315°C (392 and 600°F) are plotted in Fig. 39. The trends observed at room temperature are also evident. It can be observed that the higher dispersoid volume fraction alloys result in higher strength and lower elongation. It is also evident a lower rolling temperature results in higher strength and lower elongation. At 315°C (600°F), the effect of rolling temperature on tensile strength and elongation is less significant than at lower temperatures for the higher volume fraction alloys. The typical stress strain curve obtained from these tests is represented by Fig. 40. The behavior is one of no significant strain hardening, but gradual decrease in engineering stress is a result of broad necking. Failure is preceded by localized necking. This is the same behavior observed at room temperature. Other than due to the geometry change observed during deformation, there is no evidence of true strain softening.

Table 7 and Fig. 41 summarizes the effect of thermal exposure on the room temperature tensile behavior of the alloys. Service exposure temperatures of up to 400°C (750°F) are anticipated for these alloys and thus no significant microstructure degradation is expected up to this temperature. There is essentially no effect of a 120 h exposure at 400°C (750°F) on the properties of any of the extruded alloys. FVS0812 exhibits insignificant variations in tensile properties following 120 h or 504 h at 400°C (750°F) and 120 h at 455°C (850°F). Following 120 h at 510°C (950°F) the yield and tensile strengths of FVS0812 have been reduced by almost 10% and the elongation by nearly 50%. There is a corresponding transition in fracture morphology from the ductile cup-and-cone appearance to a more tortuous surface with irregular tear features. The microstructure has probably been severely degraded by the precipitation of angular or plate-like brittle intermetallic phases. Limited duration exposure at processing temperatures above 500°C (932°F) will be presented and discussed later in another section.

Fatigue crack growth rates were also determined for the extruded FVS0611 and FVS0812 in the L-T and T-L orientation. These are shown in Fig. 42.

Fracture toughness results for the FVS0611 and FVS0812 extrusions are presented in Table 8 and Fig. 43. These values have not been corrected for curvature of the crack front, which in most cases would increase the stated values by a few percent. In both alloys, the L-T orientation shows greater toughness than the T-L orientation; this difference is more pronounced in FVS0812. In general, FVS0611 shows greater toughness than FVS0812. This was anticipated due to the greater tensile ductility and lower strength of FVS0611. In all cases except for T-L FVS0812 specimens, the plane stress fracture toughness Kc is much greater than the corresponding ("not valid") plane strain Kq. The T-L FVS0812 specimens showed very brittle fracture surfaces, with narrow shear lips outlining flat featureless center areas. All other specimens showed wide shear lips and severely deformed and torn fracture surfaces, which accounts for the large values of Kc.

Hardness. Hardness is an indicator of tensile strength in many alloys. The hardness of the four alloys is plotted in Fig. 44 and it can be observed that the highest volume fraction alloy had the highest hardness. It is also evident that rolling at elevated temperatures reduced hardness as a result of increased dispersoid size due to coarsening. Prior work has shown that annealing at

elevated temperatures up to 500°C (932°F) has no significant effect of hardness[32]. Exposure at 600°C (1112°F) can be expected to reduce hardness due to significant coarsening of the dispersoids.

Modulus. The modulus of the alloys were measured using an acoustical resonance method.[33] The data representative of average modulus of the three rolling conditions are presented in Fig. 45. It can be observed that there is a significant increase in modulus as the volume fraction of dispersoid is increased from 16 to 27 vol%. It is also apparent that at 12.6 mpsi (86.9 x 10^3 MPa), the highest volume fraction alloy (FVS1212) did not have the 14.0 mpsi (96.6x 10^3 MPa) modulus previously reported[34] for a Al-Fe-V alloy with 12 w% Fe. The reason for this lower stiffness was not known, but it is thought to be related to the initial alloy casting procedure.

5.4 OTHER CHARACTERISTICS

The stability of the dispersoid is critical to the elevated temperature strength of the alloys. One method that can be applied to study precipitation and transformations kinetics is based upon differential scanning calorimetry (DSC). This method measures the relative heat capacity of samples as a function of temperature. Using DSC at a temperature scan rate of 10°C/ min, the results are shown in Fig. 46. No significant reactions were detected by DSC from room temperature up to approximately 625°C (1157°F) in all four alloys.

The alloys showed significant electrical conductivity differences. The conductivity of the alloy sheets is shown in Fig. 47. Clear differences in conductivity existed between alloy dispersoid volume fraction but not between different rolling conditions.

6. RESULTS AND DISCUSSION II: SUPERPLASTIC EVALUATION

6.1 SLOW STRAIN RATE(< $2x10^{-3}$ s^{-1})

Deformation behavior at the slow strain rates commonly associated with superplastic forming was investigated. The elongation achieved at 500 and 600°C (932 and 1112°F) at a strain rate of $1x10^{-4}$ s^{-1} is presented in Fig. 48. The data show that at low strain rate, although difference exist in elongation between deformation at 500 or 600°C (932 or 1112°F), all elongations were approximately under 40%. Alloy FVS0611/500 and FVS812/300 showing the highest and lowest elongation, respectively. The maximum flow stress achieved during deformation at a strain rate of $1x10^{-4}$ s^{-1} is shown in Fig. 49. Engineering stress (maximum load / initial cross section) is shown for later comparison with high strain rate tests. In addition, due to the generally non-homogeneous deformation behavior of the alloys, a calculated true stress can be subject to greater errors. The calculated true stress was typically 8% higher than the engineering stress. For the tests at 500°C (932°F), sheet fabricated at lower rolling temperatures produced the highest strength and is attributed to the effect of rolling temperature on dispersoid size as shown previously in Table 4. At 600°C (1112°F), the strengths are significantly reduced due to the introduction of thermally activated deformation.

Some evidence of localized superplasticity was observed in some of the tests. This was evident in the form of fine ligaments observed at the fracture surface. Typical ligaments are shown in Fig. 50. Ligaments have been observed in other superplastic materials and are suggestive of deformation according to the core and mantle mechanism.[35,36] Although the presence of these ligaments suggest that superplasticity occurs on a very localized level, the overall elongation data indicate that macroscopic superplasticity does not occur at low strain rates at temperatures up to 600°C (1112°F).

In many alloys, superplasticity can be improved by using a very low strain rate. This allows diffusional accommodation processes to relieve stresses (mostly at triple points of grains) arising from grain boundary deformation. Alloy 611/300 was tested at low strain rates of $2.5x10^{-6}$ s^{-1} at 500°C (932°F). The results shown in Fig. 51 indicate that at lower strain rates the flow stress was reduced as expected. However, the elongation was also reduced. The highly effective pinning of the grain boundaries by the dispersoids does not allow sufficient grain boundary deformation at low strain rates to increase ductility. Failure at very low strain rates is likely due to diffusion controlled void formation (cavitation). Additional tests at low strain rates were not pursued.

To determine the role of dispersoid condition on deformation behavior, FVS0812/400 was held at 600°C (1112°F) for 15 min prior to testing at 500°C (932°F) at a strain rate of $1x10^{-4}$ s^{-1}. The 600°C (1112°F) exposure coarsens the dispersoid and alters its interaction with the matrix. The result is shown in Table 9. Except for a reduction in strength due to the coarsened dispersoid, as expected, no difference in elongation was observed.

6.2 EFFECT OF INTERNAL STRESS ON SUPERPLASTICITY

The effect of thermally induced internal stress on superplastic deformation was investigated using pre-loaded samples and rapid temperature cycling. The highest volume fraction alloy with the largest dispersoid size (FVS1212/500) was tested as this condition can be expected

to have the highest internal stress generation. A segment of the time-temperature record for test N70 is shown in Fig. 52. It can be seen that the rate of heat-up was substantially faster than that of cool-down. While a change in temperature from 200 up to 580°C (392 to 1076°F) required less than 10 s, the overall time needed for one complete thermal cycle was approximately 400 s due to the long cool-down period needed. The results of these thermal cycles are presented in Table 10 and indicated no benefit from temperature cycling as elongation was not improved. Apparently, the very small size of the spherical dispersoids did not result in any significant internal stress despite a high dispersoid volume fraction. It should be noted that in the composite alloys in which internal stress superplasticity has been reported, the second phase has been of significantly greater size than the dispersoids in these Al-Fe-V-Si alloys.

6.3 HIGH STRAIN RATE (> $2x10^{-3}$ s^{-1})

The dependence of superplastic behavior on fine grain size is well established. As grain size is reduced, the rate at which superplasticity can take place is increased.

Enhanced Ductility at T >600°C (1112°F). The application of a high strain rate resulted in a significant increase in elongation at 600°C (1112°F). Figures 53 and 54 show the effect of high strain rate (0.1 s^{-1}) on elongation and flow stress at 400, 500, and 600°C, (752, 932, and 1112°F) respectively. At 600°C (1112°F), the data indicate a notable increase in elongation for all alloy conditions. Alloy FVS0611/500 exhibited the highest elongation gain as compared to the test data at a strain rate of $1x10^{-4}$ s^{-1}.

As temperature approaches 600°C (1112°F), the differences between alloys, such as volume fraction dispersoid and dispersoid size become less significant as deformation becomes more matrix diffusion controlled. This can be seen in Fig. 55 , where the flow stress converges at high temperatures. This is a continuation of the behavior first observed at intermediate temperatures. The effect of deformation temperature on elongation is illustrated in Fig. 56 for alloy 611/500. (The data point at 625°C (1157°F) is from a test at a strain rate of 0.05/s). It shows that in this strain rate range, temperatures at or above 600°C (1112°F) significantly increase elongation. At the highest temperature tested (625°C (1157°F)), the highest elongation was achieved. Although high elongation was possible, further tests were not performed because of significant dispersoids coarsening. In addition, the microstructural observation indicated the formation of voids (cavitation) as shown in Fig. 57.

At temperatures below 600°C (1112°F), however, strain rate has very little effect on strength and elongation as shown in Fig. 58 where the maximum flow stress and elongation is plotted against strain rate at 550°C. At all three strain rates plotted, the flow stress varied by no more than 0.48 MPa (70 psi). Elongation did not vary significantly, but it did show a better response at the middle strain rate value.

Effect of Dispersoid Condition. The effect of dispersoid condition on ductility was investigated by coarsening the dispersoids prior to test through elevated temperature exposure. Fig. 59 shows the result of different hold times prior to testing on flow stress and elongation of FVS0812/500. It is apparent that hold time does not have a significant effect on deformation behavior. Since time at this temperature would alter the dispersoid morphology, the data signifies that deformation is controlled more by temperature induced (diffusion) effects than by direct particle dislocation effects.

Dispersoid Coarsening. The effect of deformation on the microstructure in the deformed samples were investigated by TEM. TEM foils were taken from the gauge section near and far from the point of failure. The region near the grip represents thermal exposure with less deformation than that near the break. The observation indicated that deformation and plasticity at 500 and 600°C (932 and 1112°F) are primarily accommodated by the generation and movement of dislocations within the grains of the alloys. In the lowest volume fraction samples (FVS0301 and FVS0611), the presence of dislocation tangles and interaction of dislocations with the silicide dispersoids are readily apparent, especially at 500°C (932°F). Representative TEM micrographs of tested specimens are shown in Fig. 60 to 62 .

Quantitative analysis to determine the effect of deformation on grain size (Table 11) indicates that after deformation at temperatures above 500°C (932°F), alloys FVS0812 and FVS1212 showed very little change in grain size. Alloys FVS0301 and FVS0611 showed a reduction in grain size. This reduction in grain size may be indicative of partial recrystallization occurring during deformation and/or the simultaneous recovery of the deformed structure. Grain size measured in the deformed samples are very similar to the grain size measured in the initial sample sheets.

Quantitative analysis to determine the effect of deformation on average silicide dispersoid size (Table 12), indicated that deformation of the alloys at 600°C (1112°F) resulted in more coarsening of the dispersoid phase in the region nearer the break than in the region away from the break. Average particle size in the gauge section away from the break was very similar to the average size measured in the initial sample sheets. The enhanced coarsening of the silicide phase in the region near the failure point is indicative of localized deformation and strain enhanced coarsening. Increased dislocation densities enhance solute diffusion and particle coarsening either via a sweeping action of a glissile dislocation moving through a grain or directly by pipe diffusion.

Deformation of the alloys at 600°C (1112°F) also resulted in the formation of coarse needle-like Al_3Fe particles dispersed in the matrix. The presence of these needles and/or excessively coarse silicide dispersoids are expected to severely degrade the material's mechanical properties.

Biaxial Forming using High Strain Rate. Equibiaxial gas pressure forming was attempted using the FVS0611/500 alloy in a fixture similar to the fixture used for the DB studies. The pressure sequence used is shown in Table 13, and was selected to generate an approximate average strain rate of 0.01 s^{-1} when formed into a 0.90 in. (2.29 cm) dome. This was determined based upon the stress strain behavior measured during uniaxial testing. The cross section of the resulting dome is shown in Fig. 63. It can be observed that although formed, the thinning was not as uniform as desired. This reflected the low strain rate sensitivity of the alloy. The alloy did not show evidence of cavitation under this forming condition.

6.4 ESTIMATED POST PROCESSING PROPERTIES

Effect of Thermal Exposure. The properties of the Al-Fe-V-Si alloys can be retained only if the microstructure of the alloys can be preserved during thermomechanical processing. The coarsening of the dispersoids result in degraded properties. This is illustrated in Fig. 64 where the elongation and tensile strength of the alloys are plotted after exposure to 625°C

(1157°F) for 1 h, 500°C (932°F) for 1 h , 500°C (932°F) for 4 h and with no exposure (as-received condition). It is evident that the alloys are not degraded at 500°C (932°F). Tensile strength and elongation are essentially that of the as-received condition. Observation of the data show a clear trend of ductility and strength loss in the higher volume fraction alloys (FVS0812 and FVS1212) after the 625°C (1157°F) exposure. The lower volume fraction alloys (FVS0301 and FVS0611) did not show any ductility loss but indicated strength loss.

6.5 SPF ASSESSMENT

Overall, the Al-Fe-V-Si alloys show little or no strain rate sensitivity at strain rates between $1x10^{-6}$ and 0.10 s^{-1} at temperatures under approximately 550°C (1022°F). The alloys do exhibit a small strain rate sensitivity increase at strain rates near 0.01 and 0.10 s^{-1} at temperatures above approximately 600°C (1112°F). This is shown in Fig. 65 where log flow stress is plotted against log strain rate. For the group, the highest average m value is approximately 0.13. Some conditions, notably the FVS0611/500 condition, achieved higher elongation. The highest elongation specimen is shown in the before and after condition in Fig. 66. Based upon FVS0611/500, an approximate m value can be determined at 500 and 600°C (932 and 1112°F) using the measured flow stress difference between strain rates of $1x10^{-4}$ and 0.1 s-2. The calculated m value is 0.09 at 500°C (932°F) and 0.16 at 600°C (1112°F).

The Al-Fe-V-Si alloys showed very little strain hardening at room temperature, 200°C (392°F), and 300°C (572°F). This same behavior was observed at high temperatures where the typical load vs time data indicate a very rapid increase to the maximum load followed by gradual load decrease prior to localized neck formation and failure. The load reduction was attributed to diffuse necking. Calculated true stress true strain curve is shown in Fig. 67 for the highest ductility alloy condition (FVS0611/500). These true stress strain curves assume uniform deformation within the gauge section of the specimen, a situation which is difficult to satisfy for these alloys given the tendency towards localized neck formation. However, given the current data, what is evident from Fig. 67 is that the strain level at which "strain softening" (load reduction) occurs increase as the strain rate is increased. The evidence indicates that strain hardening at low strain rates, if it occurs, occurs very rapidly in the very early stages of deformation. At high strain rates and at temperature above 600°C (1112°F), there appears to be some possible enhanced plastic stability due to "strain hardening."

Because superplastic behavior can not be considered to take place at strain rate sensitivity values (m) values less than approximately 0.3, the Al-Fe-V-Si alloys can not be considered superplastic. However, at temperatures >600°C (1112°F), the increase in m at the higher strain rates offered some additional plastic stability to the deformation process and elongation was improved. The significantly higher elongations achieved at temperatures >600°C (1112°F) suggest that another deformation mechanism was operative. At these high temperatures, thermally induced dislocation climb through vacancy diffusion is possible.[7] At high temperatures where there is climb, the dispersoid particles are no longer effective at limiting slip through residual dislocation interaction (i.e., Orowan bowing). As dislocation climb is diffusion rate driven, there is an associated rate effect and a "strain rate sensitivity" might be encountered under climb conditions. The observed increase in strain rate sensitivity might be the result of such a rate dependence and could have been observed in the "strain" hardening behavior ob-

served under high strain rates. The combination of high strain rate and deformation resulted in a large number of dislocations within the matrix and evidence of dynamic recrystallization as evident from the microstructure.

THIS PAGE INTENTIONALLY LEFT BLANK

7. RESULTS AND DISCUSSION III : DIFFUSION BONDING EVALUATION

7.1 SHEAR STRENGTH OF Al-Fe-V-Si ALLOYS

The shear strength of Al-Fe-V-Si alloys in the as-rolled condition (300°C (572°F)) and after selected thermal exposures is presented in Table 14. The thermal exposures simulated a typical diffusion bonding and heat treating cycle employed during the study of dissimilar (Al-Fe-V-Si/7475) bonds. The thermal exposures included heating at 516°C (961°F) for 4 h followed by slow cooling, which represents an "as-bonded" or annealed condition, and 516°C (961°F) /4 h followed by heat treatment to the "T6" aged condition (482°C (900°F)/1 h, WQ + 121°C (250°F)/24 h), which is a typical strengthening heat treatment for 7000 series aluminum alloys, such as 7475. The data show that there was no effect of thermal exposure on shear strength in alloys containing up to 27 volume percent dispersoids. However, thermal exposure of the FVS 1212 alloy (36 %) caused a loss of shear strength of approximately 24 %.

Effect of Dispersoid Volume Percent and Thermal Exposure on Shear Strength. The effect of dispersoid volume percent and thermal exposure on the shear strength of high temperature alloys is shown by Fig. 68. For comparison, the estimated shear strength of these alloys in the as-rolled condition, based on 60 % of the ultimate tensile strength is also shown. Since there is no reported shear strength data for these alloys, the estimated values are viewed only as a first approximation. It can be seen that the actual shear strength of these alloys increases with dispersoid volume percent, although not in the nearly linear manner as the estimated values. The shear strengths of the 8 and 16 volume percent alloys agree with the estimated values, while the strengths for the 27 and 36 % alloys are considerably lower (30 and 34 %, respectively) than those estimated. Also, it can be seen that thermal exposure had no effect on the shear strength of the 8, 16, and 27 % dispersoid alloys, but did cause a consistent drop in shear strength for the 36 % alloy. This reduction in shear strength might be due to the result of additional precipitation or coarsening of particles located at prior particle boundaries. Prior particle boundaries inherent from the powder metallurgy fabrication process are often a significant source of weakness.

The effect of rolling temperature and thermal exposure up to 516°C (960°F) on shear strength of sheet FVS0301 and FVS0611 alloys is shown in Fig. 69. In general, the shear strengths of these two alloys decrease with rolling temperature, as expected, and also show reasonable agreement with estimated values of shear strength based on 60% of the as-rolled sheet ultimate strength. These results also indicate that thermal exposure of this type does not degrade the properties of these alloys. However, beyond 516°C (960°F), high temperature exposure of the base metal drastically reduces shear strength, as shown in Fig. 70. The data at 600 and 625°C (1112 and 1157°F), (from Table 15) represent shear strength values of high temperature alloy (similar) diffusion bonds, where failure in many cases occurred in the base metal adjacent to the bondline. This strongly suggests that the alloy is no longer stable beyond approximately 516°C (960°F).

Shear Failure Mode in Al-Fe-V-Si Alloys. The fracture surfaces of unbonded, as-rolled FVS0812 and FVS1212 after shear testing at room temperature are shown by the SEM fractographs in Fig. 71 and 72. Shear testing of these alloys typically resulted in brittle fracture surfaces

consisting of relatively flat multiple steps or ledges, which is considered fairly common to materials made by powder metallurgy (PM) technology. The ledges may have been caused by prior particle boundaries and oxide distributions that can influence fracture paths and result in low shear strengths, as was observed for these materials. Brittle fracture surfaces and low fracture toughness in T-L oriented specimens are typical of many PM alloys. The width of the ledges vary, but appear to be of the order of the ribbon thickness size (25 μm) of the rapidly solidified product. Apparent microstructural non-uniformities in the appearance of layers or laminations were observed in all alloys. The typical appearance of these non-uniformities is represented in Fig. 73. These striations are the result of the alinement of the comminuted ribbon (powder) during the alloy consolidation process of extrusion. Additional directionality is achieved during subsequent rolling.

7.2 DIFFUSION BOND BETWEEN Al-Fe-V-Si ALLOYS (SIMILAR BONDS)

Similar Bond Shear Strength. The effect of diffusion bonding pressure and time on the shear strength of the high temperature sheet alloys is presented in Table 15 and Fig. 74. Diffusion bonding conditions, bonding results and bond shear strength are summarized in Table 15. In general, these conditions produced three groups of results: diffusion bonded specimens that were capable of being machined and tested (DB); specimens that were weakly bonded and broke during machining or subsequent handling (DB/BDM); and specimens for which no bonding was observed (DNB). Most experiments were conducted on the alloys that had been rolled into sheet at 500°C (932°F), since they represented the most ductile condition for their respective compositions and, thus, the most likely to bond. A limited number of bonding experiments were conducted on alloys rolled at 300°C (572 °F) to verify initial results.

It can be seen from Table 15 that diffusion bonding, which resulted in measurable shear strengths, occurred only when the bonding temperature was ≥ 600°C (1112°F). More specifically, bonding occurred at 600°C (1112°F) when the bonding pressure was 6.90 MPa (1000 psia), and at 625°C (1157°F) when the pressure was 0.7 to 2.8 MPa (100 to 400 psia), as shown in Fig. 74. The ability to bond at 600°C (1112°F) appears to be directly related to the enhanced interfacial contact that should occur at the highest bonding pressure. The shear strength of bonds made at 600°C (1112°F) are slightly higher. This is attributed to somewhat less dispersoid coarsening at that temperature. Thus, the results indicate that higher bonding pressure was beneficial in slightly lowering bonding temperature and increasing resultant shear strengths.

In general, the shear strengths of most of the conditions tested are considered to be low and range between 69.0-103 MPa (10-15 ksi). In many specimens, shear failure occurred in base metal adjacent to the bondline and, thus, these values may be considered a reasonable measure of the shear strength of the high temperature alloys after short time (up to 4 h) exposure at 600 and 625°C (1112 and 1157°F). The average shear strength for 1100-0 and 7475-0 (as-DB) aluminum also are shown in Fig. 74 for comparison. The results indicate that dispersoid coarsening during bonding contributes to lower shear strength and that the resultant shear strengths approach that of the soft, aluminum matrix. The effect of bonding time on shear strength for two selected conditions is shown in Fig. 75. It can be seen that bonding time has very little affect on strength, even after short bonding times. Thus, alloy coarsening and softening must occur at high rates at temperatures ≥ 600°C (1112°F).

Bond Interface Microstructure. The effect of diffusion bonding pressure on the bond interface microstructure and shear strength of FVS301/500 after bonding at 600°C (1112°F) for 4 h at 0.7, 2.8 and 6.9 MPa (100, 400, and 1000 psia) is shown in Fig. 76. The specimens bonded at the two lower pressures were characterized by weak bonds that broke at the shear test region during the test specimen machining operation. The intact halves of each specimen were utilized for metallographic examination. A comparison of the bond interfaces shows that the bondline of each couple is planar but with increasing bonding pressure, the interface becomes less continuous and defined, as is the case for the bond made at 6.90 MPa (1000 psia). Shear failure in bonds made at pressures ≤ 2.8 MPa (400 psia) occurred along the bond interface, whereas in bonds made at 6.90 MPa (1000 psia), shear occurred along the interface, or in material adjacent to the interface, or both. Shear failure in FVS611/500, bonded at 600°C (1112°F) for 1.25 h under 6.90 MPa (1000 psia), in which material adjacent to the bond interface fractured, is shown in Fig. 77. This indicates that the bond strength was similar to that of the base material. In general, bonds with highly discontinuous interfaces and where shear is mixed, are considered to be of high quality and, thus, desirable.

A comparison of two bonds in FVS301/300 and FVS0301/500 material, bonded at 625°C (1157°F) for 4 h under 2.8 MPa (400 psia) is shown in Fig. 78. Close examination reveals that the bondlines in each are free of porosity and voids and are mainly discontinuous but are decorated with particles and needles. The Al_3Fe needles are mainly oriented parallel to the bondline or normal to the applied bonding pressure. A silicide depleted zone is visible around each needle. The average bond shear strength of each specimen was approximately the same, although, before diffusion bonding, the FVS301/300 sheet was about 35% stronger. These results indicate that bonding under these conditions leads to extensive particle coarsening and drastic loss in strength.

The effect of bonding time and temperature on the bond interface and strength of FVS611/500 is shown by light micrographs in Fig. 79 and 80. The effect of time on bonding at 625°C (1157°F) at 2.8 MPa (400 psia) for 1,2, and 4 h is shown in Fig. 79. In addition to dispersoid particle coarsening in each condition, it can be seen that bonding at 4 h led to a less distinct and more discontinuous interface than the shorter times. The less distinct interface did not lead to higher shear strength but it did result in a more consistent bond quality, as indicated in Table 15. For example, the 1 h bond condition exhibited considerable failures during sample machining and handling so that only one shear test was actually conducted for that condition. The beneficial effect of temperature on bonding FVS611 is shown in Fig. 80. A bond made at 516°C (960°F) and 2.8 MPa (400 psia) easily broke during subsequent handling; its bondline is well defined and continuous. The 625°C (1157°F)/ 0.7 MPa (100 psia) bond exhibits a more desirable interface which indicates that higher temperatures lower yield strength, and help to achieve good surface contact that is required for bonding. Coarsening in the 625°C (1157°F) bond lead to the relatively low shear strength that is common in these materials after overheating.

The interfaces of bonds made in FVS0812 and FVS1212 after bonding at 600°C (1112°F) for 4 h under 6.9 MPa (1000 psia) are shown in Fig. 81. Under these conditions, the higher strength alloys also exhibit discontinuous bondlines and extensive coarsening. Distinct Al_3Fe needles oriented in a direction normal to the applied bonding pressure may be observed.The fracture surface of an FVS812 shear specimen is seen to be adjacent to the barely discernible

interface, that indicates that the shear strength of the bond was comparable to that of the base metal. The higher volume fraction alloys (FVS0812 and FVS1212) are more difficult to bond because of their inherent higher creep resistance. This makes the initial stage of bonding, that of surface contact, very difficult using low pressures. The use of high pressures, such as 6.90 MPa (1000 psi) is not practical and the use of higher temperatures (>>600°C(1112°F)) would only increase the dispersoid coarsening problem.

TEM micrographs of FVS812, shown in Fig. 82 after bonding at 600°C (1112°F) for 4 h under 6.90 MPa (1000 psia), indicate that these bonding conditions promote significant coarsening of the silicide phase and copious formation of needle-like Al_3Fe and possibly Al_3V intermetallic particles. In general, the diffusion bond was very difficult to discern by TEM because only an apparently fine oxide layer was present at the interface and clustering of the silicide particles along the interface had not occurred. These results indicate that the conditions required to DB these alloys and the resultant evolution in microstructure are expected to severely degrade the material's mechanical properties following bonding.

Bond Fracture Appearance. The shear fracture surfaces of FVS301/300 bonds and FVS0301/500 bonds, bonded at 625°C (1157°F) for 4 h is shown by the SEM fractographs shown in Fig. 83. Although bonded at different pressures, the fracture surfaces are quite similar. They are mainly characterized by relatively featureless islands approximately 10 μm wide with evidence of coarsened dispersoids or Al_3Fe needles. Also, the islands of each surface have small, elongated, ductile tear ridges characteristic of shear. The average shear strength for each was virtually the same.

7.3 DIFFUSION BOND BETWEEN Al-Fe-V-Si ALLOY AND 7475 (DISSIMILAR DIFFUSION COUPLES)

The difficulty encountered during high temperature DB of Al-Fe-V-Si alloys to itself is dispersoid coarsening which results in properties degradation. If the properties can not be retained, then DB is an unlikely joining technique for strength critical applications. To retain full strength in the Al-Fe-V-Si alloys, the bonding temperature used must not result in microstructural coarsening. This can be done if bonding can be done at low temperatures. Dissimilar bonding offers such a possibility as what is considered high for one alloy might not be considered high for another. A dissimilar alloy which can bond to the Al-Fe-V-Si alloys might offer a novel opportunity to produce hybrid structures.

Dissimilar Bond Shear Strength. The shear strength of dissimilar bonds between high temperature alloys rolled at 300°C (572°F) and 7475 aluminum alloy are summarized in Table 16. Diffusion bonds were produced with fine-grained, superplastic 7475 Al for times from 1-22 h, under 0.7 MPa (100 psia) at 516°C (960°F), which is the optimum superplastic temperature for 7475. Diffusion bonds also were made for each of the alloys for 4 h and subsequently heat treated to the T6 condition. The results show that relatively high strength bonds were produced for all conditions and for times as short as 1 h. For example, after 1 h the shear strength of the FVS 812 dissimilar couple is approximately 75 % that of the as-received base metal.

The effect of diffusion bonding time on as-bonded shear strength is shown in Fig. 84. The average shear strength of as-bonded 7475/7475 aluminum alloy also is shown for comparison.The results indicate that bond shear strength is time dependent and that bond

strengths comparable to that of as-bonded 7475/7475 couples were attained after relatively short times for the FVS812 (27%) and FVS1212 (36%) alloys. After long time bonding at 22 h, the shear strength of all dissimilar bonds converged at the same level of 117-124 MPa (17-18 ksi), the 8% and 16% alloys having steadily increased to that level, while the 27% and 36% alloys declined from their previous highs. These changes in shear strength with time are attributed, in part, to diffusion across the interface during bonding.

The systematic effect of dispersoid content and time on the shear strength of dissimilar bonds also is shown in Fig. 85. It is clear that the FVS812 (27%) alloy consistently exhibited the highest shear strengths for times up to 4 h and, most impressively, also for the shortest times. Longer bonding times appear to enhance bond strength in the 8% and 16% alloys and degrade strength in the other alloys. After 22 h, the shear strengths of the FVS0301 and FVS0611 dissimilar bonds were about 90 and 65% of their respective base metals.

The effect of a post-bond heat treatment to the T6 strengthening condition on the shear strength of dissimilar bonds is shown in Fig. 86. The shear strength of the unbonded high temperature base metal also is shown for comparison. It can be seen that heat treatment to the T6 condition results in sizeable gains in shear strength in alloys up to 27% dispersoids and results in no change in the 36% alloy. For example, the shear strength of the FVS0812 alloy increases about 22% from the as-bonded condition to approximately 172 MPa (25 ksi) after diffusion bonding at 516°C (960°F)/0.7 MPa (100 psia)/2 h and heat treating. This is equivalent to approximately 90% base metal shear strength. In comparison, the same heat treatment given to a 7475/7475 couple, diffusion bonded in a similar manner, would result in a strengths of approximately 317MPa (46 ksi), a gain of about 110%. A comparison of the dissimilar bond strength in the as-DB and as-Db+T6 with the base alloy strength shows an almost parallel relationship. Of significance is the nearly consistent drop in shear strength for the FVS1212 (36%) alloy. In general, these results indicate that high shear strengths in dissimilar bonds may be limited by base metal shear strength and compositional gradients at the bond interface.

Dissimilar Bond Interface Microstructure. The interface microstructure between each of the high temperature alloys and 7475 aluminum alloy after diffusion bonding at 516°C (960°F) at 0.7 MPa (100 psia) for the times indicated are shown in Fig. 87 and 88. In each case, the bondline is planar and is free of porosity or other voids. Coarsening adjacent to the interface is apparent in the FVS alloys after a bonding time of 22 h. These visual microstructural changes may also be the result of interdiffusion which is known to have occurred extensively on both sides of the couples. Also, it can be seen that a diffusion zone exists in the 7475 alloy of each dissimilar couple at both bonding times.

The bondline does not appear to be continuous in the FVS0301 alloy, but it seems to be in the other alloys. This is most likely due to the higher volume percentages of dispersoids in those alloys. The discontinuous interface of the FVS0301 dissimilar couple bonded for 4 h indicates that a relatively strong bond was formed in that particular specimen. In fact, even though the average shear strength of FVS0301/4 h bonds was low because of scatter (79 ±34 MPa (11.5±5 ksi)), the maximum strength of the specimen shown (112 MPa (16.3 ksi)) was comparable to that of FVS0301/22 h bonds (122±3 MPa (17.7±0.5 ksi)) and shear fracture occurred in the FVS0301 material, away from the bond. Thus, the appearance of the bond interface can serve as a guide to bond quality.

TEM micrographs of dissimilar bonds between FVS0812 and 7475 aluminum alloy in the as-bonded and heat treated condition (T6) after bonding at 516°C (960°F) for 2 h at 0.7 MPa (100 psia) are shown in Fig. 89 and 90, respectively. TEM of areas directly adjacent to the interface, in both conditions, indicate that a significant amount of interdiffusion has occurred due to interdiffusion between the dissimilar metals. Diffusion bonding was performed without the coarsening or transformation of the $Al_{13}(Fe,V)_3Si$ silicide phase.

The effect of bonding time on interface diffusion between FVS0812 and 7475 aluminum alloy after bonding at 516°C (960°F) at 0.7 MPa (100 psia) is shown by the light micrographs in Fig. 91. Even after 1 h, the visible diffusion zone in the 7475 alloy is about 50 mm (1.97 in.) indicating that intimate surface contact and bonding was attained. The extent of interdiffusion across the interface of dissimilar couples was determined by performing energy dispersive spectroscopic (EDS) analysis on bonds between FVS0812 and 7475 aluminum alloy after bonding at 516°C (960°F) and 0.7 MPa (100 psia) for 1, 4, and 22 h, as shown in Fig. 92. The concentration profiles of the major alloying elements were determined at approximately 20-30 micron increments across the interface. In addition, wave length dispersive spectroscopy (WLDS) was performed on the same dissimilar couple after a 2 h bonding cycle, in increments of one micron across the interface, as shown in Fig. 93. In general, the analytical results are in reasonable agreement and show that interdiffusion of Zn, Cu,and Mg is extensive even after 1-2 h For example, after 1 h, Cu and Zn (Fig. 92) have diffused approximately 200 μm across the interface into the FVS0812 alloy. Bonding at longer times resulted in extended diffusion zones at least 300 μm wide. The slope of the diffusion profiles for Fe and V are steep indicating limited diffusion. After 22 h, Si diffusion into 7475 Al is relatively sizeable. The presence of Cu, Zn, and Mg in the FVS0812 matrix is assumed to be deleterious since the phases that form are unstable at high temperatures. Furthermore, the reduction of Cu, Zn, and Mg in 7475 Al adjacent to the interface will result in localized weakening of the 7475, especially after strengthening heat treatments.

The influence of interdiffusion on the mechanical properties of dissimilar bonds is illustrated by the effect of bonding time and heat treatment on microhardness across the interface of bonds after bonding at 516°C (960°F) at 0.7 MPa (100 psia), as shown in Fig. 94 and 95. The effect of 1 and 22 h bonding times on the hardness profile of as-bonded specimens between FVS0812 and 7475 aluminum alloy is shown in Fig. 94. After 1 h, a hardness gradient in the FVS0812 extends approximately 125 μm from the interface and, after 22 h, it is approximately 300 mm from the interface. The hardness of the 7475 Al is relatively unchanged, but there is a slight increase near the interface after 22 h, that may be attributed to diffusion. The effect of post-bond heat treatment to the T6 condition on the hardness of dissimilar bonds between FVS0812/7475 and FVS1212/7475 after bonding at 516°C (960°F) for 2 h at 0.7 MPa (100 psia) is shown in Fig. 95. It can be seen that a hardness gradient exists on the 7475 aluminum side of both couples and extends approximately 125 μm from the interface and that the hardness of the 7457 near the interface is comparable to the as-bonded condition, shown in Fig. 94. Both Al-Fe-V-Si alloys exhibit smaller than expected hardness gradients away from the interface. It is possible that diffusion of Cu, Zn, and Mg into the Al-Fe-V-Si alloys, followed by the T6 heat treatment, had a strengthening effect.

Dissimilar Bond Fracture Appearance. Fractographs of shear test specimens representing dissimilar diffusion bonds are shown in Fig. 96 to 98. Typical results for as-bonded

FVS0301/7475 and FVS0611/7475 couples after bonding at 516°C (960°F) for 22 h under 0.7 MPa (100 psia) are shown in Fig. 96. In the 22 h bonds, fracture occurred through the Al-Fe-V-Si alloys, adjacent to the interface. The fracture surface of each alloy was characterized by small, elongated dimples. In the 1 and 2 h bonds, fracture occurred along the bondline; the fracture surface appeared flatter and had far fewer ductile appearing dimples. The 4 h bonds were characterized by a mixture of shear failures either along the bondline or through the Al-Fe-V-Si alloys.

Fracture specimens of FVS0812/7475 after bonding at 516°C (960°F) under 0.7 MPa (100 psia) for 2 and 22 h are shown in Fig. 97. In each, fracture occurred in the Al-Fe-V-Si alloy away from the bond interface, which was typical for all 22 h bonds. In the 1, 2, and 4 h bonds with FVS0812/7475, the fracture path was mixed between bondline and Al-Fe-V-Si alloy failure.Thus, since there was only small scatter in shear strength values, the mixed fracture paths indicate that the shear strength at the bondline or in material away from the interface were approximately comparable. Typical fracture surfaces for both 2 and 22 h bonds are shown in Fig. 98. For each, elongated dimples with ductile tear ridges were observed. In general, the appear-'ance of fracture surfaces of FVS1212/7475 couples were similar to those of the FVS0812/7475 series.

7.4 DB ASSESSMENT

DB of Al-Fe-V-Si alloys. The results of this work suggest that diffusion bonding of the rapidly solidified Al-Fe-V-Si alloys can be achieved at temperature and pressure combinations with virtually no macro deformation. Bond shear strengths achieved were approximately that of the matrix material. However, due to the instability of the dispersoid at the temperature needed for diffusion bonding, significant dispersoid coarsening and transformation occurred and the matrix mechanical properties were significantly reduced. Similar to the results obtained in the deformation work, exposure to temperatures above 500°C (932°F) caused rapid coarsening of the dispersoids and the formation of large needle-like Al_3Fe particles. Once significantly coarsened, the dispersoids no longer offered strengthening and the shear strength of the diffusion bonds was mainly determined by the matrix strength which was 69-103 MPa (10-15 ksi). Higher DB gas pressures reduced the temperature required for bonding, but no bonds were achieved at temperatures below 600°C (1112°F) at pressures up to 6.9 MPa (1000 psi), in any of the Al-Fe-V-Si alloys. Using gas pressures bonding at relatively low pressures, it appears that the Al-Fe-V-Si alloys require a homologous temperature greater than 0.95 for bonding, which is similar to 7475 Al alloy. The dispersoids are thermally stable up to a homologous temperature of approximately 0.76 or approximately 500°C (932°F). The effect of higher DB temperatures was not further investigated because of the extensive coarsening already observed at 600°C (1112°F).

Consideration of the diffusion bonding process suggests that high temperatures are beneficial for two reasons. First, diffusion rate is highly controlled by temperature, so that the time needed for bonding is clearly decreased with increasing temperature. Second, and perhaps more important, the yield stress needed to deform surface asperities during the first stage of bonding is significantly reduced. For the creep resistant Al-Fe-V-Si alloys, very high temperatures are required to reduce the "flow" stress to a level that is compatible with conventional gas pressure diffusion bonding. At these temperatures, the accompanying coarsening of strengthening dispersoids and resultant losses in the properties are unfortunate by-products. However, the

decrease in yield stress of the Al-Fe-V-Si alloys at temperatures above 600°C (1112°F) is not mainly due to dispersoid coarsening but rather to the availability of another deformation mechanism based upon diffusion controlled dislocation climb. Thus, if the strengthening dispersoids remained stable at high enough temperatures to reduce the flow stress to that compatible with gas pressure bonding, it is quite possible that surface deformation and matrix bonding could occur without significant degradation in room temperature properties. The inherent fine grain microstructure would enhance the bonding process by allowing oxide disruption through extensive localized surface deformation. Furthermore, in extremely fine-grained material, new dislocations can be continually supplied to support deformation since potential dislocation sources are available at grain boundaries. [38] Source and sink mobility at boundaries may dictate the behavior of fine-grained superplastic alloys. [39] Thus, it may be possible that dispersion strengthened alloys can be bonded without significant strength loss if the dispersoids remain stable.

Effect of Small Grain Size. The experimental evidence suggests that the fine grain size of the Al-Fe-V-Si alloys enhances diffusion bonding. This effect was evident by comparing bonding data for dissimilar couples, as shown in Fig. 99. It can be seen that alloys with smaller grain sizes achieve maximum strength faster than those with larger grain sizes. It is significant that this effect was operative at 516°C (960°F), representing a homologous temperature of approximately 0.78 for the Al-Fe-V-Si alloys and 0.95 for the 7475 alloy. At increased bonding time, such as 22 h, measurements of compositional gradients across the bond interface suggest that bond strength can be reduced by the interdiffusion of elements between the dissimilar alloys. The better bonding ability of the smaller grain size alloys can be attributed to the easier localized deformation of the fine grain surface, which offers a mechanism for the fragmentation of the thin inherent surface oxide layer and thus enabling diffusion bonding to occur at a faster rate.

Diffusion Bonding of Dissimilar Alloys. The work on diffusion bonding of fine-grained 7475 aluminum alloy to Al-Fe-V-Si alloys indicates that viable joints can be made at temperatures without significant dispersoid coarsening. This is particularly encouraging since the bonding of the Al-Fe-V-Si alloys to itself was only possible at temperatures that caused detrimental dispersoid coarsening and loss of strength. The shear strength of dissimilar bonds was limited by base metal shear strength and compositional gradients at the bond interface. This is indicated by a comparison of normalized shear strengths (i.e., the ratio of bond strength to that of base metal) for dissimilar Al-Fe-V-Si alloy bonds in the T6 condition and similar Al-Fe-V-Si alloy bonds, as shown in Fig. 100. It can be seen that dissimilar bonds with strengths up to 90% that of the Al-Fe-V-Si alloy base metal were attained, which are high compared with the low strengths of the similar Al-Fe-V-Si alloy bonds. Full strength probably was not achieved due to interdiffusion of alloying elements between the 7475 and Al-Fe-V-Si alloys, since many shear samples showed failure away from the bond line. In general, the results of this work indicate that the fabrication of hybrid dissimilar alloy structures based upon the enhanced bonding behavior of these important materials is possible.

8. CONCLUSIONS

Superplastic deformation of the Al-Fe-V-Si alloys was not possible due to effective pinning of grain boundaries by dispersoids. However, enhanced ductility (up to 300% elongation for FVS0611/500) can be achieved at temperatures above 600°C (1112°F) using strain rates typically between 0.1 and 1 s^{-1}. This enhanced ductility is likely the result of an increase in strain rate sensitivity at high temperatures where the limiting deformation mechanism changes from dislocation glide to thermally (diffusion) controlled dislocation climb. The deformed microstructure under these conditions indicated substantial dislocation generation and some dynamic recrystallization. At temperatures above 600°C (1112°F), rapid coarsening of the dispersoids and their transformation to primary Al_3Fe resulted in significant degradation of mechanical properties. Furthermore, the coarsening was amplified by strain during the deformation process. At temperatures below 500°C (932°F), strain-enhanced coarsening was also observed to a lesser degree. Non-strain induced coarsening was significantly less at 500°C (932°F) as compared to 600°C (1112°F).

Diffusion bonding of the Al-Fe-V-Si alloys was possible at temperatures at or above 600°C (1112°F). Although the bond strength approached that of the matrix, significant reduction in the alloy strength occurred due to extensive dispersoid coarsening and transformation at or above 600°C (1112°F). Dissimilar diffusion bonds between the Al-Fe-V-Si alloys and fine-grained, superplastic 7475 aluminum alloy were produced at 516°C (960°F) for short times and low pressures without harmful dispersoid coarsening. Dissimilar bonds with shear strengths up to 90% that of the Al-Fe-V-Si base metals were attained. The excellent dissimilar bonds were limited by lower than expected base metal shear strength and compositional gradients due to interfacial diffusion. It was also apparent that the fine grain size of the Al-Fe-V-Si alloys enhanced diffusion bonding by reducing bonding time and pressure.

THIS PAGE INTENTIONALLY LEFT BLANK

9. REFERENCES

1 C.J. Pellerin, Superplastic Forming, ed. S.P. Agrawal, ASM, Metals Park, OH, 1985, p 63.

2 J. Williamson, Superplastic Forming of Structural Alloys, eds. N. Paton and C. Hamilton, TMS-AIME, Warrendale, PA, 1982, p 291.

3 E. D. Weisert, Superplastic Forming, ed. S.P. Agrawal, ASM, Metals Park, OH, 1985, p 84.

4 J. Kennedy, Superplasticity and Superplastic Forming, eds. C.H. Hamilton and N.E. Paton, "The Metallurgical Society," Warrendale, PA, 1988, p 523.

5 K. Okazaki and D.J. Skinner, Scripta Met., Vol. 18, 1984, p 911.

6 D.J. Skinner and K. Okazaki, Scripta Met., Vol. 18, 1984, p 905.

7 C.M. Adam, J.W. Simon, and S. Langenbeck, Rapid Solidification Processing Principles and Technologies III, ed. R. Mehrabian, NBS, Washington DC, 1983, p 629.

8 A.K. Gogia, P.V. Roa, and J.A. Sekhar, J. Mats. Sci., Vol. 20, 1985, p 3091.

9 D.J. Skinner, R.L. Bye., D.Raybould, and A.M. Brown, Scripta Met., Vol.20, 1986, p 867

10 D.J. Skinner, R.L. Bye, D. Raybould, A.M. Brown, and M.S. Zedalis, Proc. of Struct. Metals by Rapid Solidification, eds. F.H. Froes and S.J. Savage, ASM, Metals Park, OH, 1987, p. 291.

11 D. Munson, J. Inst. Metals., Vol. 95, 1967, p 217.

12 D.J. Skinner, Dispersion Strengthened Aluminum Alloys, eds. Y.W. Kim and W.M. Griffith, TMS, 1988, p 181.

13 M. Cooper, Acta Cryst., Vol. 23, 1967, p 1106.

14 A.J. Barnes, Superplasticity in Aerospace, eds. H.C. Heikkenen and T.R. McNelley, TMS, 1988.

15 W.A. Backofen, I.R. Turner, and D.H. Avery, Trans. Am. Soc. Met., Vol. 57, 1964, p 980.

16 K.A. Padmanabhan and G.J. Davies, eds. . Superplasticity, MRE, SPRINGER-VERLAG, N.Y., 1980.

17 J.H. Hollomon, Trans. AIME, 162, 1945, p 268.

18 F.A. Nichols, Acta Metall. Vol. 28, 1980, p 663.

19 E.W. Hart, Acta Metakll., Vol. 15, 1967, p 351.

20 G.J. Davis, J.W. Edington, C.P. Cutler, and K.A. Padmanabhan, J. Mater. Sci., Vol. 5, 1970, p 1091.

21 R.C. Grifkins, Met. Trans. A, Vol. 7, 1976, p 1225

22 M.J. Mayo and W.D. Nix, submitted to Acta Met.

23 D.H. Avery and W.A. Backofen, Trans. Am. Soc. Met., Vol. 58, 1965, p 551.

24 D.L. Holt and W.A. Backofen, Trans. Am. Soc. Met., Vol. 59, 1966, p 755.

25 M.Y. Wu and O.D. Sherby, Scripta Metall., Vol. 18, 19874, pp 773-776.

26 M.Y. Wu, J. Wadsworth, and O.D. Sherby, Scripta Metall., Vol. 21, 1987, pp 1159-1164.

27 P.G. Partridge, Superplasticity, AGARD Lecture Series No. 154, 1987, p 5-1.

28 T.D. Byun and P. Yavari, Superplasticity in Aerospace Aluminum Proceedings, eds. R. Pearce, and L. Kelly, SIS, Cranfield, Bedford, England, 1985, p 285.
29 J. Kennedy and E. Ting, U.S. Patent # 4,732,312, 22 March 1988.
30 E. Heyn, "The Metallographist," Vol. 5, 1903, p 39.
31 G.M. Pharr, M.S. Zedalis, D.J. Skinner and P.S. Gilman, Dispersion Strengthened Aluminum Alloys, eds. Y.W. Kim and W.M. Griffith, TMS, 1988, p 309
32 R.E. Franck and J.A. Hawk, Scripta Met. Vol. 23, 1989, pp. 113-118
33 Rooney, Papazian, Balmoth, and Adler, to be published in 5 Int. Al-Li, 1989
34 D.J. Skinner, K. Okazaki, and M.A. Colin. Rapidly Solidified Powder Aluminum Alloys, ASTM 809, eds. M.E. Fine and E.A. Starke, ASTM, Philadelphia, 1986, pp. 211-236
35 J. Kennedy, unpublished work, Grumman.
36 M.J. Mayo and W.D. Nix, Superplastic Forming of Structural Alloys, eds. C.H. Hamilton and N.E. Paton, TMS/AIME, Warrendale, PA, 1988.
37 J. Weertman, J. Appl. Phys., Vol.28, 1957, p 362.
38 J.K. Gregory, J.C. Gibeling and W.D. Nix, Met Trans, Vol 16A, 1985, p 777.
39 H.J. Frost and M.F. Ashby, Deformation-Mechanism Maps, Pergamon Press, New York, 1982, p 128.

Table 1. Chemical Composition of Experimental Al-Fe-V-Si Alloys

Alloy	Vol. % (silicides)	Composition (weight %)				
			Fe	V	Si	Al
FVS0301	8	nominal	2.78	0.25	0.54	bal.
		actual	3.04	0.23	0.63	bal.
FVS0611	16	nominal	5.47	0.49	1.06	bal.
		actual	5.77	0.46	1.16	bal.
FVS0812	27	nominal	8.5	1.3	1.7bal.	
		actual	8.83	1.22	1.76	bal.
FVS1212	36	nominal	11.7	1.15	2.4bal.	
		actual	12.7	1.06	3.12	bal.

Table 2. Alloy Sheet Quantity Produced

Alloy	Compact	Roll Temp °C (°F)	Total Sheet m^2 ($in.^2$)
FVS0301	C395	300 (572)	.22 (340)
Ext@385°C	C394	400 (752)	.22 (340)
(725°F)	C396	500 (932)	.22 (340)
FVS0611	C379	300 (572)	.26 (400)
Ext@385°C	C377	400 (752)	.22 (340)
(725°F)	C378	500 (932)	.12 (180)
FVS0812	C381	300 (572)	.26 (400)
Ext@385°C	C383	400 (752)	.26 (400)
(725°F)	C384	500 (932)	.25 (380)
FVS1212	C400	300 (572)	.18 (280)
Ext@427°C	C399	400 (752)	.25 (380)
(800°F)	C398	500 (932)	.26 (400)

(Sheet thickness approximately = 2.0 mm, typical width= 10.2 cm)

Table 3. Alloy Average Grain Size

Alloy	Extrusion (μm)	Sheet (μm)
FVS0301 as-extruded	1.25	
FVS0301/300		1.23
FVS0301/400		1.19
FVS0301/500		1.08
FVS0611 as-extruded	0.87	
FVS0611/300		0.78
FVS0611/400		0.87
FVS0611/500		1.19
FVS0812 as-extruded	0.42	
FVS0812/300		0.33
FVS0812/400		0.41
FVS0812/500		0.44
FVS1212 as-extruded	0.29	
FVS1212/300		0.30
FVS1212/400		0.32
FVS1212/500		0.32

Table 4. Average Dispersoid Particle Size

Alloy		Dispersoid Size Extrusion (nm)	Sheet (nm)
FVS0301	as-extruded	30	
FVS0301/300			40
FVS0301/400			65
FVS0301/500			138
FVS0611	as-extruded	27	
FVS0611/300			58
FVS0611/400			40
FVS0611/500			96
FVS0812	as-extruded	25	
FVS0812/300			53
FVS0812/400			31
FVS0812/500			43
FVS1212	as-extruded	47	
FVS1212/300			33
FVS1212/400			83
FVS1212/500			76

Table 5. Average Longitudinal Tensile Strength of Extruded Alloys

Alloy	Temp. °C (°F)	0.2 Yield MPa (ksi)	UTS MPa (ksi)	Elong. %	Area Reduction %
FVS0301	R.T.	167 (24.2)	217 (217)	26.8	85
	149 (300)	143 (20.8)	165 (23.9)	23.9	80
	232 (450)	125 (18.1)	134 (19.4)	23.1	80
	316 (600)	106 (15.3)	107 (15.5)	24.4	77
FVS0611	R.T.	258 (37.4)	311 (45.1)	22.3	71
	149 (300)	222 (32.2)	248 (36.0)	13.5	52
	232 (450)	192 (27.9)	206 (29.8)	17.3	52
	316 (600)	160 (23.2)	163 (23.7)	16.8	50
FVS0812	R.T.	391 (56.7)	444 (64.4)	17.1	55
	149 (300)	337 (48.9)	369 (53.5)	8.9	37
	232 (450)	293 (42.5)	310 (45.0)	11.3	37
	316 (600)	231 (33.5)	238 (34.5)	11.8	39
FVS1212	R.T.	514 (74.5)	553 (80.2)	9.4	23
	149 (300)	437 (63.3)	457 (66.3)	5.8	21
	232 (450)	373 (54.1)	390 (56.6)	6.9	22
	316 (600)	272 (39.5)	290 (42.1)	8.5	15

Table 6. Average Longitudinal Tensile Strength of Rolled Sheet

Alloy	Strength		Elong. %
	0.2 Yield MPa (ksi)	UTS MPa (ksi)	
FVS0301/300	172 (25.0)	203 (29.5)	19.1
FVS0301/400	133 (19.3)	180 (26.1)	27.0
FVS0301/500	104 (15.1)	148 (21.5)	30.7
FVS0611/300	298 (41.9)	317 (45.9)	17.6
FVS0611/400	212 (30.7)	248 (36.0)	9.5
FVS0611/500	116 (16.8)	181 (26.2)	27.7
FVS0812/300	430 (62.4)	454 (65.8)	13.3
FVS0812/400	392 (56.8)	416 (60.3)	17.4
FVS0812/500	271 (39.3)	342 (49.6)	18.0
FVS1212/300	500 (72.5)	530 (76.9)	9.4
FVS1212/400	482 (69.9)	503 (73.0)	12.1
FVS1212/500	413 (59.9)	448 (65.0)	13.3

Table 7. Average Longitudinal Tensile Strength of Extruded Alloys After Thermal Exposure

Alloy	Exposure °C (°F)/hr	0.2 Yield MPa (ksi)	UTS MPa (ksi)	Elong. %	R.A. %
FVS0301	399 (750)/120	159 (23.1)	207 (30.0)	27.2	85
FVS0611	399 (750)/120	254 (36.9)	306 (44.4)	24.0	70
FVS0812	399 (750)/120	394 (57.1)	450 (65.3)	17.7	55
FVS1212	399 (750)/120	519 (75.2)	554 (80.4)	6.8	18
FVS0812	399 (750)/504	397 (57.5)	446 (64.6)	17.8	57
FVS0812	454 (850)/120	390 (56.5)	446 (64.6)	15.7	51
FVS0812	510 (950)/120	358 (51.9)	414 (60.0)	9.9	25

Table 8. Average Room Temperature Fracture Toughness Based Upon Extruded Alloys

Alloy	Orientation	Kq MPa√m (ksi√in)	Kc MPa√m (ksi√in)
FVS0611	L-T	23.5 (21.4)	100 (91.0)
	T-L	19.1 (17.4)	58.6 (53.3)
FVS0812	L-T	28.8 (26.2)	87.2 (79.3)
	T-L	14.1 (12.8)	15.5 (14.1)

Table 9. Effect of Dispersoid Coarsening on Deformation at 500°C (932°F)

Sample FVS0812/400 Strain rate=$1x10^{-4}$ s^{-1}, test temperature= 500°C(932°F)			
Hold Time at 600°C (1112°F)	Max. Eng. Stress MPa (ksi)	Max. True Stress MPa (ksi)	Elongation %
No hold	64 (9.28)	71 (10.3)	26
Hold 15 min.	56 (8.12)	61 (8.84)	26

Table 10. Internal Stress Superplasticity Test

FVS1212/500 at a constant stress of 8.62 MPa (1250 psi)				
Test ID	T_{max} °C (°F)	T_{min} °C (°F)	Duration min.	Results
N68	520 (968)	200 (392)	1860	Test stopped- no elongation measured
N70	580 (1076)	200 (392)	1200	Test stopped- no elongation measured
N69	620 (1148)	200 (392)	55	Sample failed at 65% elongation

Table 11. Grain Size After High Temperature Deformation

Alloy Condition	Defor. Temp. °C (°F)	Strain Rate s^{-1}	Approx. Elong. %	Grain Size Sheet µm	*Grip µm	*Break µm
FVS0611/500	600 (1112)	0.01	200	1.19	1.30	0.73
FVS0301/500	500 (932)	0.1	40	1.08	1.05	0.86
FVS0611/500	500 (932)	0.1	45	1.19	1.50	0.75
FVS0812/500	500 (932)	0.1	38	0.44	0.40	0.39
FVS0812/300	600 (1112)	2.2	87	0.33	0.23	0.25
FVS1212/300	600 (1112)	2.2	150	0.30	0.26	0.32
FVS1212/500	600 (1112)	2.2	140	0.32	0.26	0.26

* final size in gage section near grip or break

Table 12. Dispersoid Size After High Temperature Deformation

Alloy Condition	Defor. Temp. °C (°F)	Strain Rate s^{-1}	Approx. Elong. %	Dispersoid Size Sheet nm	*Grip nm	*Break nm
FVS0611/500	600 (1112)	0.01	200	96	110	210
FVS0301/500	500 (932)	0.1	40	138	110	160
FVS0611/500	500 (932)	0.1	45	96	155	200
FVS0812/500	500 (932)	0.1	38	43	40	75
FVS0812/300	600 (1112)	2.2	87	53	47	60
FVS1212/300	600 (1112)	2.2	150	33	100	100
FVS1212/500	600 (1112)	2.2	140	76	90	160

* final size in gage section near grip or break

Table 13. Pressure Sequence for Equibiaxial Forming of FVS0611/500 Alloy

Dome radius=1.14 cm (0.45 in.) Sheet thickness= 2 mm (.080 in.), at 600°C (1112°F)	
Time, s	Pressure, MPa (psi)
0	0 (0)
12	.28 (40)
60	.69 (100)
1200	.69 (100)

Table 14. Effect of Thermal Exposure on Shear Strength of Alloys

Vol % Dispersoid	Rolling Temp, °C (°F)	Shear Strength, MPa (ksi)		
		As-Rolled	516°C (960°F)/4 h	516°C (960°F)/4 h + T6 (1)
8	300 (572)	142±7(20.6±1)	132.4±(19.2±2)	-
8	400 (752)	-	120±7(17.4±1)	-
8	500 (932)	-	118.6±3(17.2±0.5)	-
16	300 (572)	181.3±7(26.3±1)	175.8±3(25.5±0.5)	184±7(26.7±1)
16	400 (752)	-	151±3(21.9±0.5)	-
16	500 (932)	-	111±3(16.1±0.5)	-
27	300 (572)	193.1±3(28±0.5)	186.9±7(27.1±1)	180.6±3(26.2±0.5)
36	300 (572)	213±7(30.9±1)	162.7±21(23.6±3)	160±7(23.2±1)

(1) 482°C (900°F)/1 h, WQ + 121°C (250°F)/24 h

Table 15. Effect of Temperature and Pressure on Shear Strength of Diffusion Bonds

°C/MPa/h (°F/psia/h)	Vol % Dispersoid	Alloy (1)	Compact No.	Bonding Results (2)	DB Shear Strength, MPa (ksi)
	8	301	396	DNB	-
516/0.7/4	16	611	378	DNB	-
(960/100/4)	27	812	384	DNB	-
	36	1212	398	DNB	-
516/0.7/16 (960/100/16)	8	301	396	DNB	-
550/0.7/4 (1022/100/4)	8	301	396	DNB	-
550/0.7/16 (1022/100/16)	8	301	396	DNB	-
	8	301	396	DB/BDM	-
600/0.7/4	16	611	378	DB/BDM	-
(1112/100/4)	27	812	384	DNB	-
	36	1212	398	DNB	-
	8	301	395(3)	DB/BDM	-
625/0.7/2	16	611	379(3)	DB/BDM	-
(1157/100/2)	27	812	381(3)	DNB	-
	36	1212	400(3)	DNB	-
	8	301	396	DB (two BDM)	66.2±14(9.6±2)
	8	301	395(3)	DB (two BDM)	55.2(8) (4)
625/0.7/4	16	611	378	DB	75.8±1(11 ± 0.2)
(1157/100/4)	16	611	379(3)	DB/BDM	-
	27	812	384	DNB	-
	27	812	381(3)	DB/BDM	-
	36	1212	398	DNB	-
	36	1212	400(3)	DNB	-
	8	301	396	DNB	-
516/2.8/4	16	611	378	DB/BDM	-
(960/400/4)	27	812	384	DNB	-
	36	1212	398	DNB	-
	8	301	396	DB/BDM	-
600/2.8/4	16	611	378	DB/BDM	-
(1112/400/4)	27	812	384	DNB	-
	36	1212	398	DB/BDM	-

Table 15. (continued)

°C/MPa/h (°F/psia/h)	Vol % Dispersoid	Alloy (1)	Compact No.	Bonding Results (2)	DB Shear Strength, MPa (ksi)
625/2.8/1 (1157/400/1)	16	611	378	DB (8 BDM)	81.4(11.8) (4)
625/2.8/2 (1157/400/2)	16	611	378	DB (7 BDM)	83.4±7(12.7±1)
	8	301	396	DB	78.6±3(11.4 ± 0.5)
	8	301	395(3)	DB	73.8±7(10.7±1)
625/2.8/4	16	611	378	DB	77.9±7(11.3 ± 1.0)
(1157/400/4)	16	611	379(3)	DB (4 BDM)	89.6±3(13±0.5)
	27	812	384	DB/BDM	-
	27	812	381(3)	DB/BDM	-
	36	1212	398	DB/BDM	-
	36	1212	400(3)	DB/BDM	-
	8	301	396	DB/BDM	-
516/7/4	16	611	378	DB/BDM	-
(960/1000/4)	27	812	384	DB/BDM	-
	36	1212	398	DNB	-
	8	301	396	DB/BDM	-
550/7/4	16	611	378	DNB	-
(1022/1000/4)	27	812	384	DNB	-
	36	1212	398	DNB	-
	8	301	396	DB	82.7±7(12±1)
600/7/1.3	16	611	378	DB	89.6±7(13±1)
(1112/1000/1.3)	27	812	384	DB/BDM	-
	36	1212	398	DNB	-
	8	301	396	DB	104.8±10(15.2±1.5)
600/7/4	16	611	378	DB/BDM	-
(1112/1000/4)	27	812	384	DB	80.7±4(11.7±0.6)
	36	1212	398	DB	100.7±19(14.6±2.7)

Notes: (1) Rolling Temp.=500°C (932°F), except as noted
(2) DB=bonded, DNB=did not bond, BDM=broke during machining or handling
(3) Rolling Temp = 300°C (572°F)
(4) one test only

Table 16. Shear Strength of Dissimilar Diffusion Bonds

Dissimilar DB Couple (1)	As-DB, 516°C/0.7 MPa(960°F/100 psia) time indicated				As-DB + T6(2)	
	1 h	2 h	4 h	22 h	2 h	4 h
	σs,MPa(ksi)	σs,MPa(ksi)	σs,MPa(ksi)	σs,MPa(ksi)	σs,MPa(ksi)	σs,MPa(ksi)
Alloy 301/7475	50.3±35(7.3±5)	65.5±35(9.5±5)	79.3±35(11.5±5)	130.3±3(18.9±0.5)	-	122±21(17.7±3)
Alloy 611/7475	78.6±35(11.4±5)	81.4±41(11.8±6)	102±28(14.8±4)	118±14(17.1±2)	-	130.3±41(18.9±6)
Alloy 812/7475	145.5±14(21.1±2)	143.7±7(20.7±1)	135±7(19.6±1)	113.8±3(16.5±0.5)	174.4±7(25.3±1)	166.2±14(24.1±2)
Alloy 1212/7475	124±14(18±2)	129.6±14(18.8±2)	139.3±7(20.2±1)	126.2±14(18.3±2)	148.2±14(21.5±2)	142±21(20.6±3)

(1) Rolling Temperature of HTA Alloys = 300°C(572°F)
(2) 482°C(900°F)/1 h (WQ) + 121 °C(250°F)/24 h

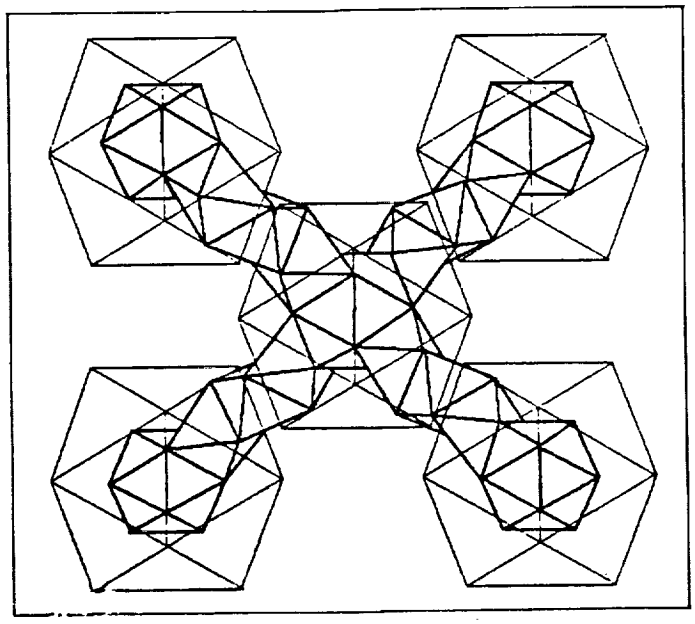

Fig. 1 Structure of Silicide Dispersoid

Fig. 2 TEM Micrograph of FVS0301 Alloy Extrusion

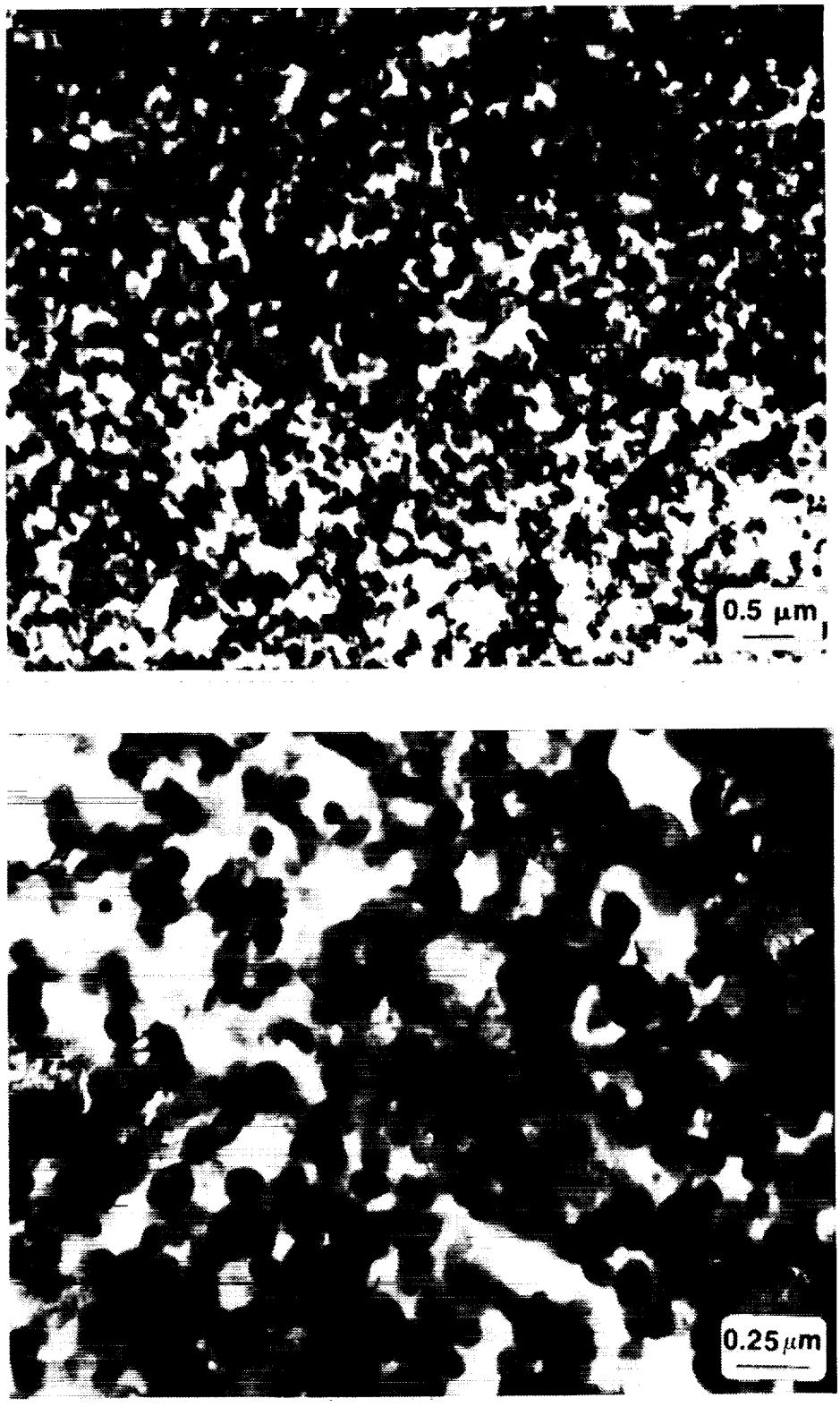

Fig. 3 TEM Micrograph of FVS1212 Alloy Extrusion

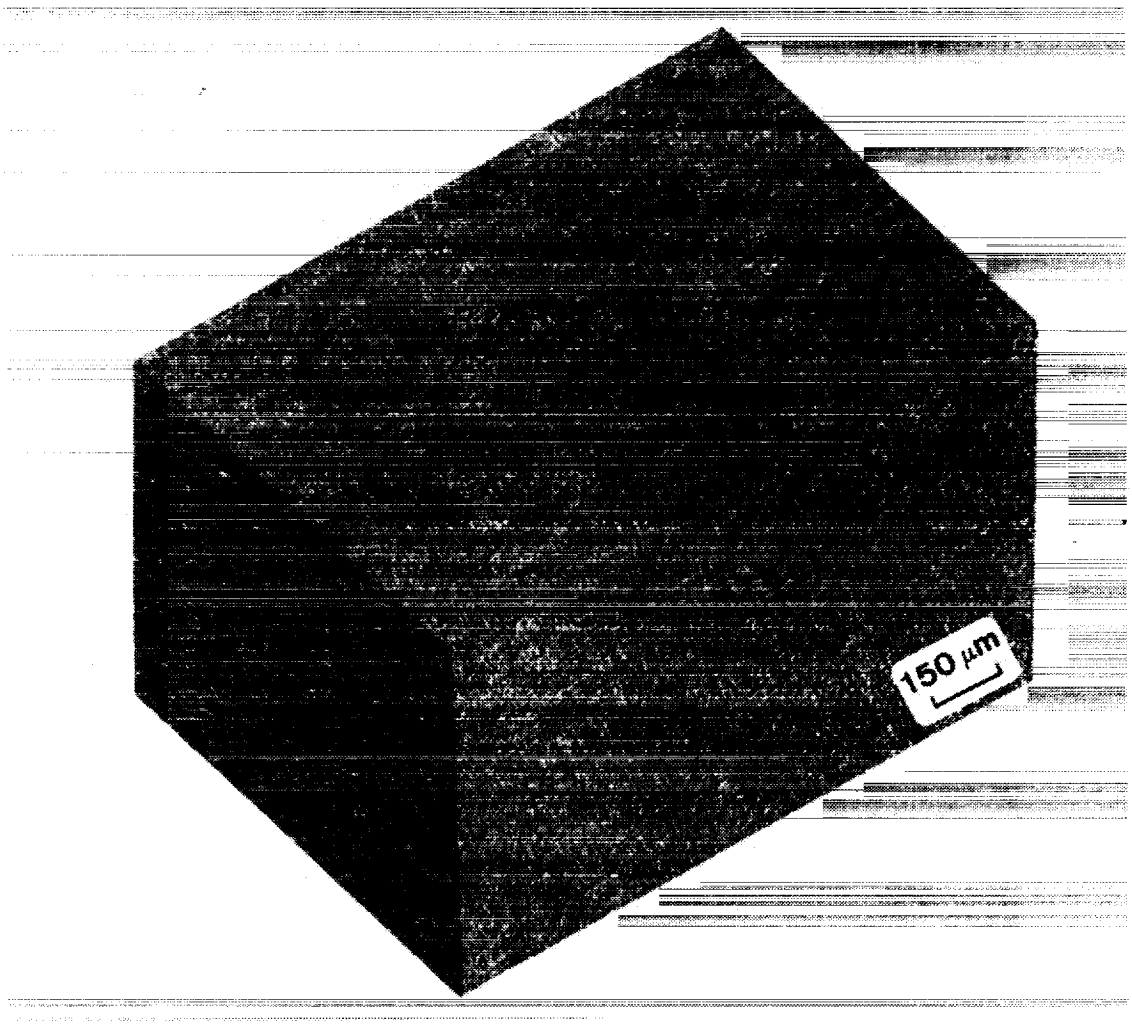

Fig. 4 Optical Micrographs of FVS0301/300 Sheet

ORIGINAL PAGE
BLACK AND WHITE PHOTOGRAPH

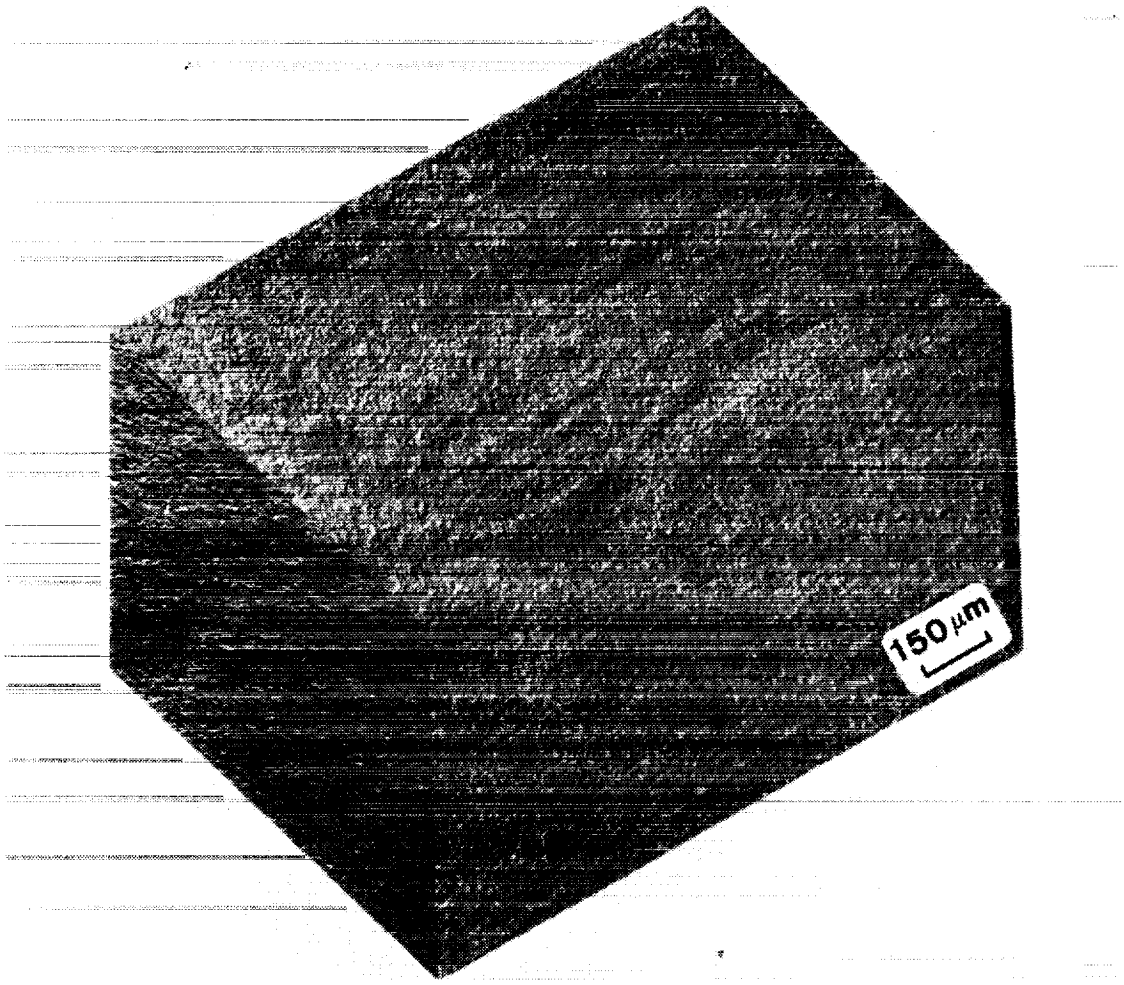

Fig. 5 Optical Micrographs of FVS0301/400 Sheet

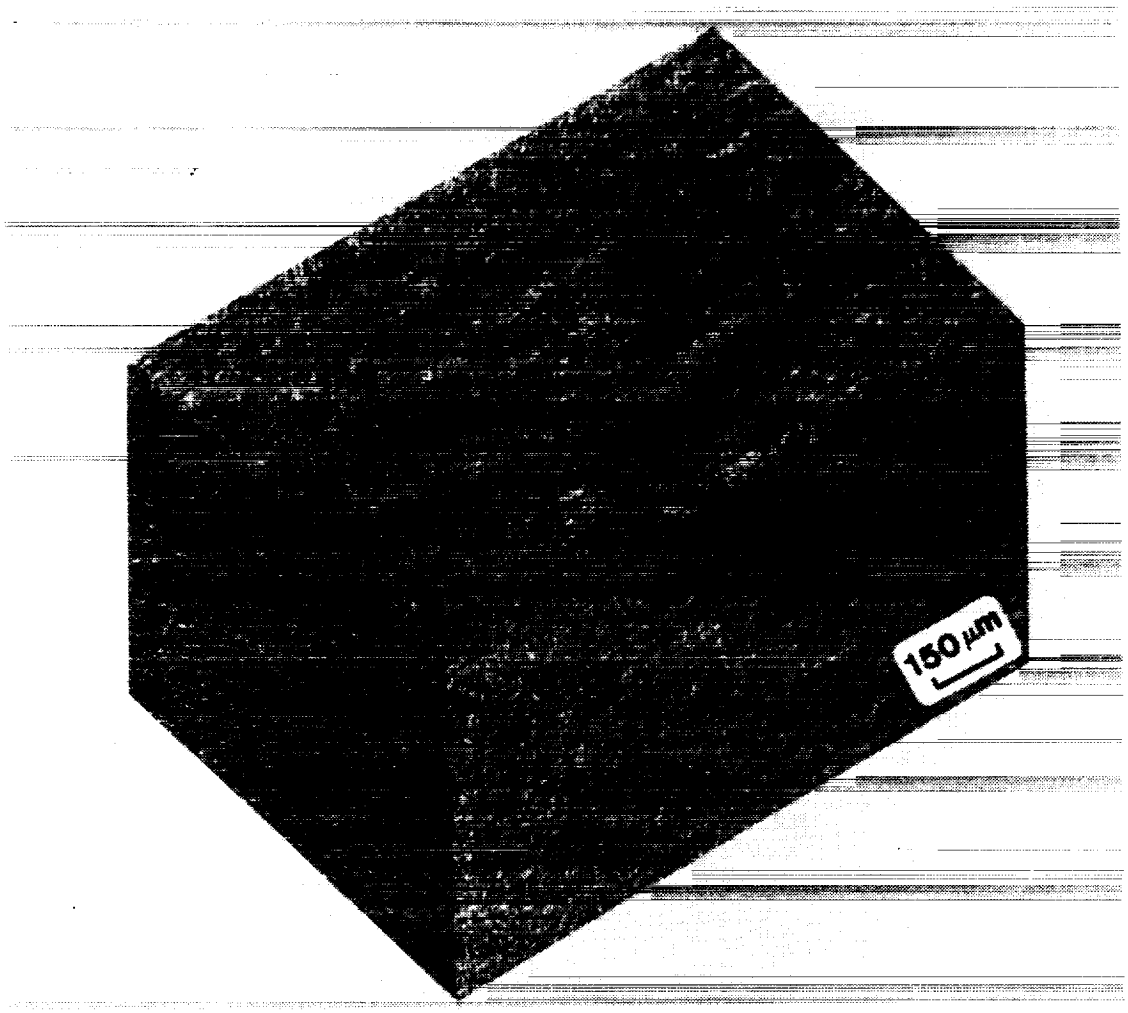

Fig. 6 Optical Micrographs of FVS0301/500 Sheet

ORIGINAL PAGE
BLACK AND WHITE PHOTOGRAPH

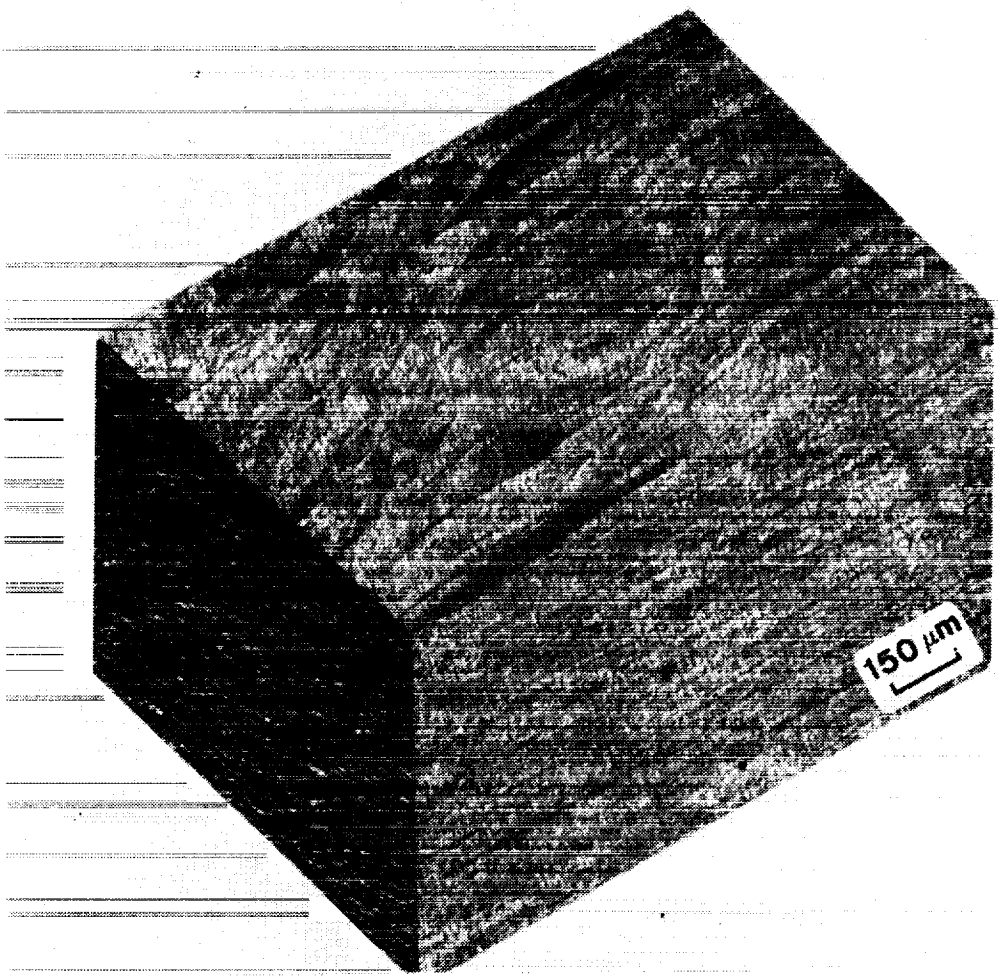

Fig. 7 Optical Micrographs of FVS0611/300 Sheet

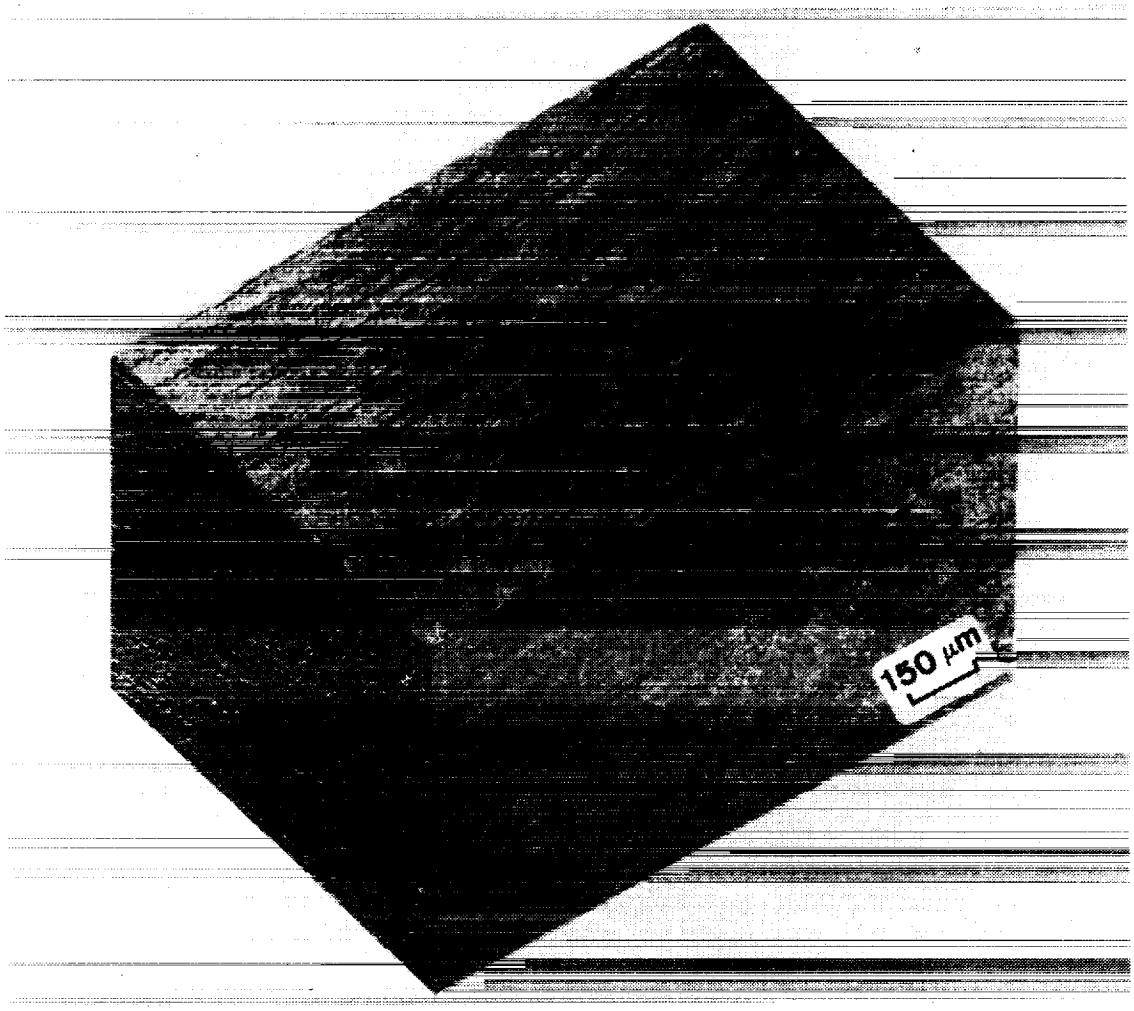

Fig. 8 Optical Micrographs of FVS0611/400 Sheet

ORIGINAL PAGE
BLACK AND WHITE PHOTOGRAPH

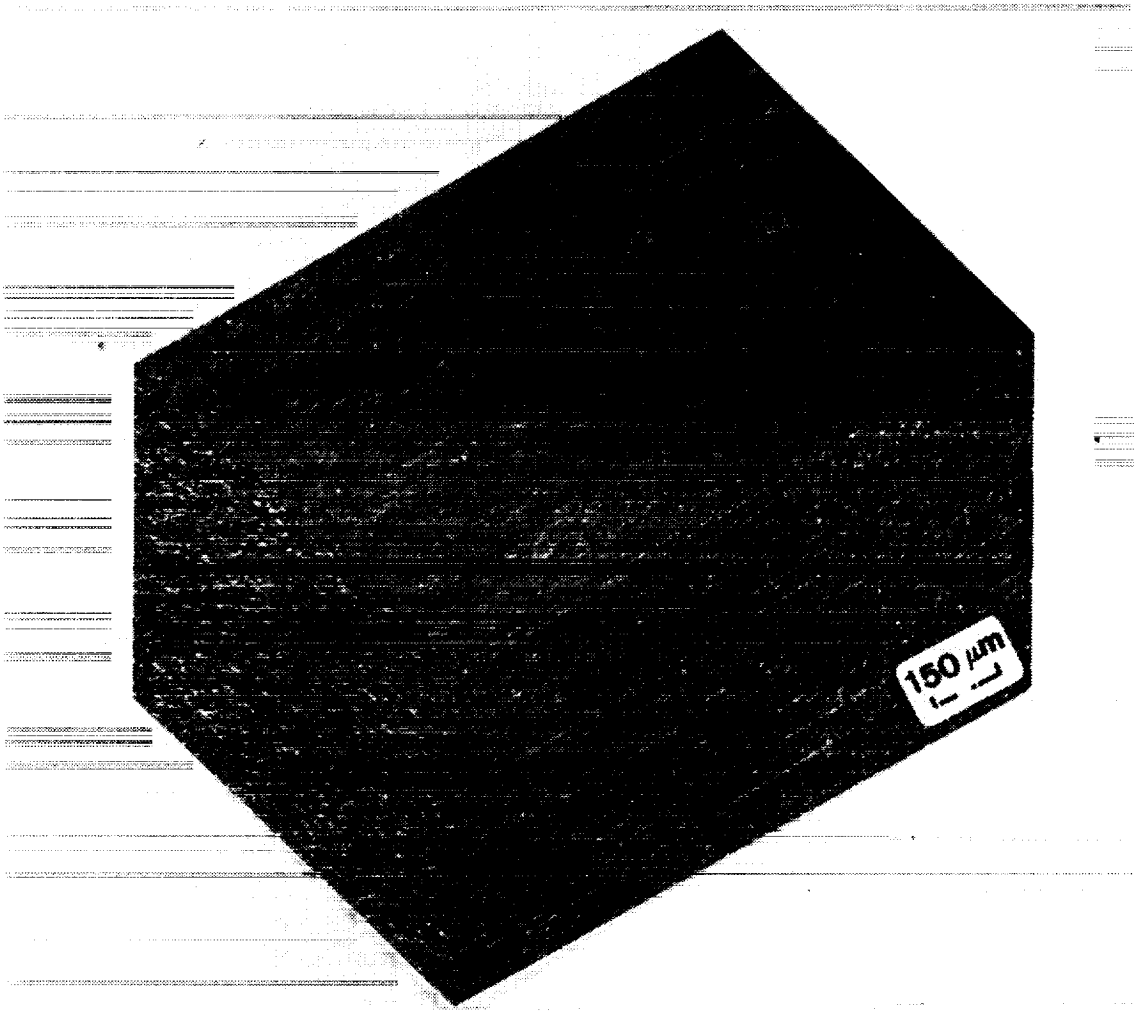

Fig. 9 Optical Micrographs of FVS0611/500 Sheet

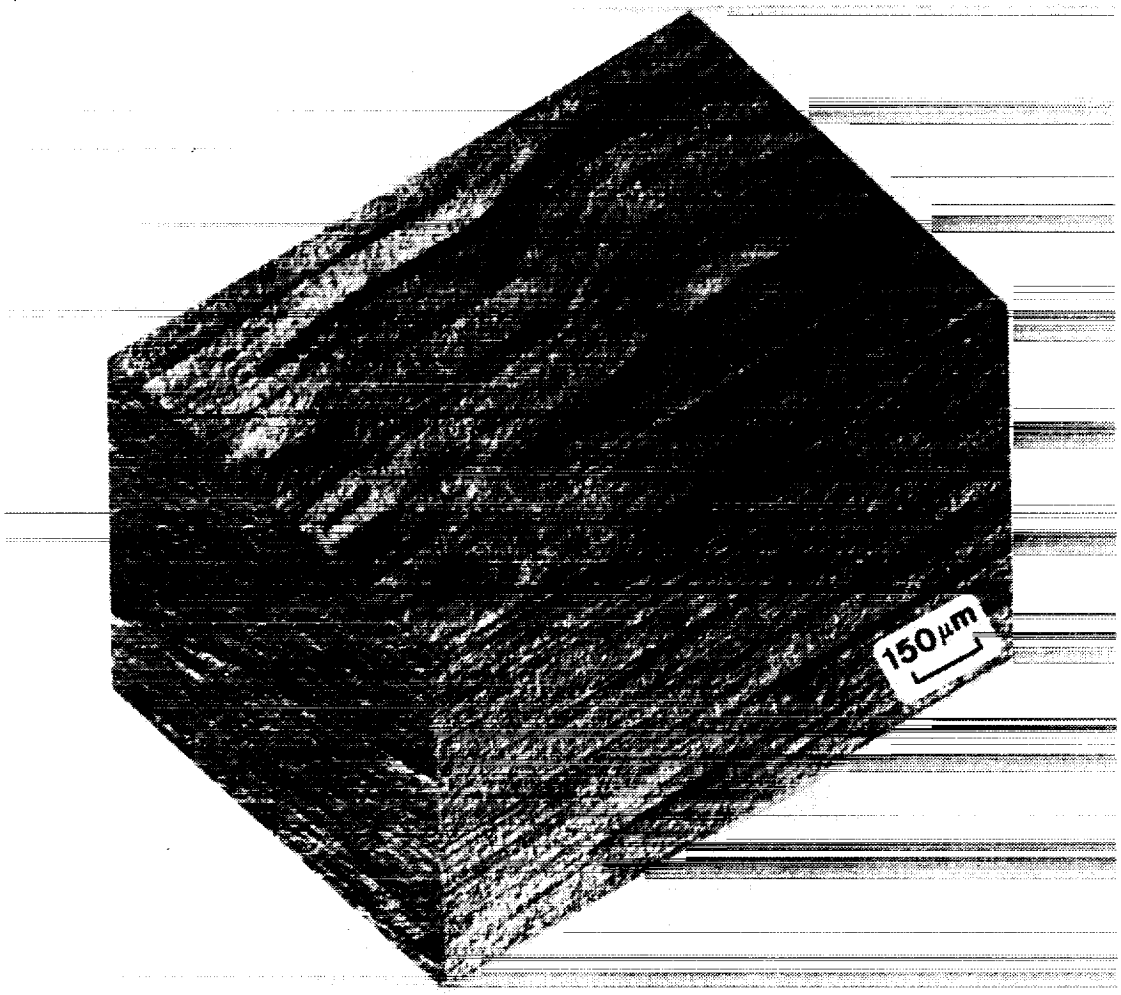

Fig. 10 Optical Micrographs of FVS0812/300 Sheet

ORIGINAL PAGE
BLACK AND WHITE PHOTOGRAPH

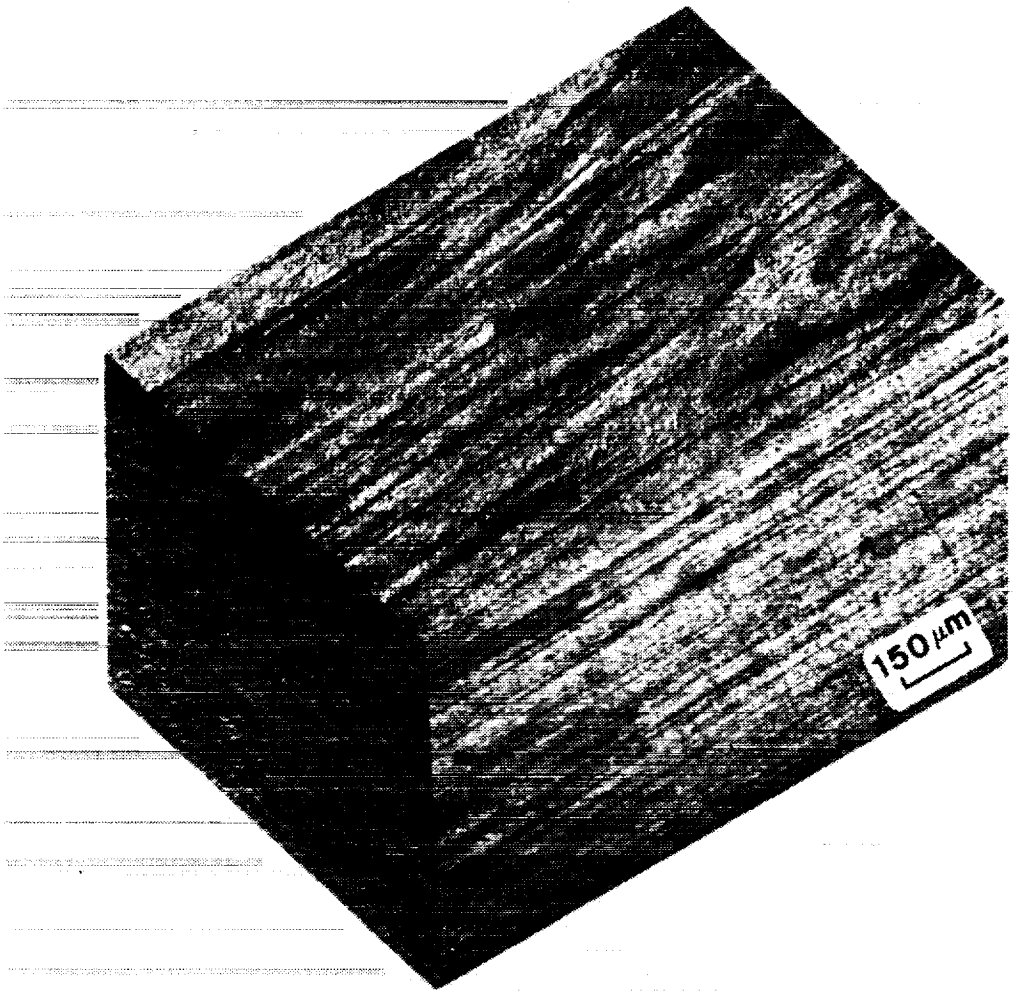

Fig. 11 Optical Micrographs of FVS0812/400 Sheet

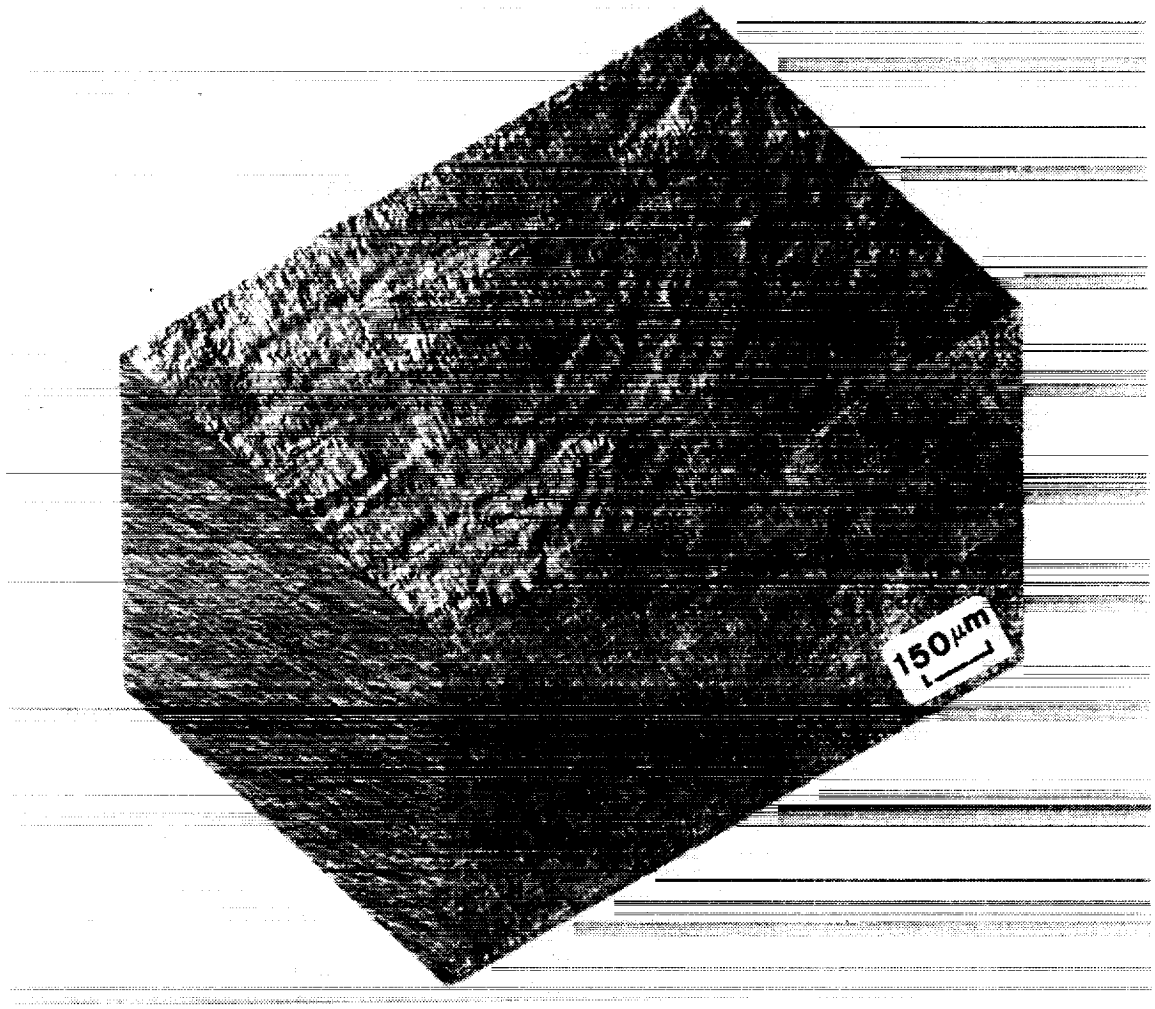

Fig. 12 Optical Micrographs of FVS0812/500 Sheet

ORIGINAL PAGE
BLACK AND WHITE PHOTOGRAPH

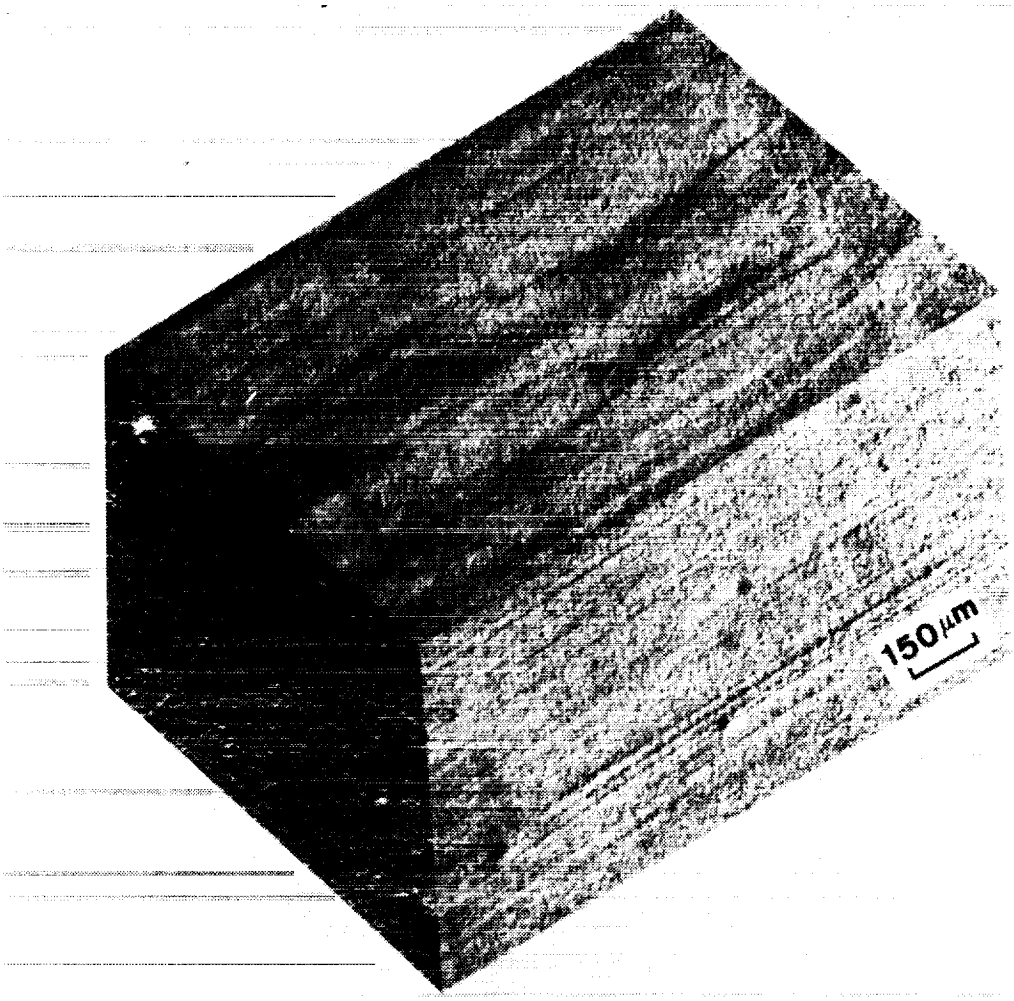

Fig. 13 Optical Micrographs of FVS1212/300 Sheet

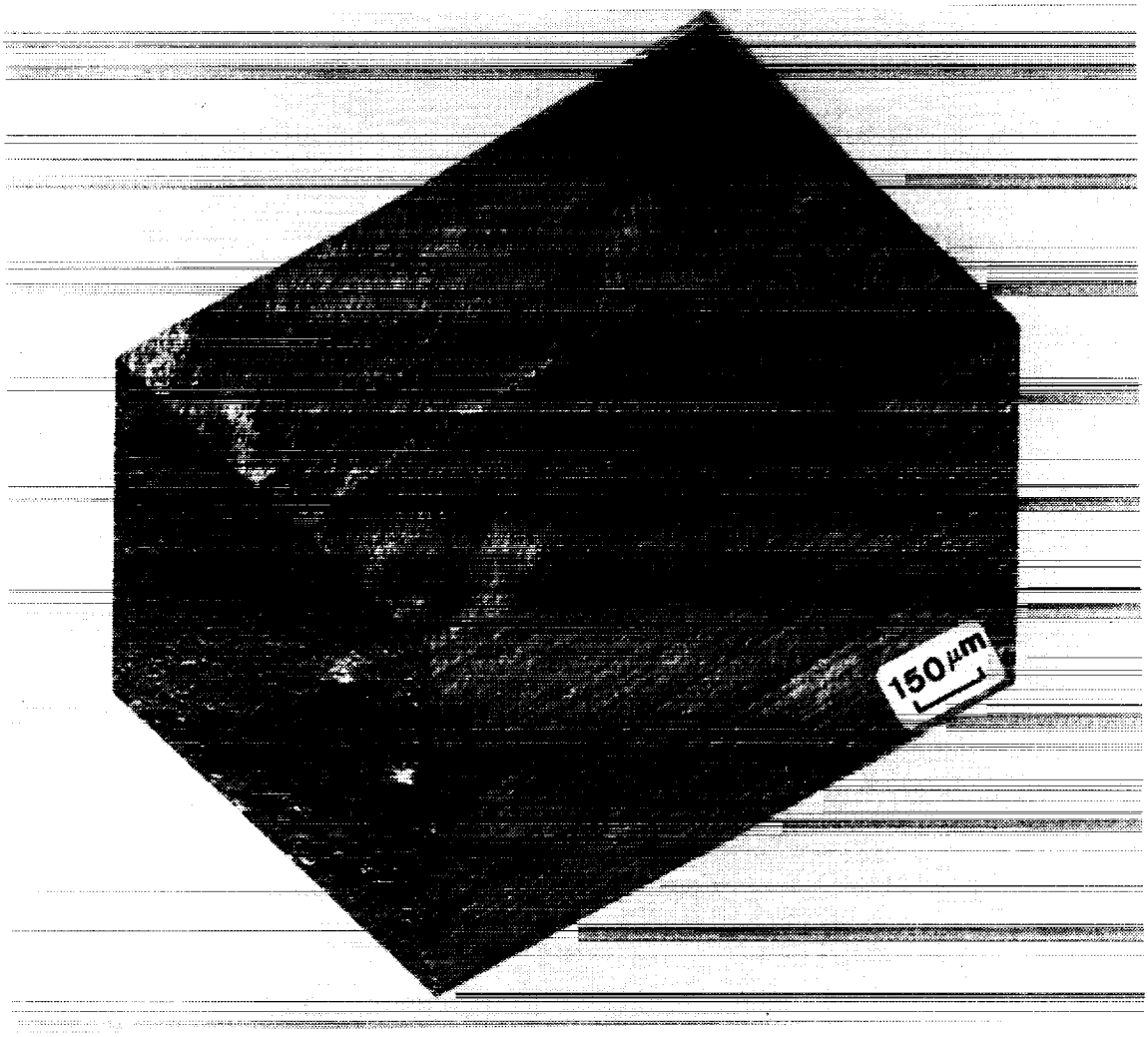

Fig. 14 Optical Micrographs of FVS1212/400 Sheet

ORIGINAL PAGE
BLACK AND WHITE PHOTOGRAPH

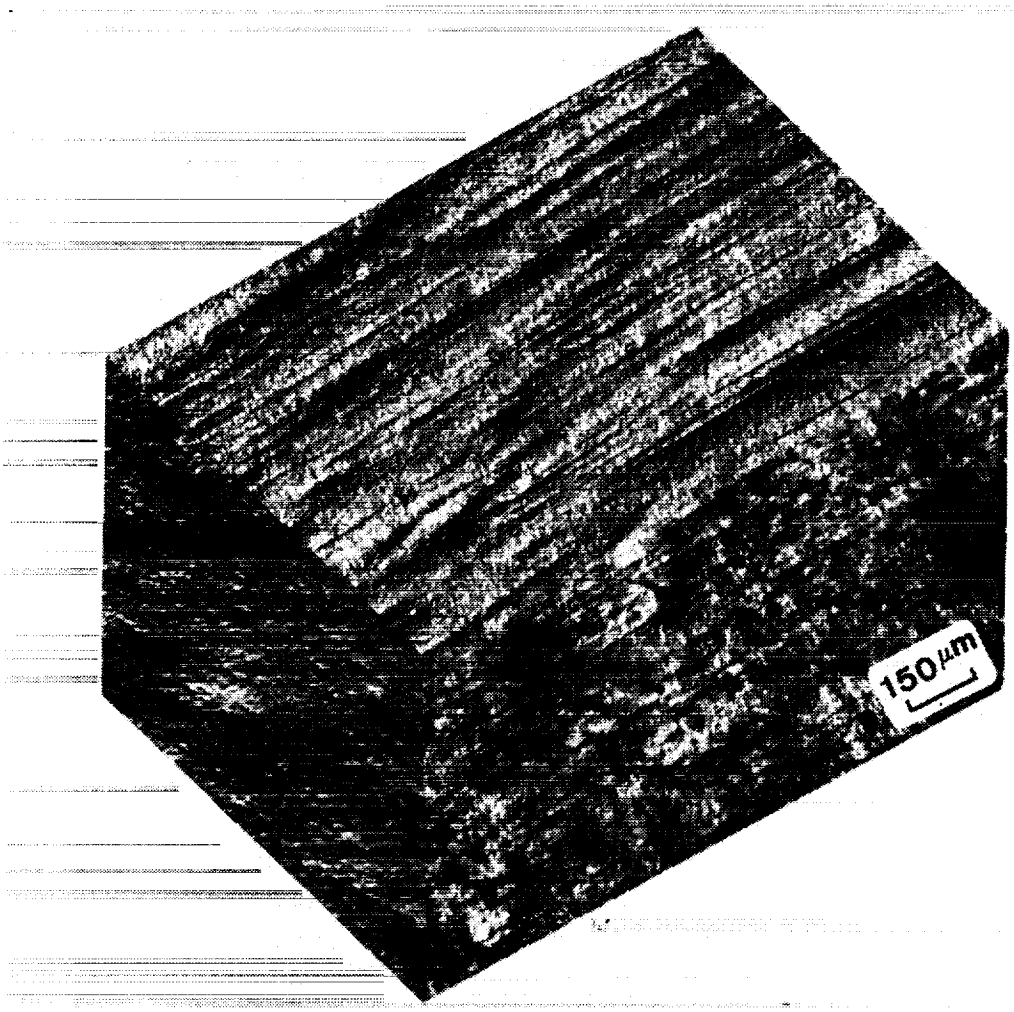

Fig. 15 Optical Micrographs of FVS1212/500 Sheet

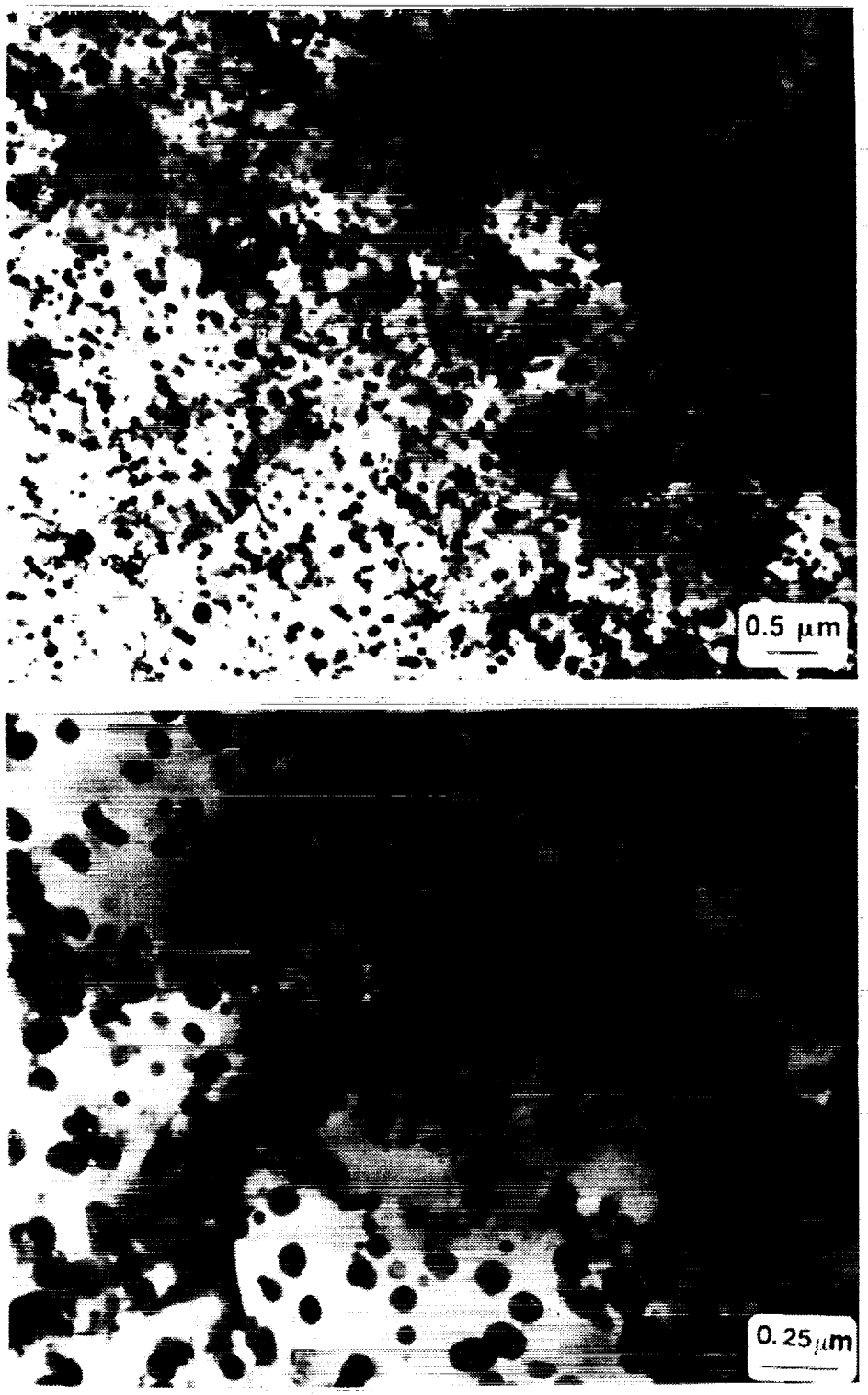

Fig. 16 TEM Micrographs of FVS0301/300 Sheet

ORIGINAL PAGE
BLACK AND WHITE PHOTOGRAPH

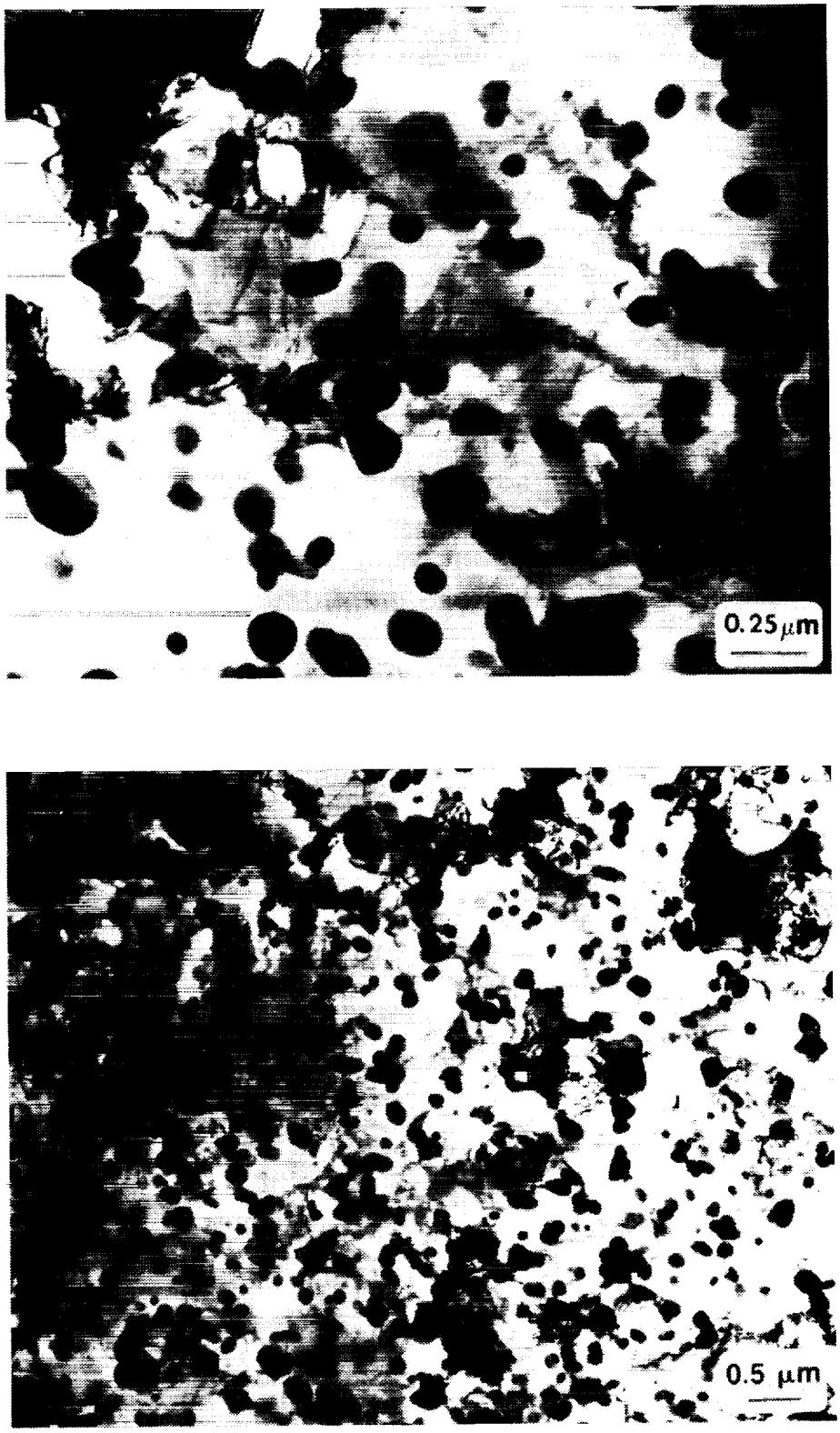

Fig. 17 TEM Micrographs of FVS0301/400 Sheet

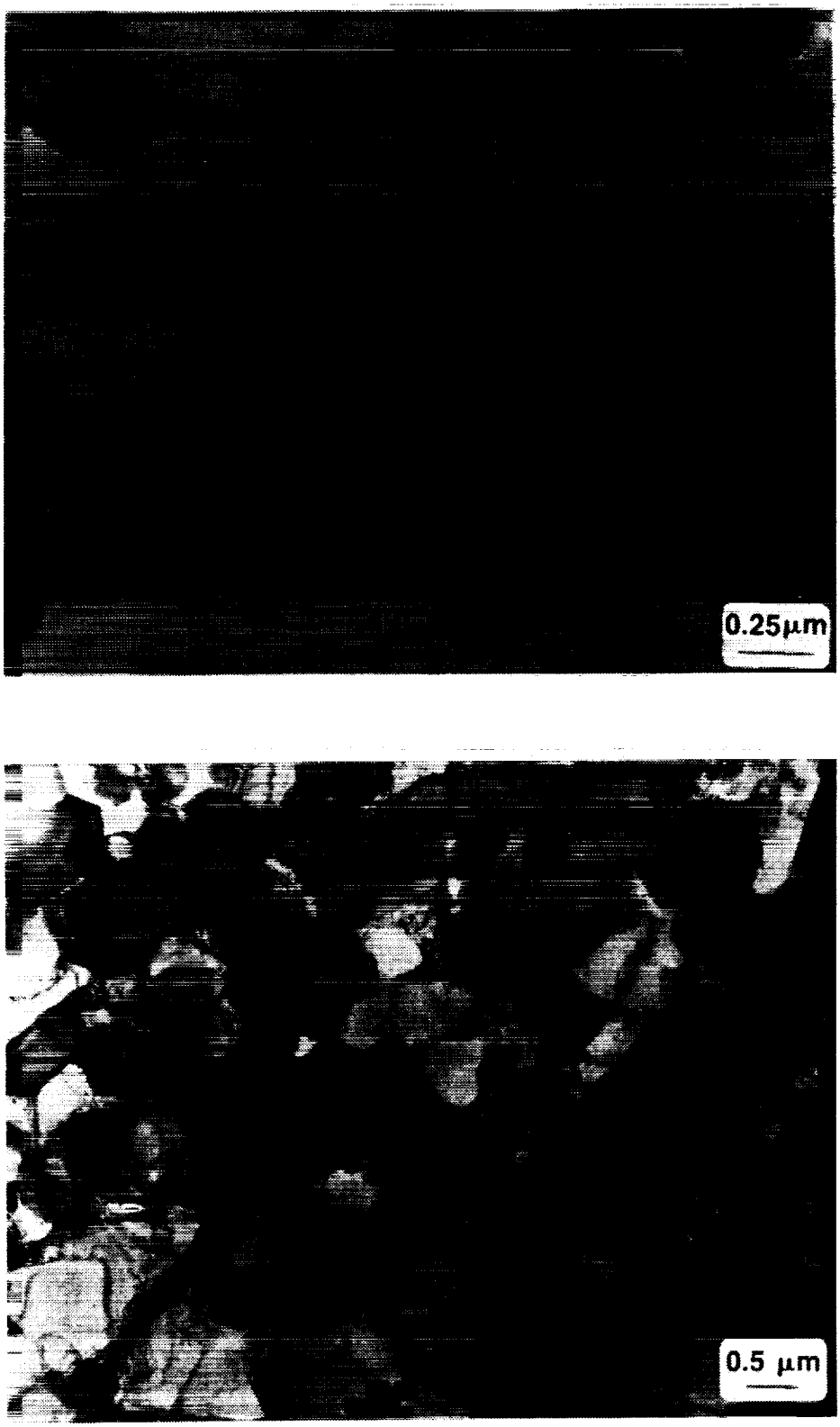

Fig. 18 TEM Micrographs of FVS0301/500 Sheet

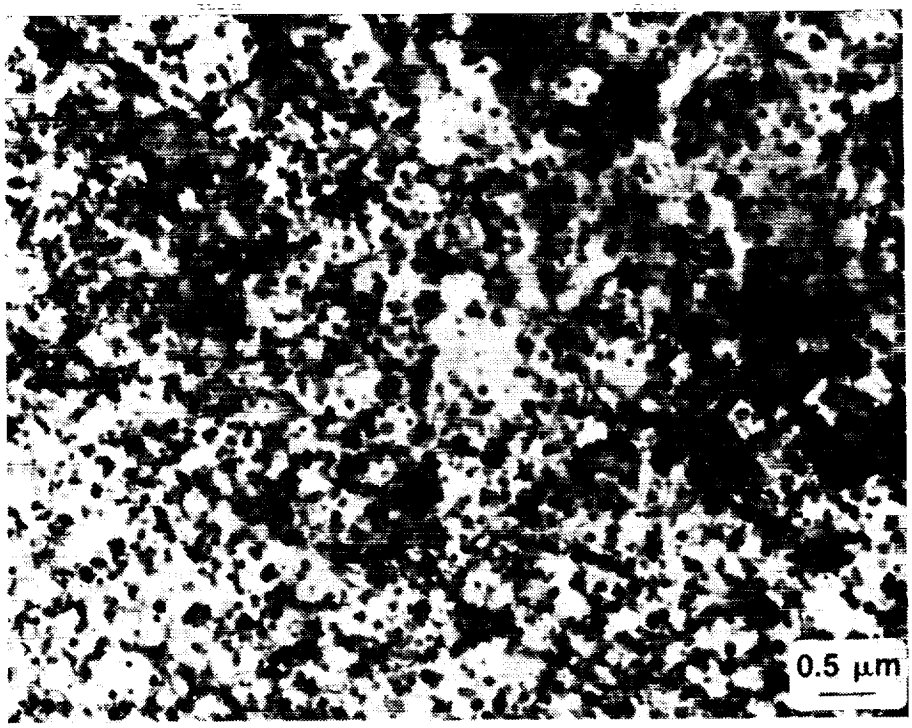

Fig. 19 TEM Micrographs of FVS0611/300 Sheet

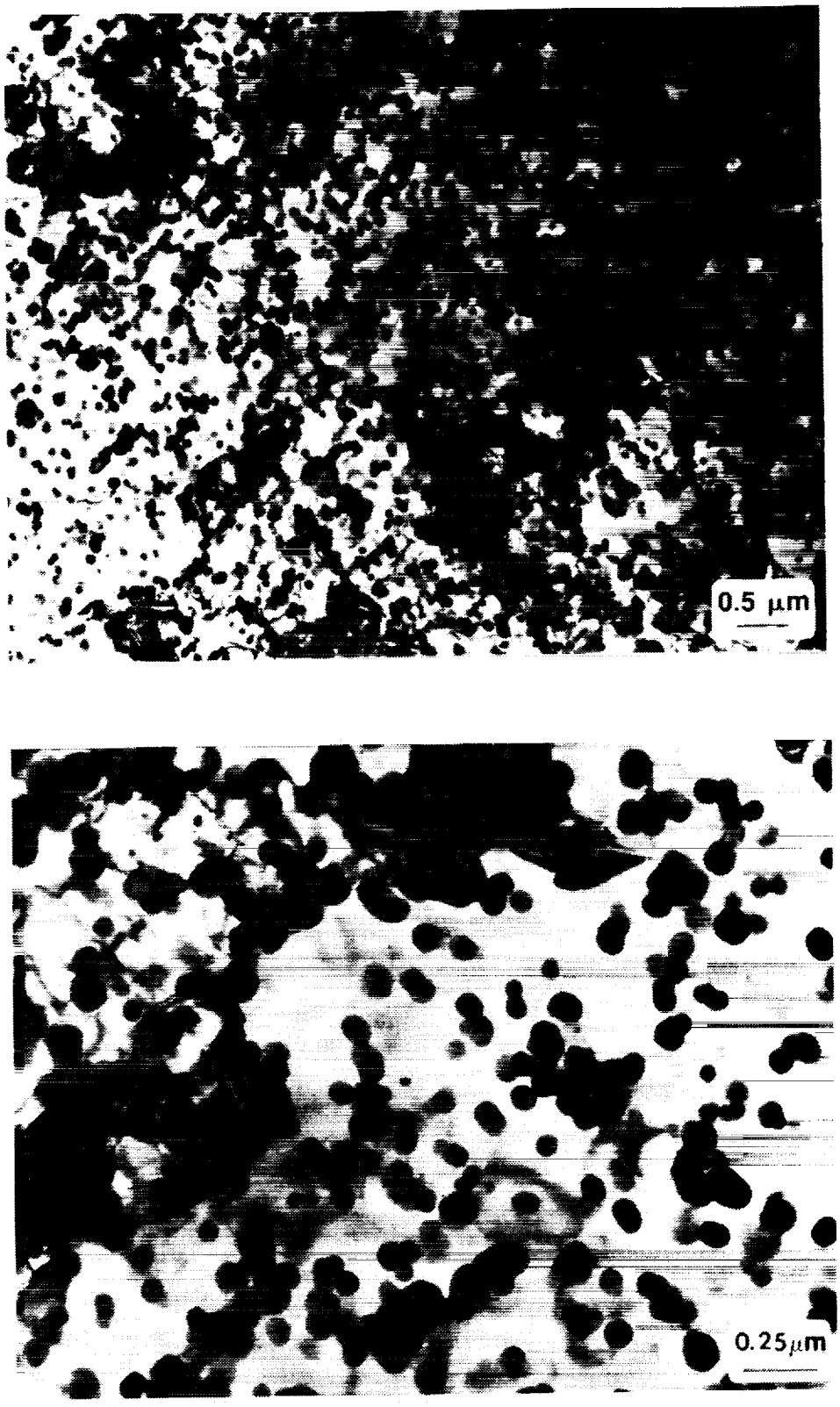

Fig. 20 TEM Micrographs of FVS0611/400 Sheet

Fig. 21 TEM Micrographs of FVS0611/500 Sheet

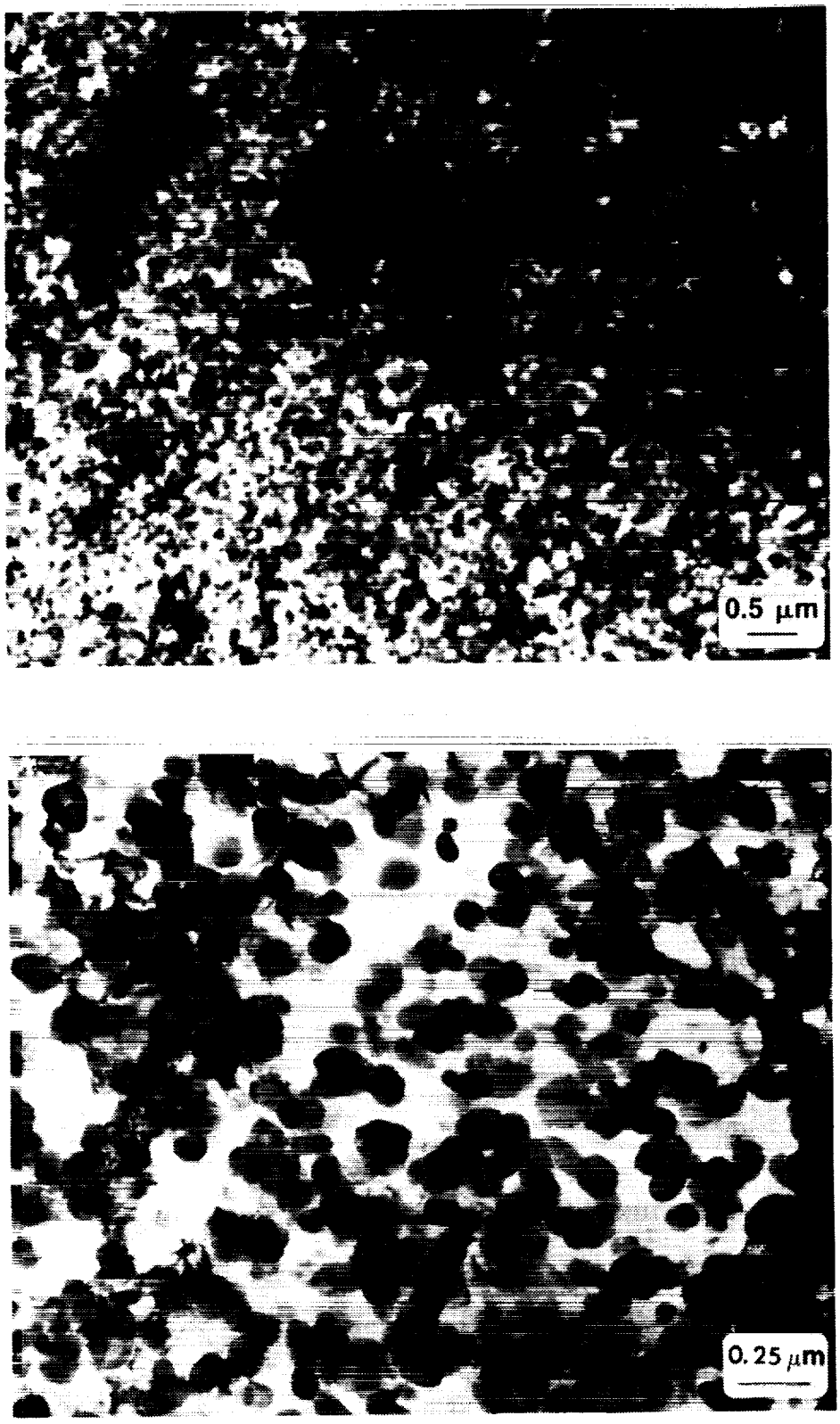

Fig. 22 TEM Micrographs of FVS0812/300 Sheet

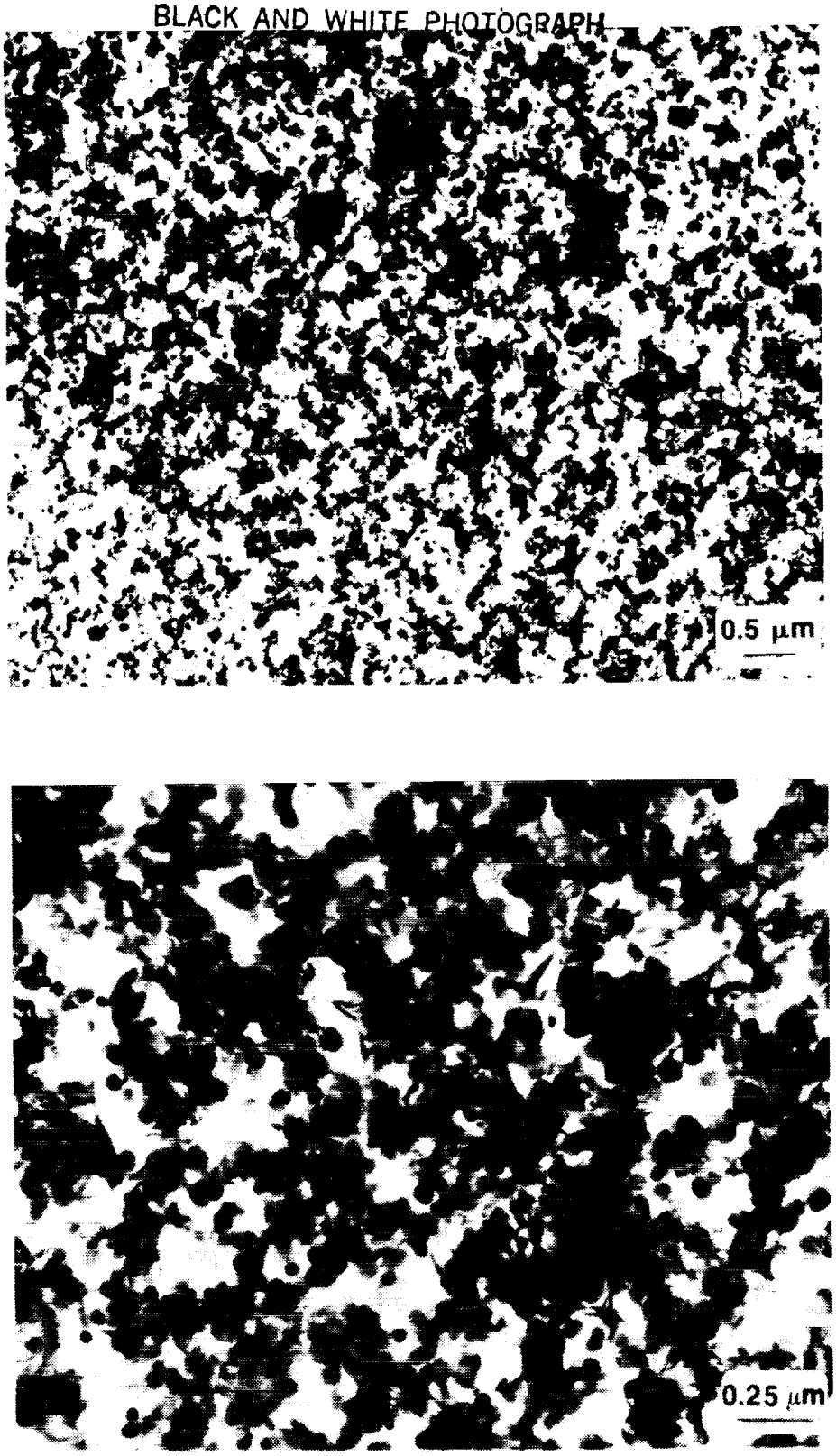

Fig. 23 TEM Micrographs of FVS0812/400 Sheet

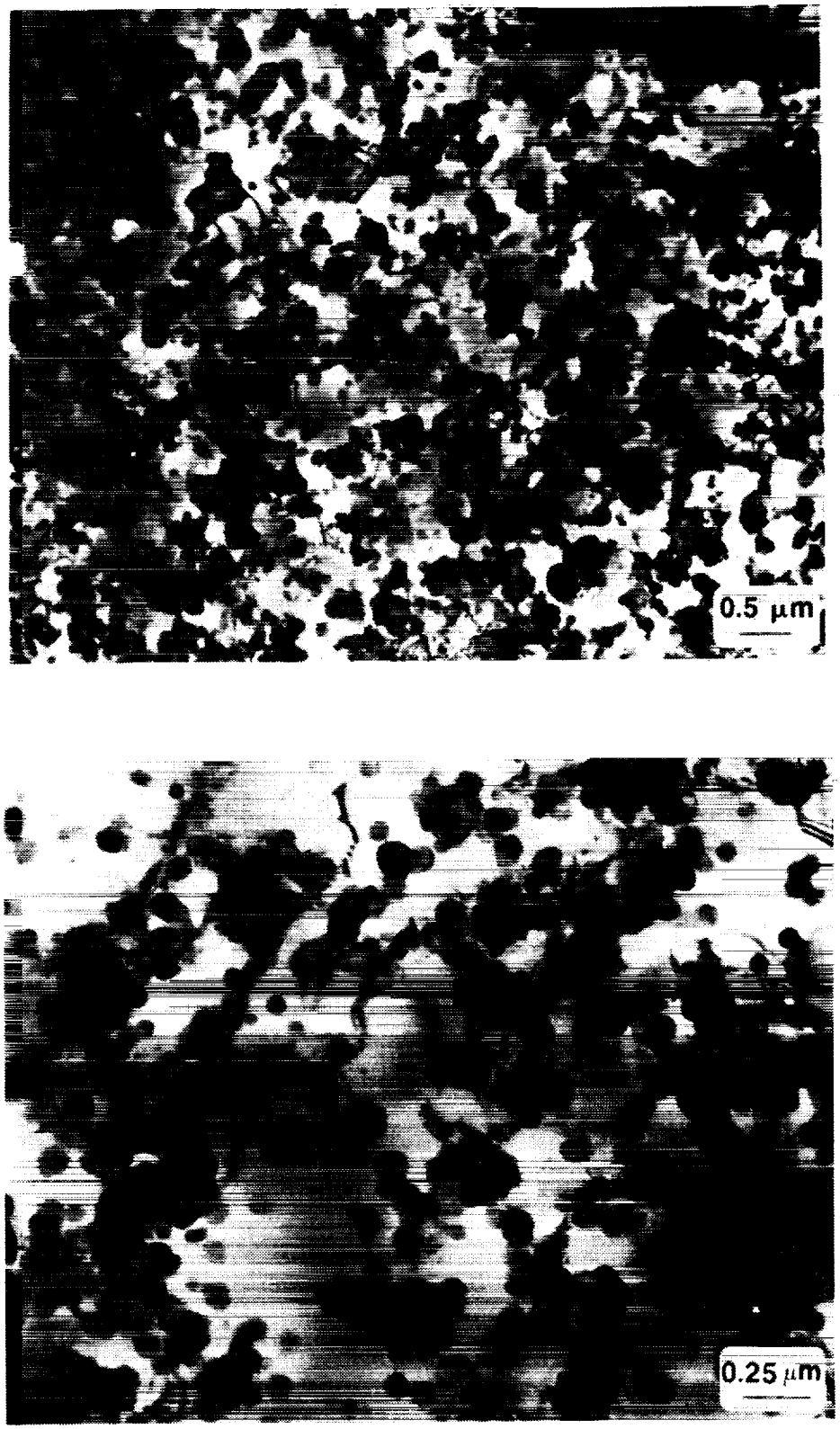

Fig. 24 TEM Micrographs of FVS0812/500 Sheet

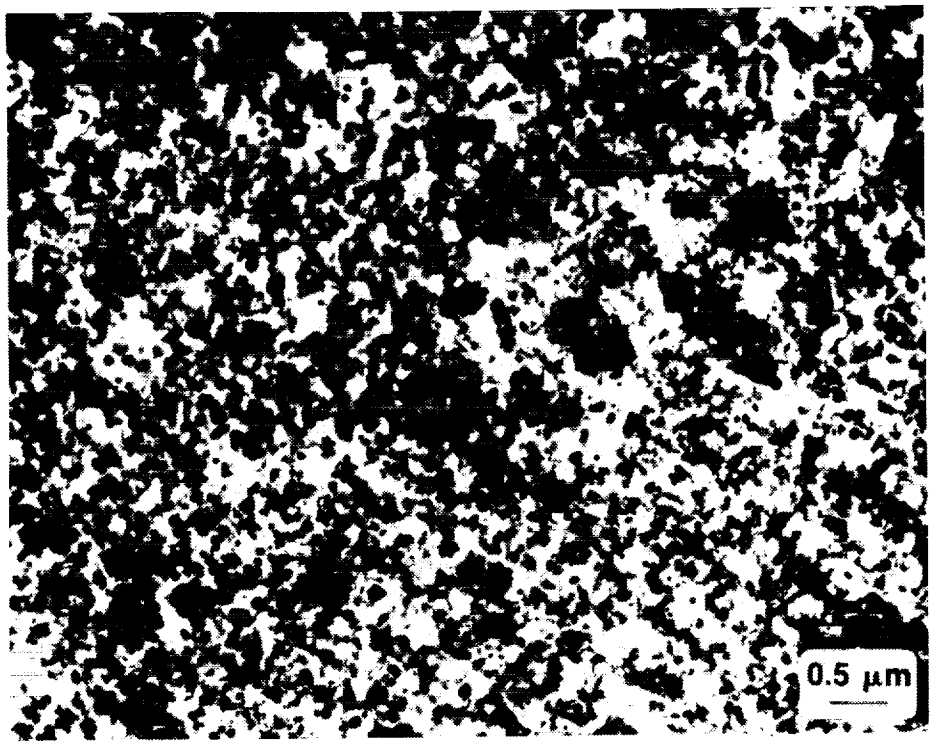

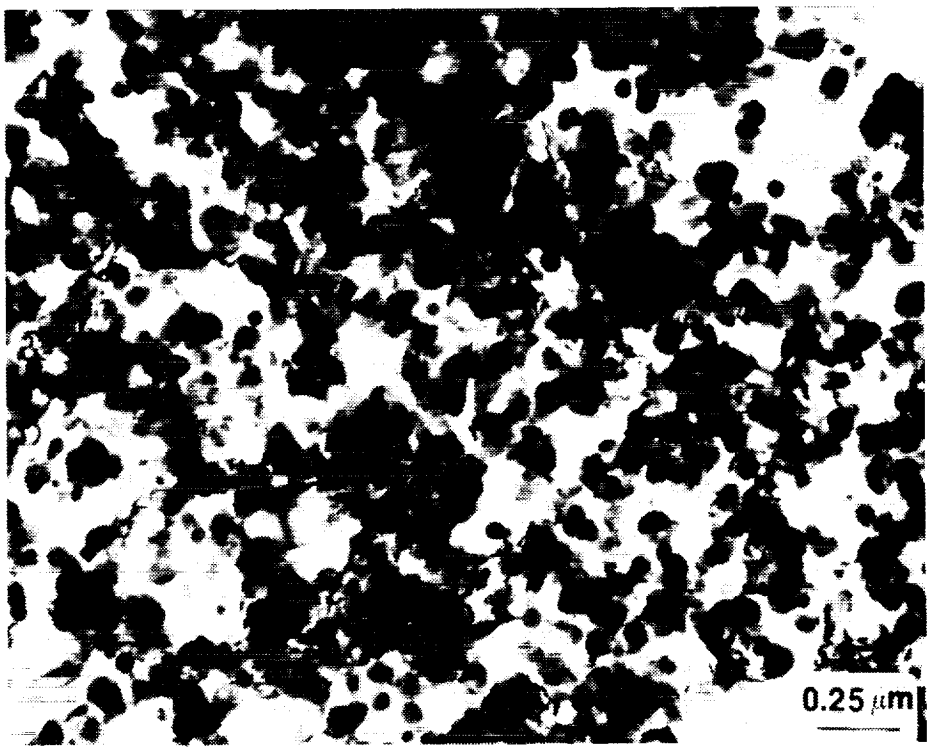

Fig. 25 TEM Micrographs of FVS1212/300 Sheet

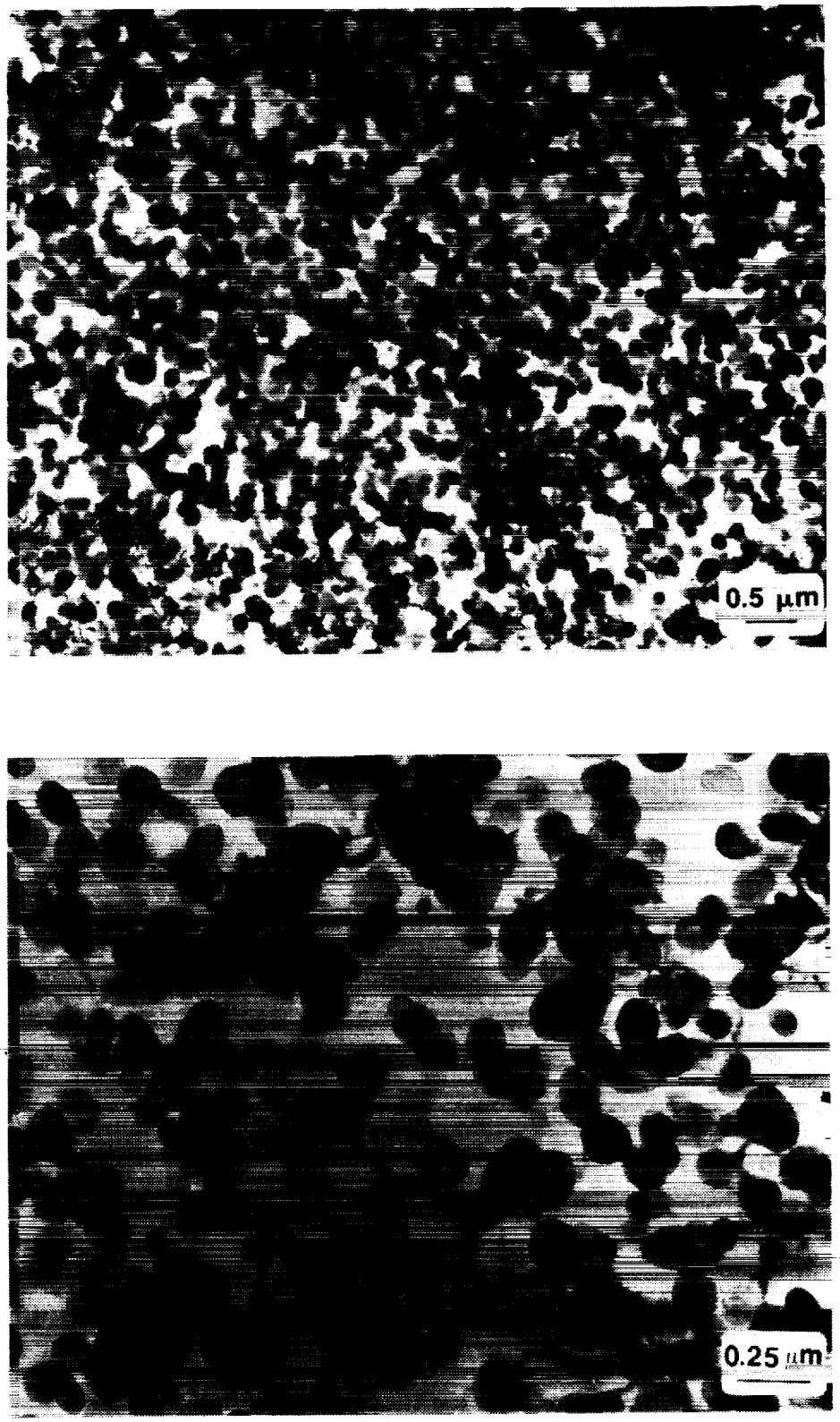

Fig. 26 TEM Micrographs of FVS1212/400 Sheet

ORIGINAL PAGE
BLACK AND WHITE PHOTOGRAPH

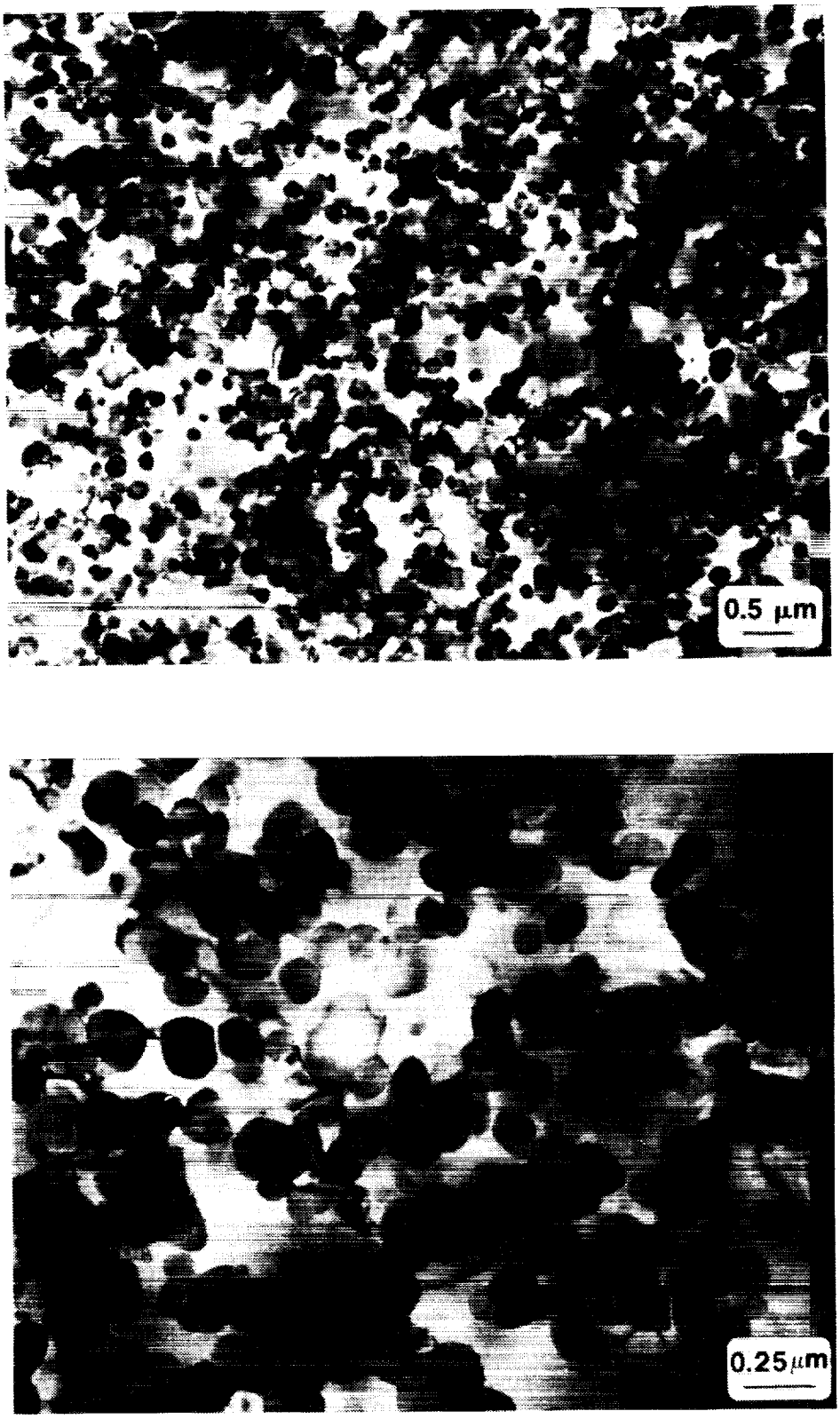

Fig. 27 TEM Micrographs of FVS1212/500 Sheet

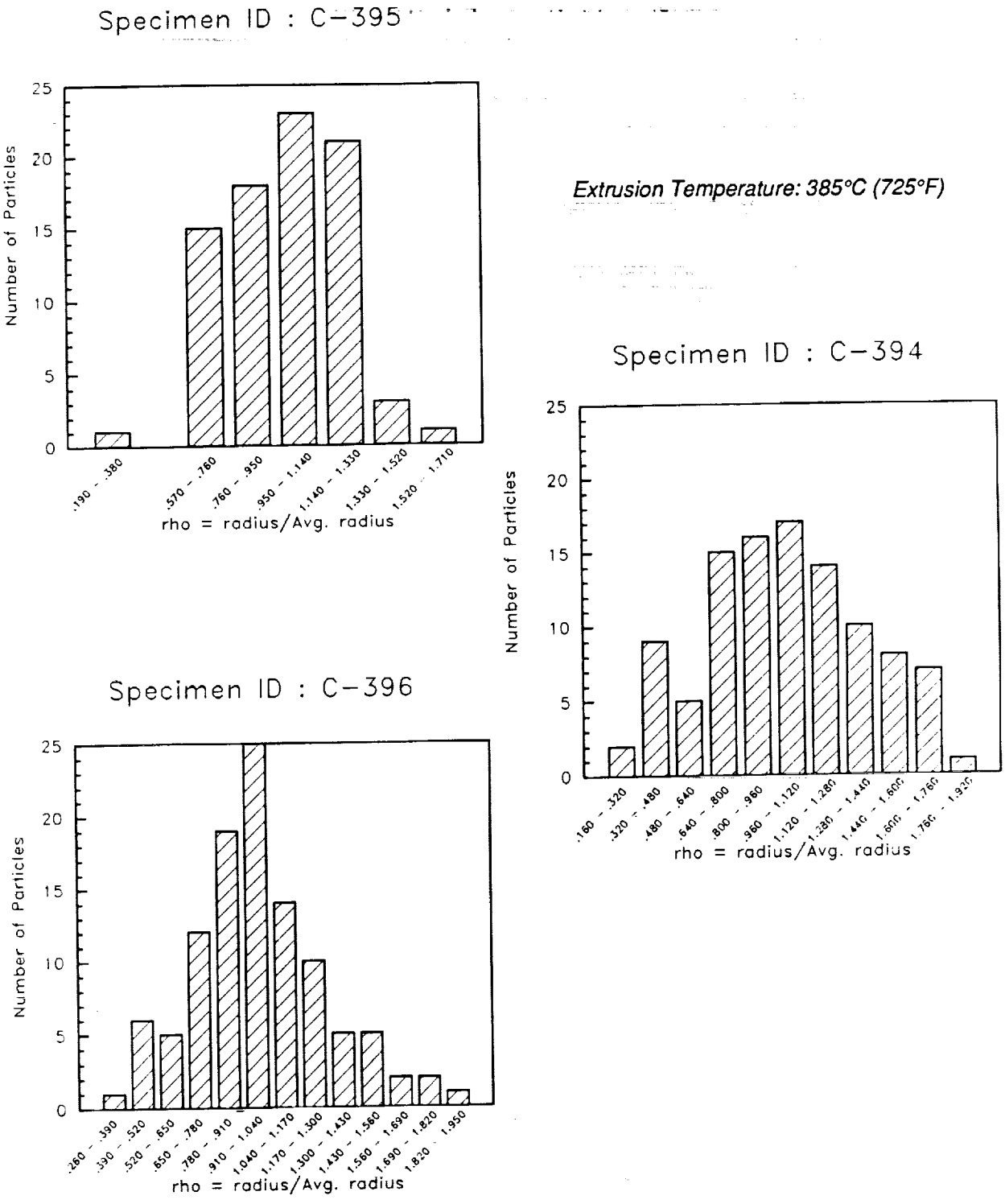

Fig. 28 Dispersoid Size Histogram for FVS0301 As-Extruded

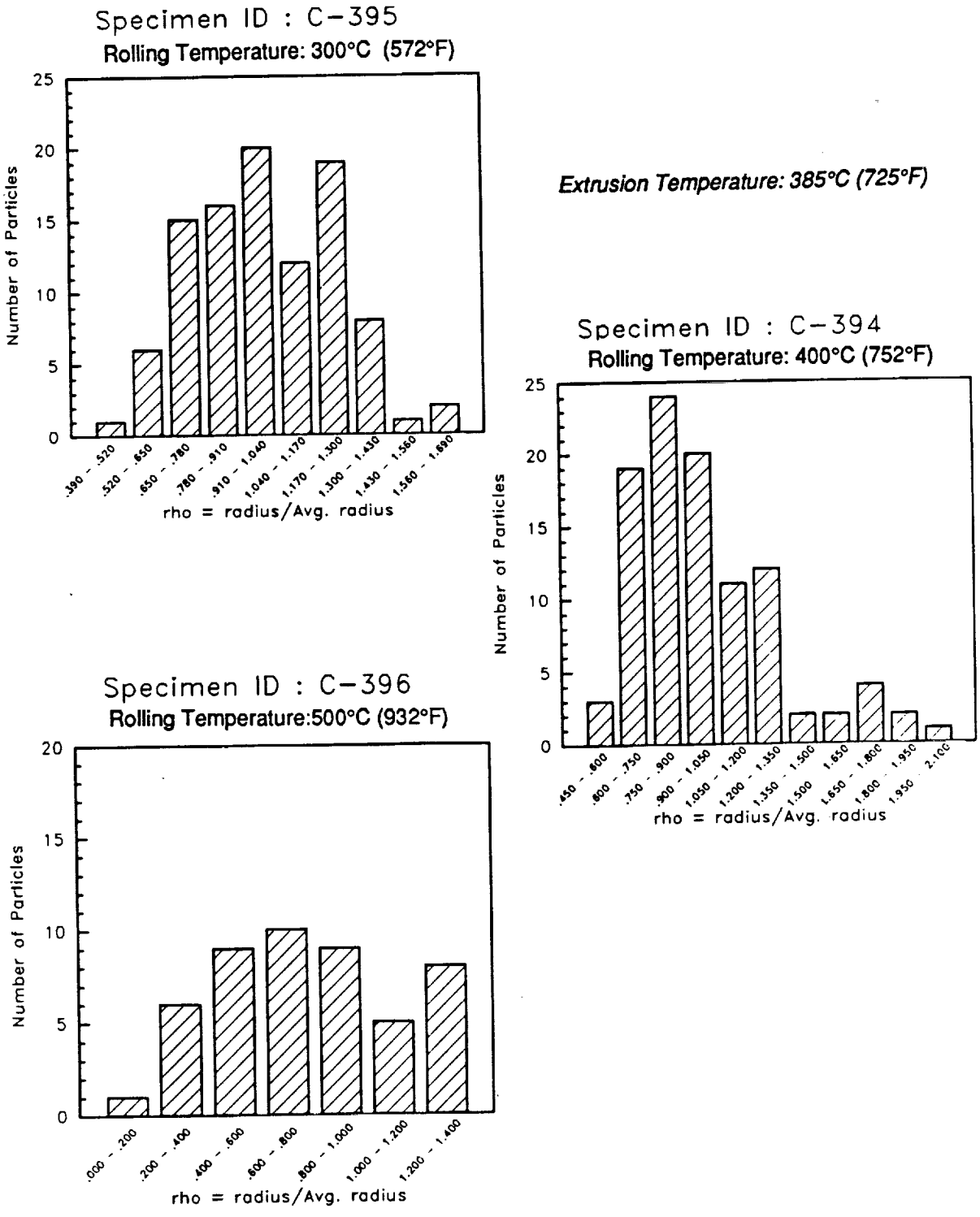

Fig. 29 Dispersold Size Histogram for FVS0301/300, FVS0301/400, and FVS0301/500

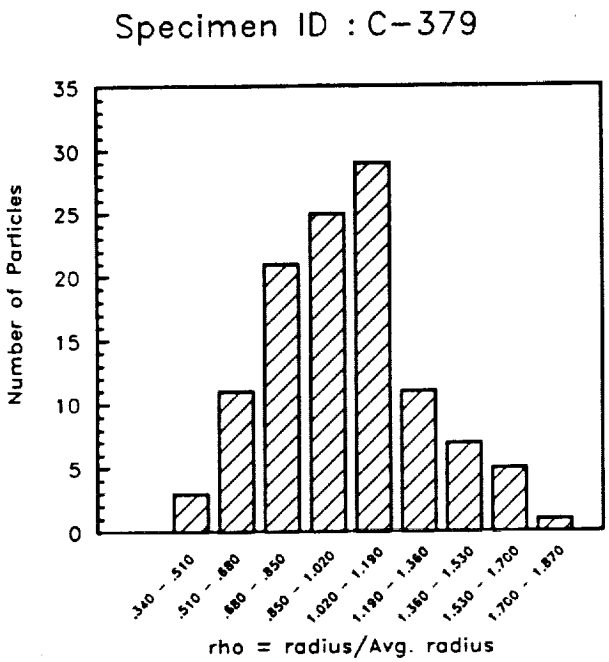

Extrusion Temperature: 385°C (725°F)

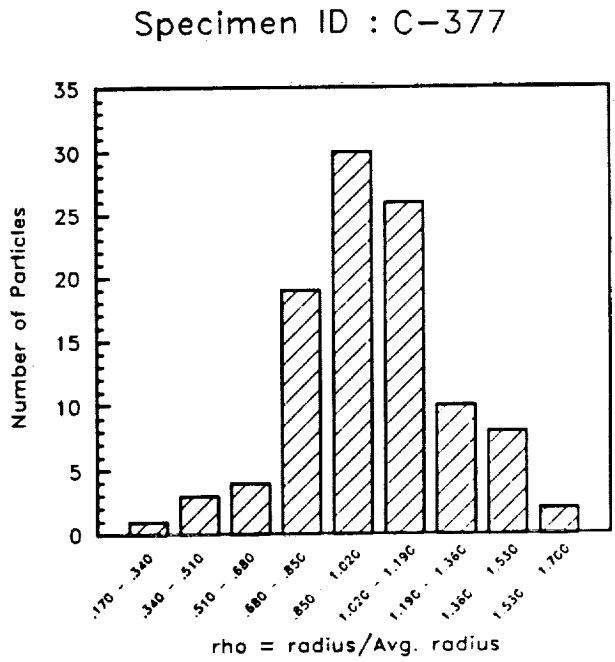

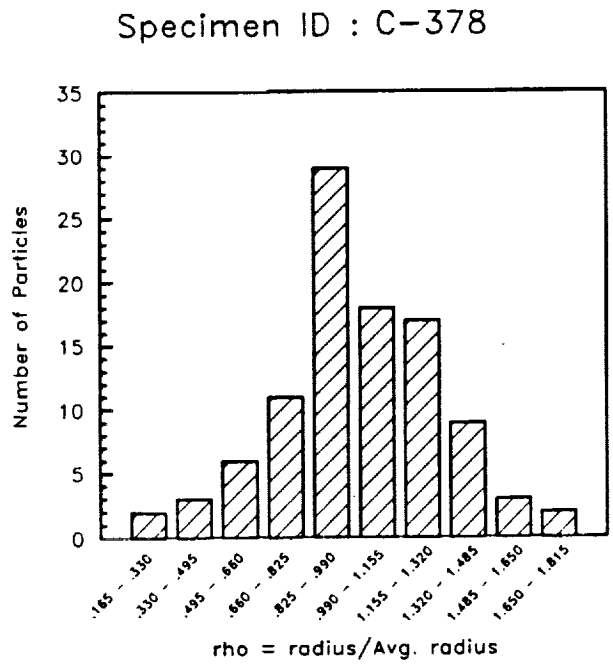

Fig. 30 Dispersoid Size Histogram for FVS0611 As-Extruded

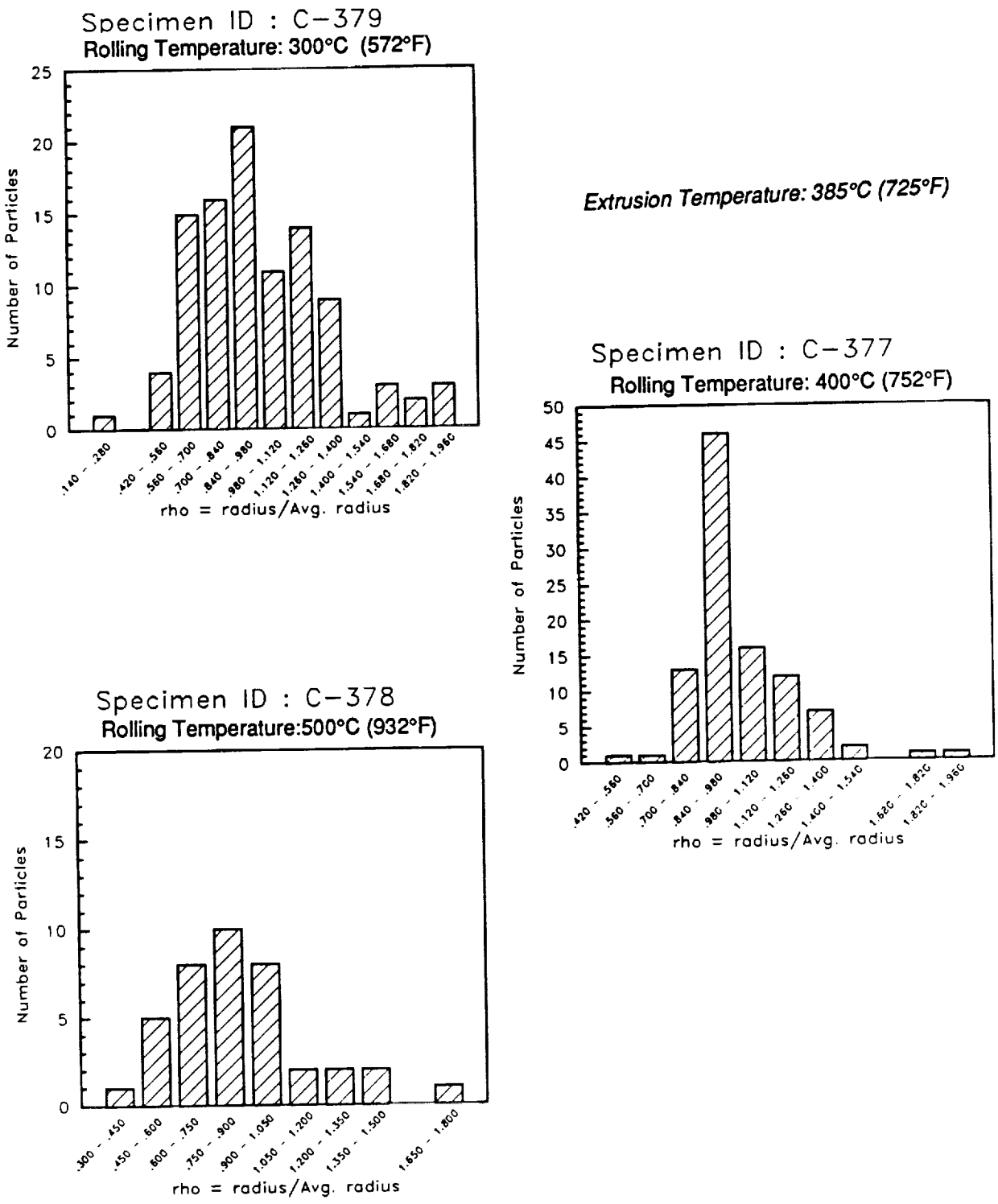

Fig. 31 Dispersoid Size Histogram for FVS0611/300, FVS0611/400, and FVS0611/500

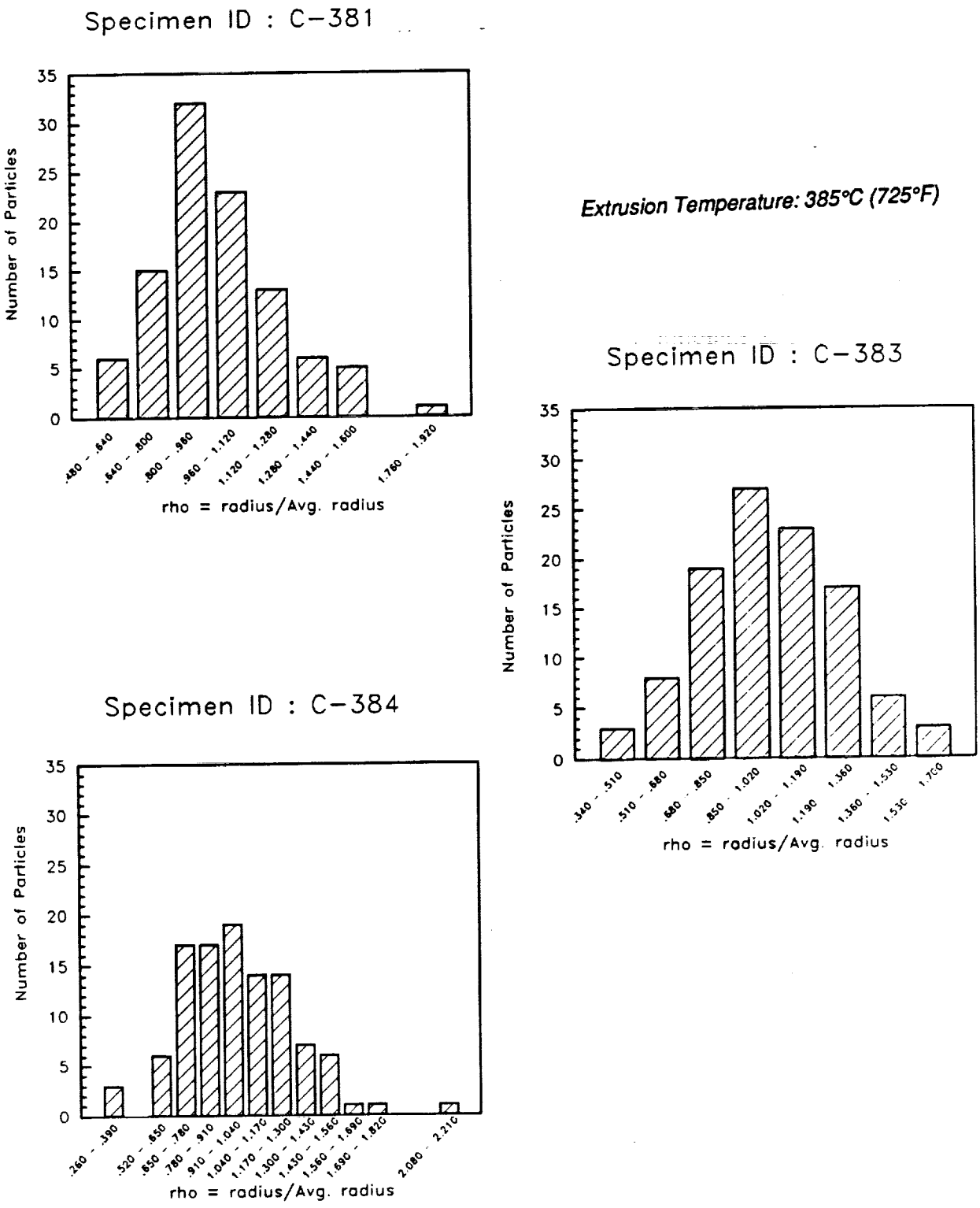

Fig. 32 Dispersoid Size Histogram for FVS0812 As-Extruded

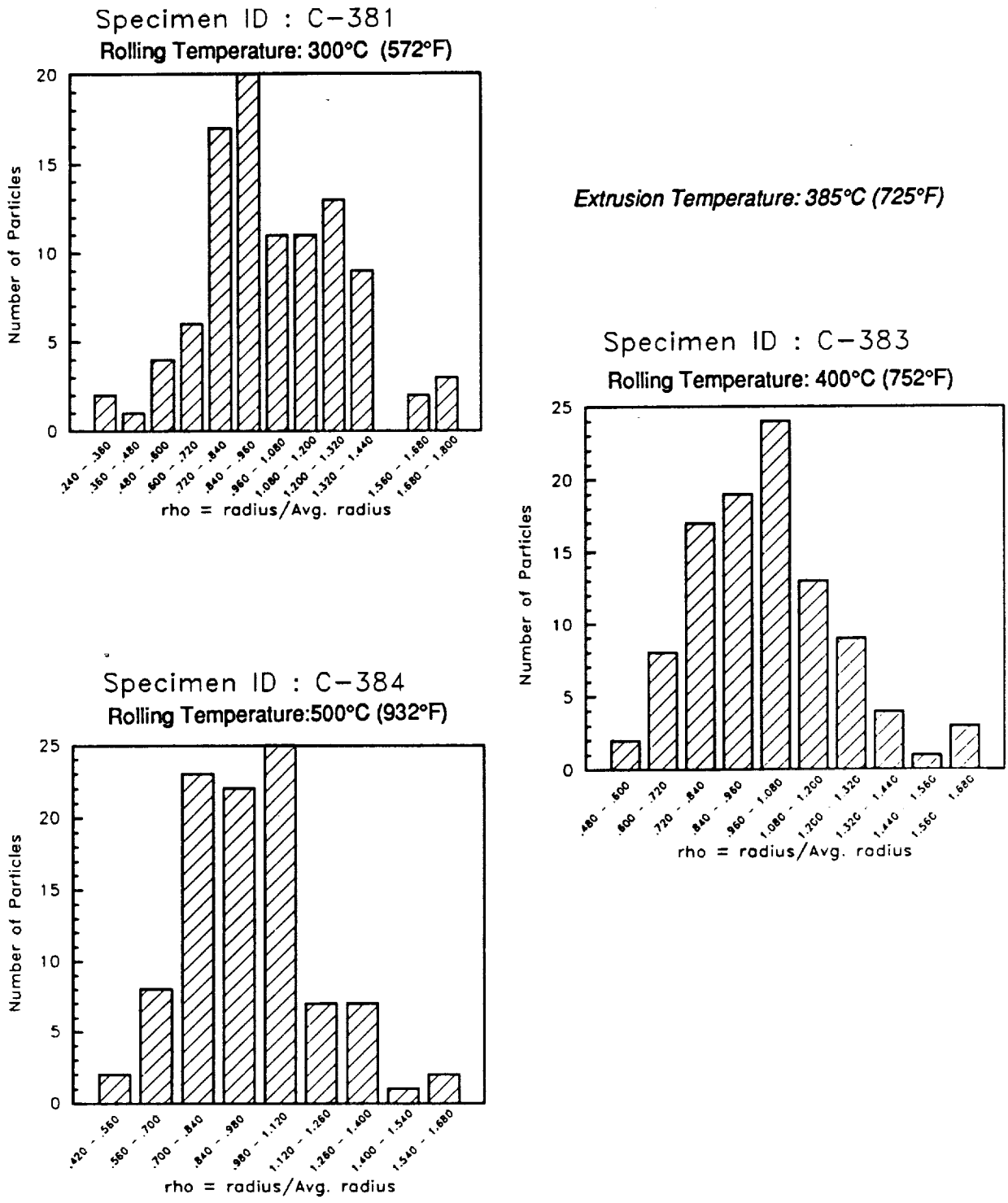

Fig. 33 Dispersoid Size Histogram for FVS0812/300, FVS0812/400, and FVS0812/500

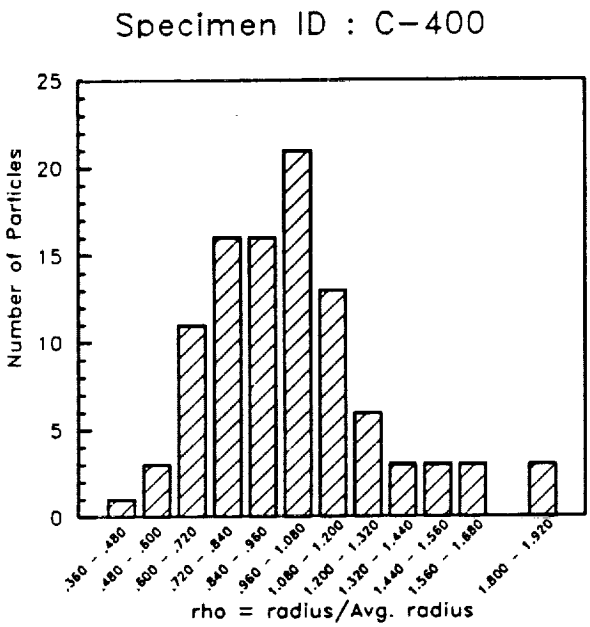

Extrusion Temperature: 427°C (800°F)

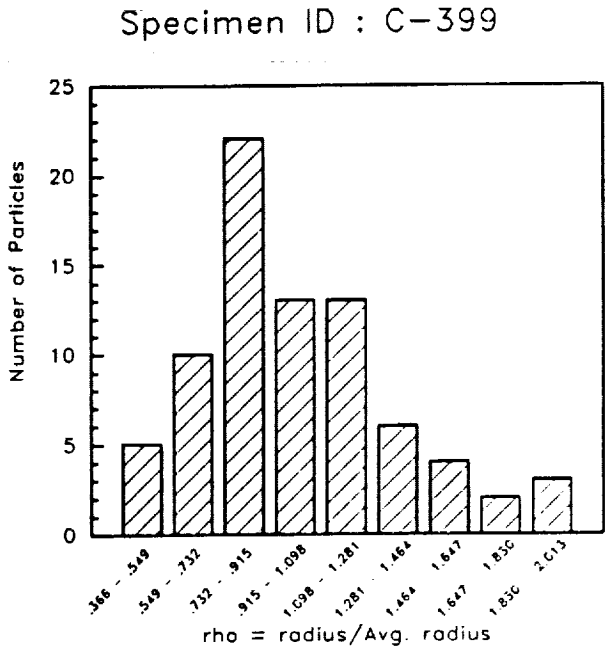

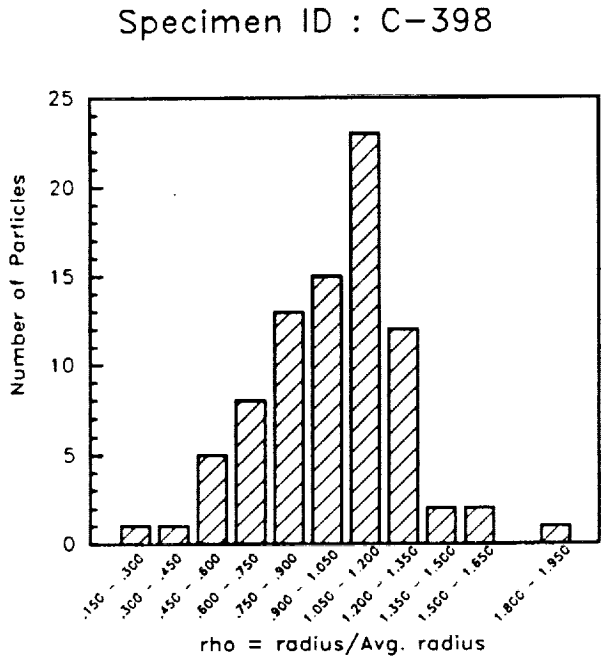

Fig. 34 Dispersoid Size Histogram for FVS1212 As-Extruded

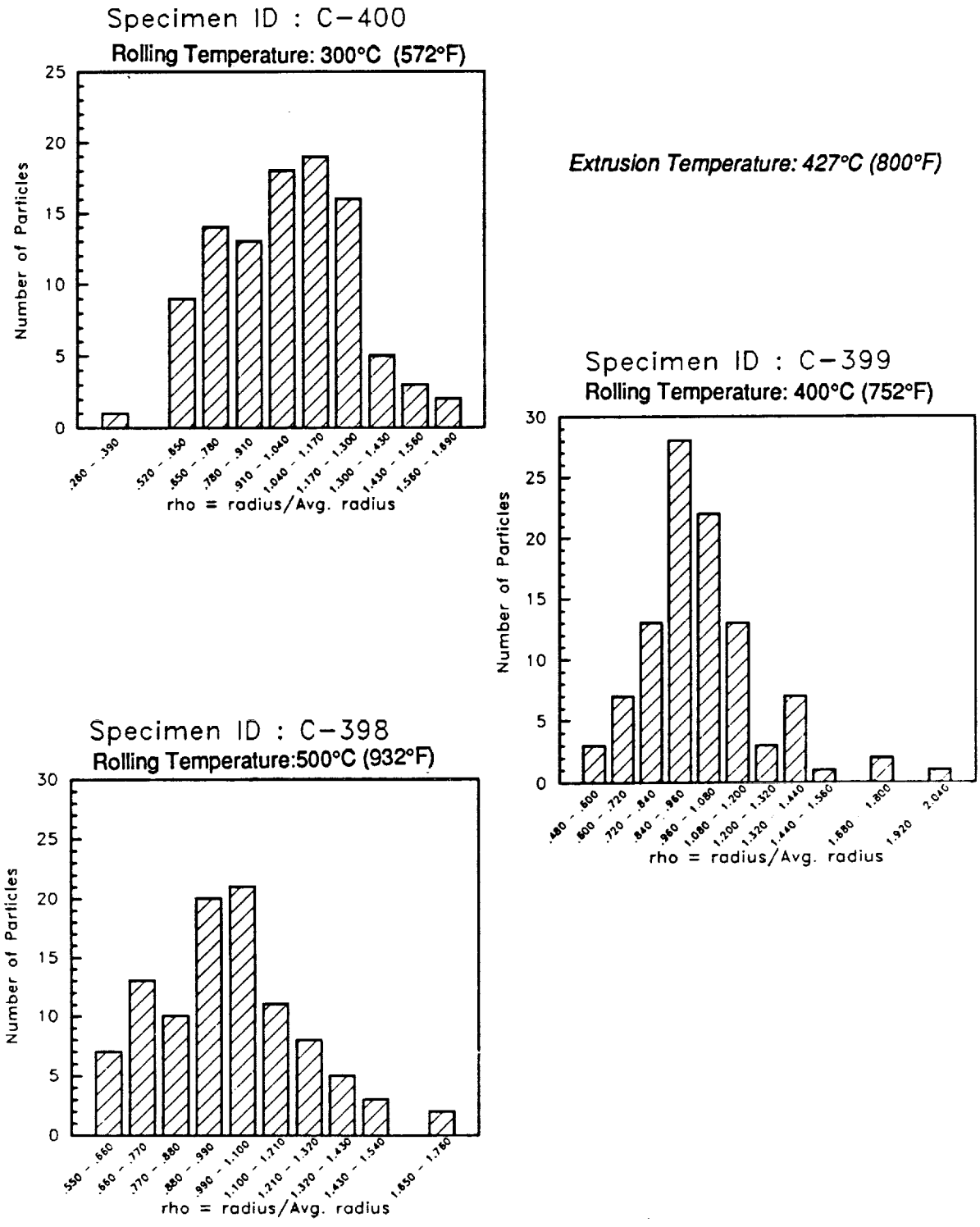

Fig. 35 Dispersoid Size Histogram for FVS1212/300, FVS1212/400, and FVS1212/500

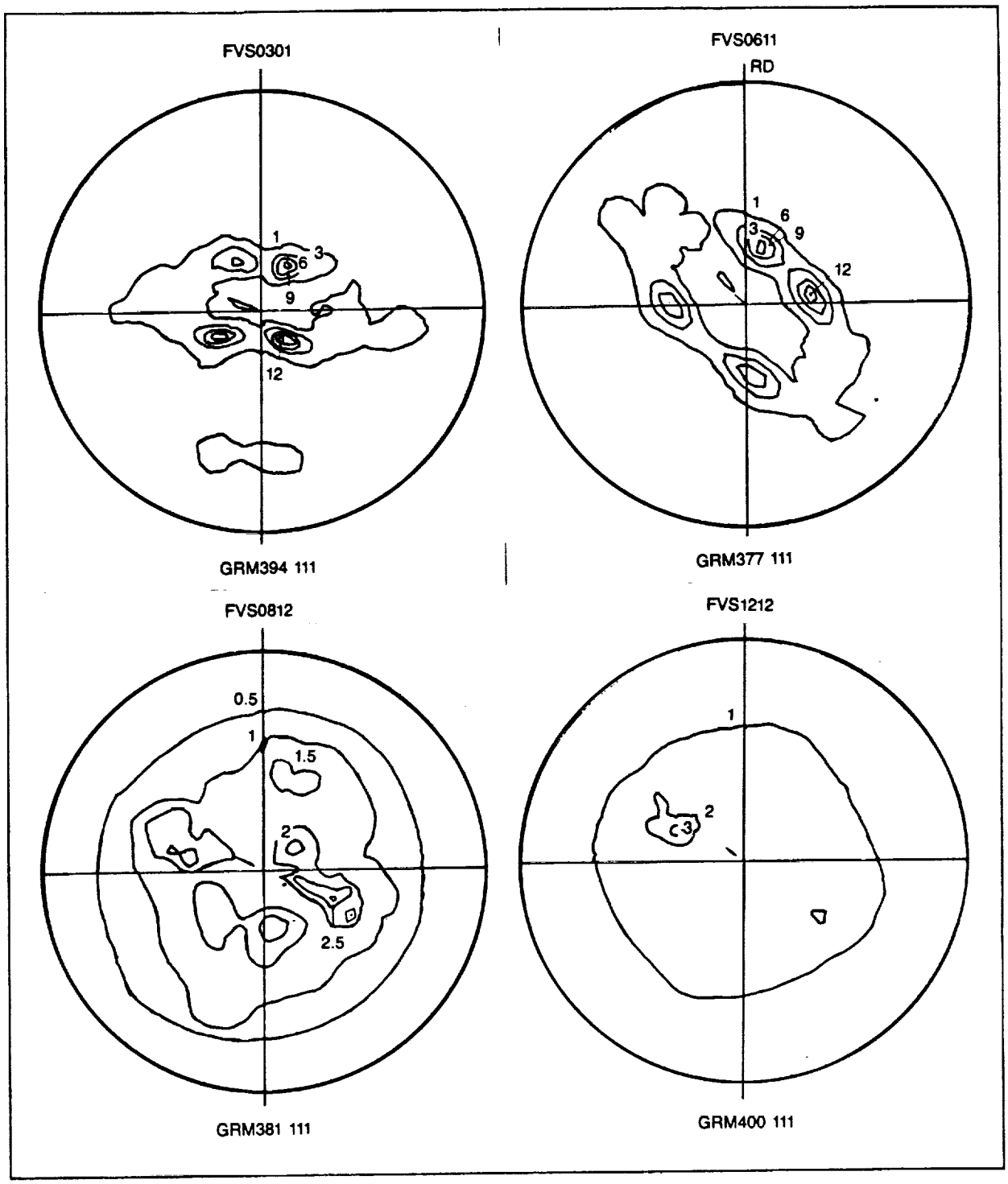

Fig. 36 X-Ray (111) Pole Figures for Alloy Extrusions

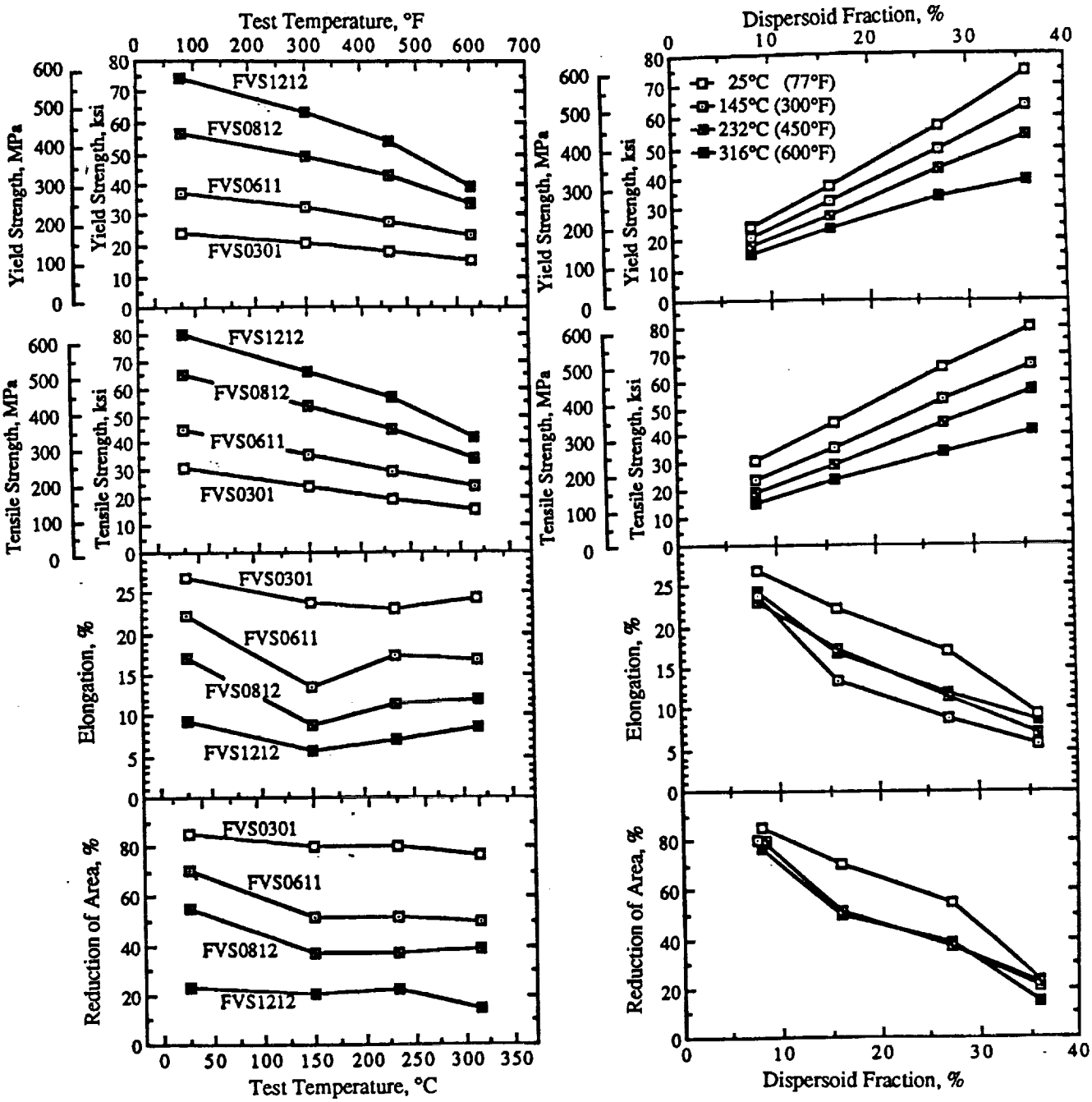

Fig. 37 **Effect of Test Temperature and Volume Fraction (Silicide) Dispersoid on Tensile Properties of Extruded Alloys**

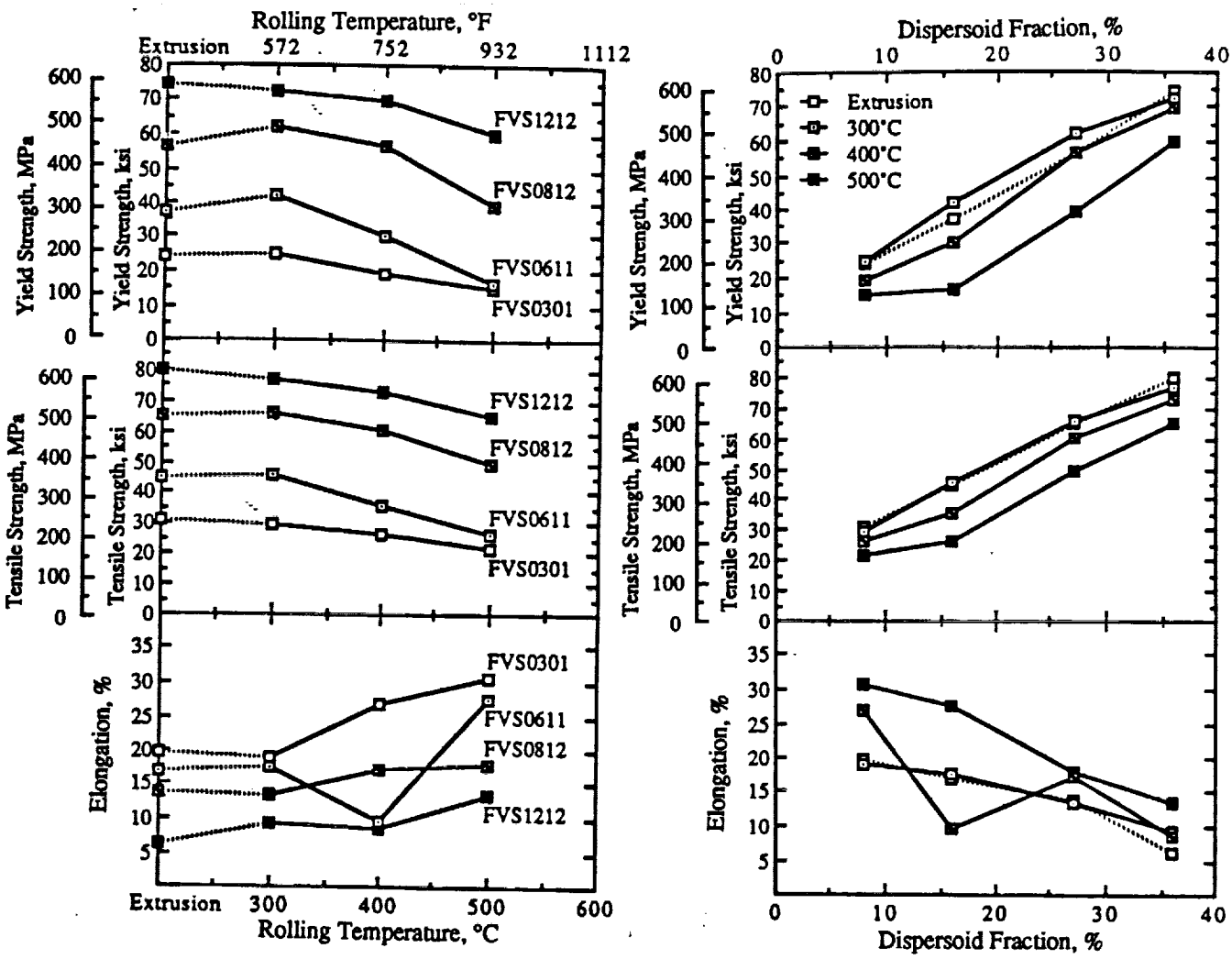

Fig. 38 Effect of Rolling Temperature and Volume Fraction (Silicide) Dispersoid on Room Temperature Tensile Properties of Sheet

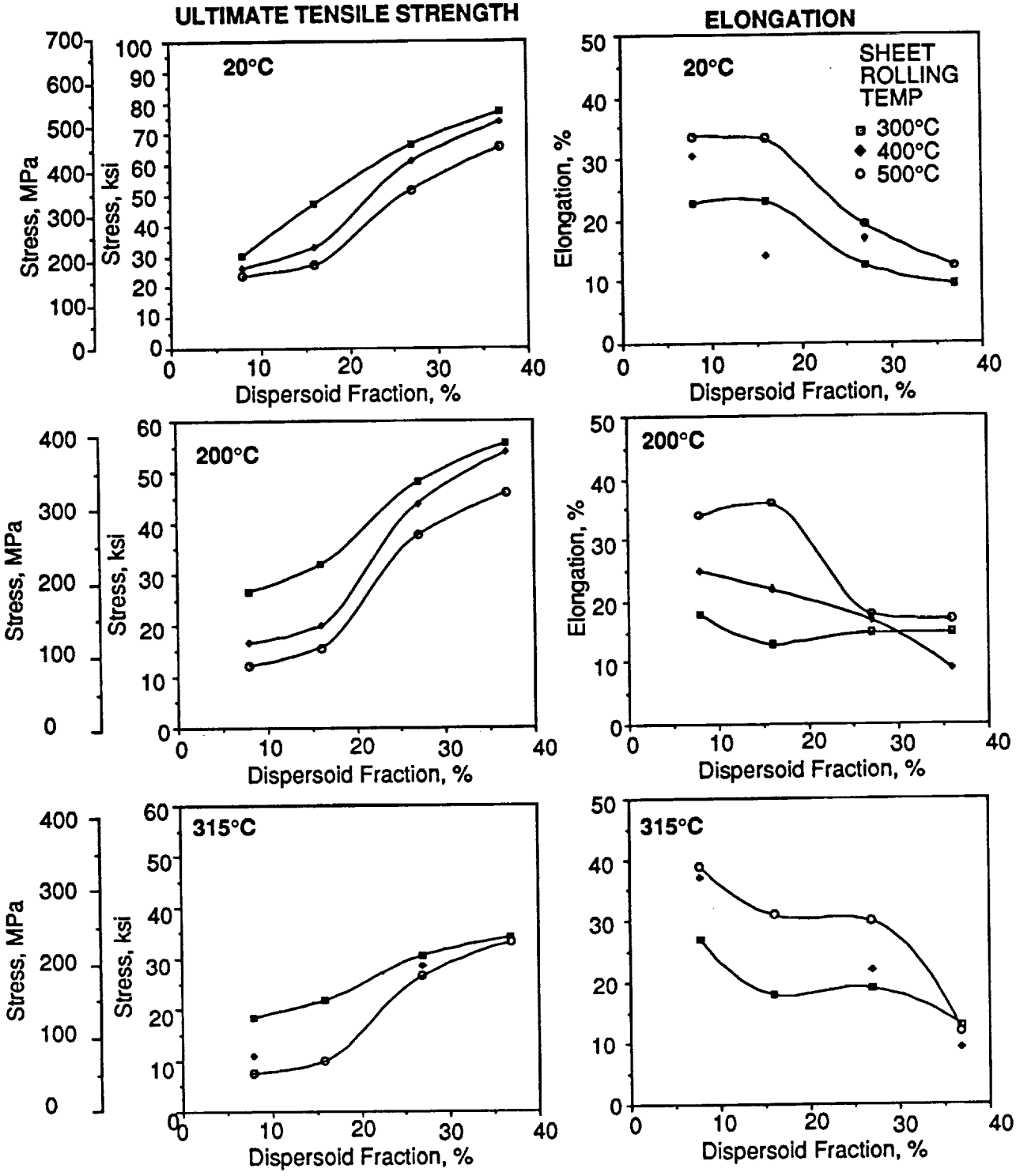

Fig. 39 Tensile Properties of Al-Fe-V-Si Sheets at 200 and 300°C (392 and 572°F)

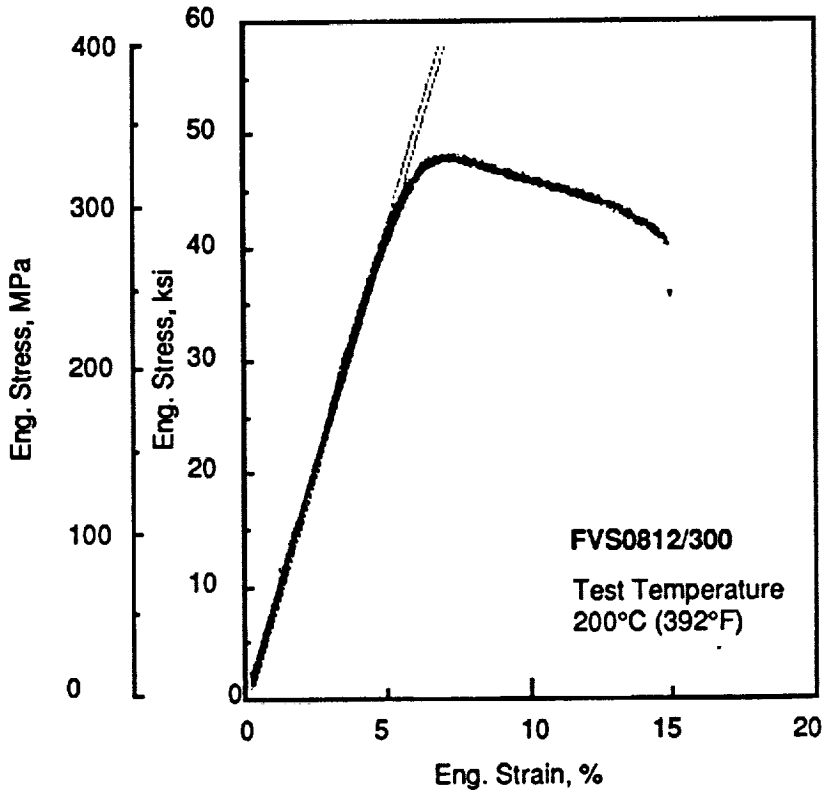

Fig. 40 Characteristic Engineering Stress Strain Curve for Al-Fe-V-Si Alloys

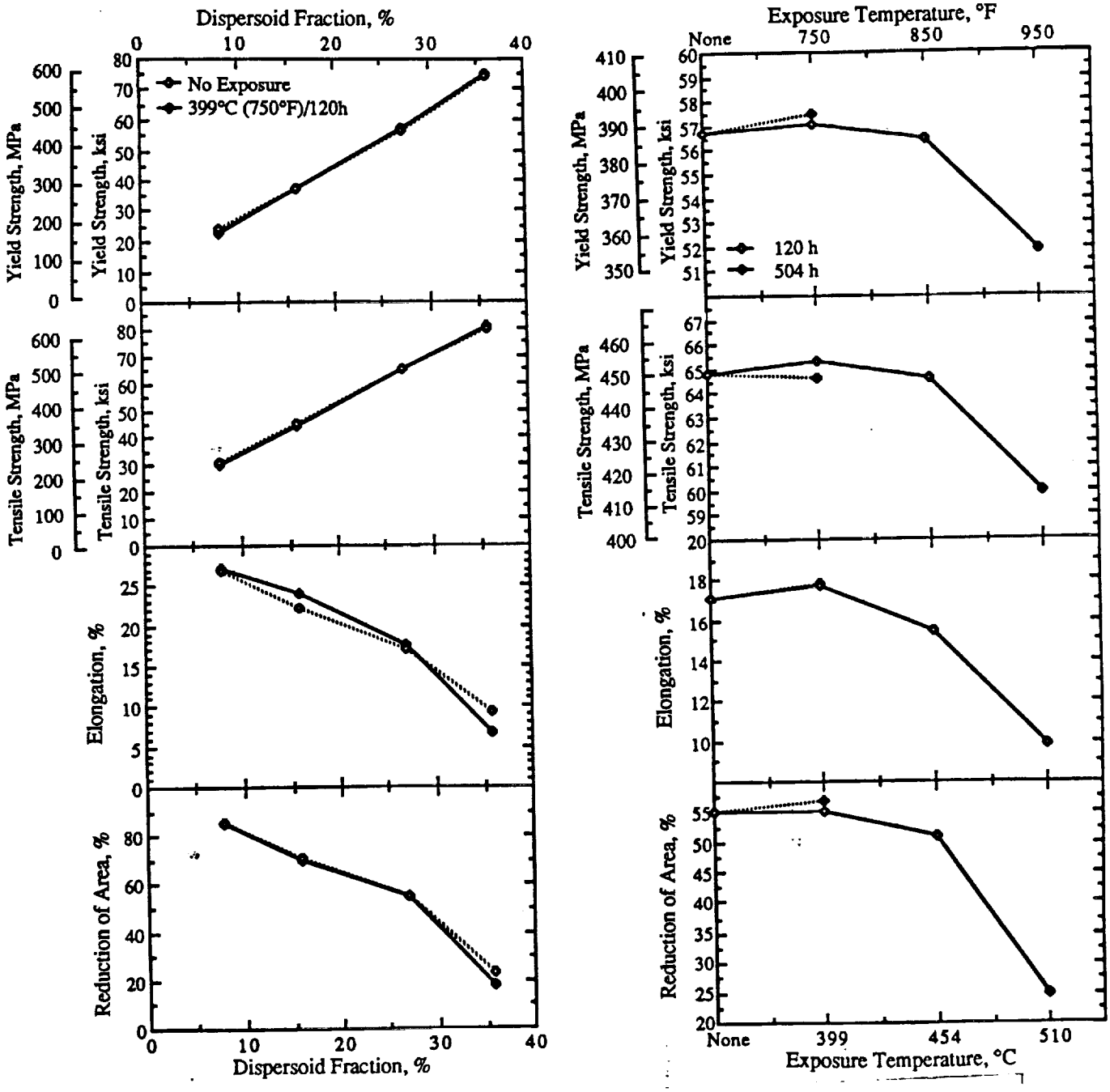

Fig. 41 **Effect of Thermal Exposure and Volume Fraction (Silicide) Dispersoid on Room Temperature Tensile Properties of Extruded Alloys**

C-2

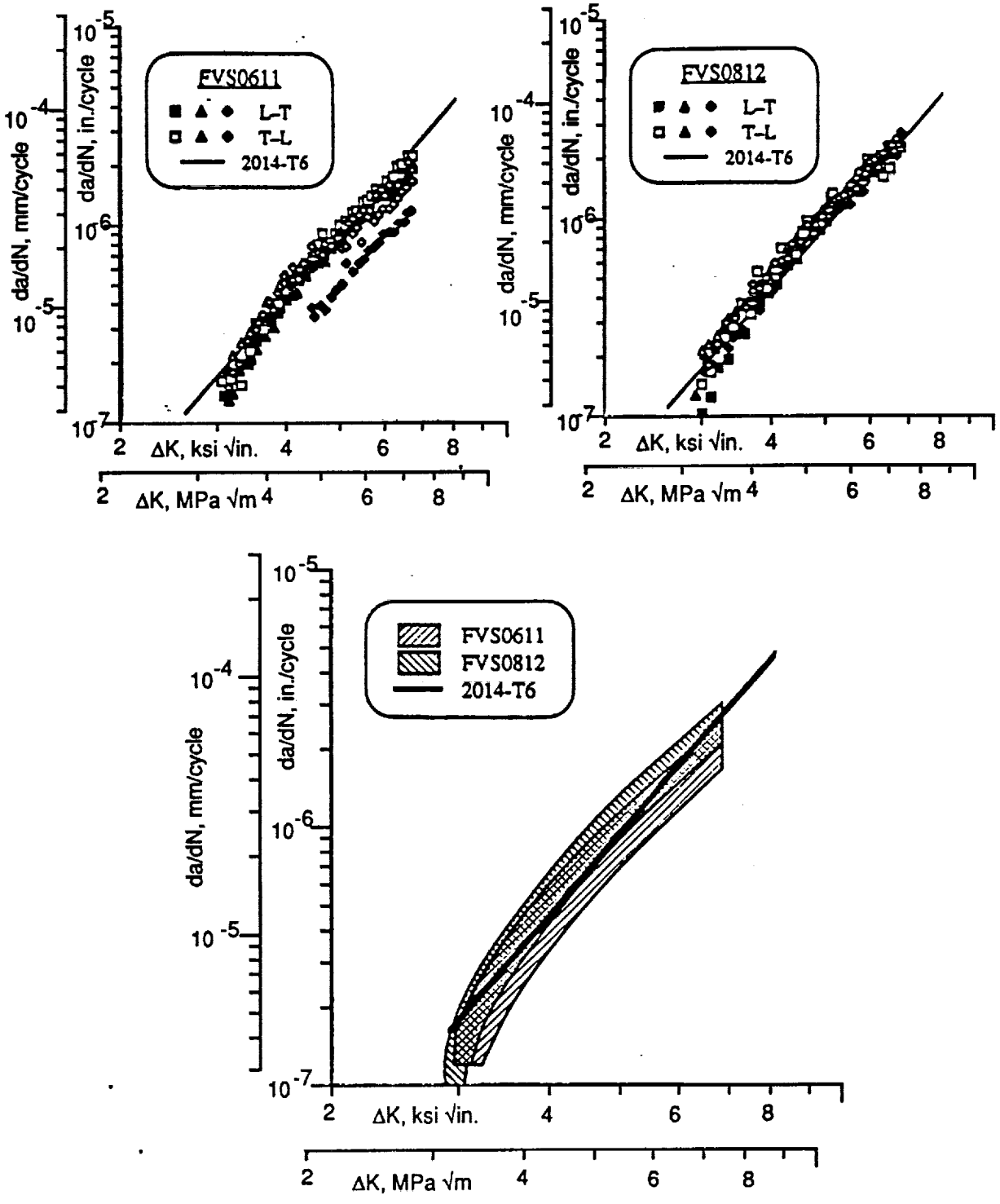

Fig. 42 Fatigue Crack Growth Rate for Extruded FVS0611 and FVS0812 in the L-T and T-L Orientation

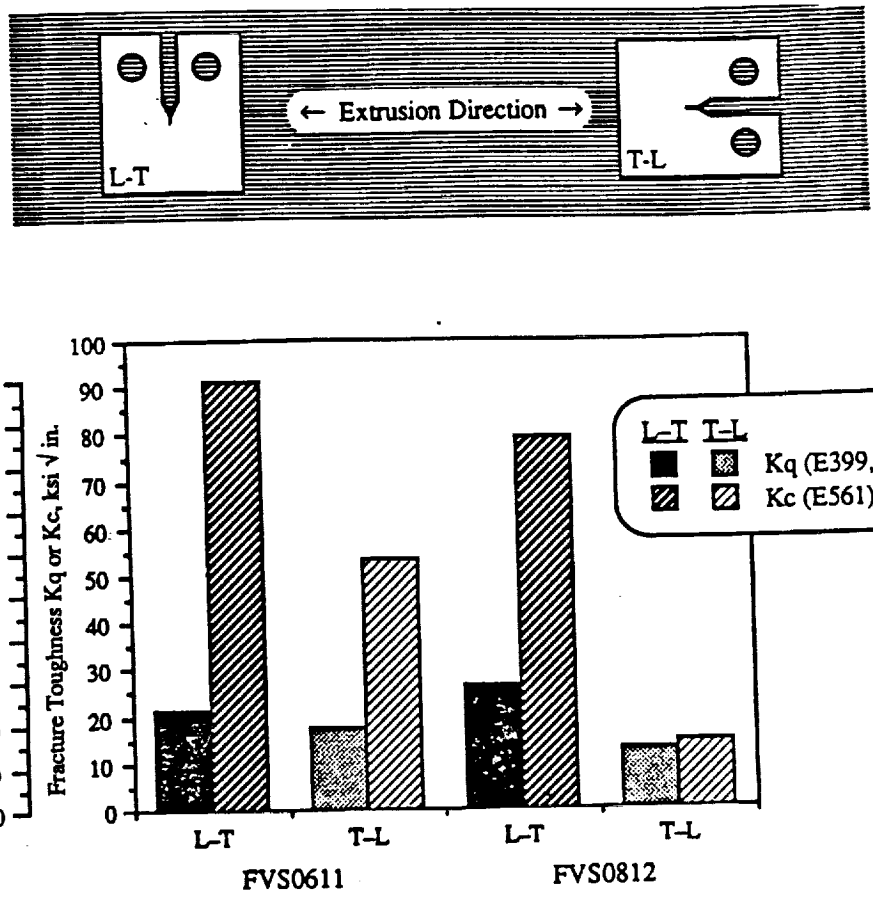

Fig. 43 Fracture Toughness for FVS0611 and FVS0812 Extrusions

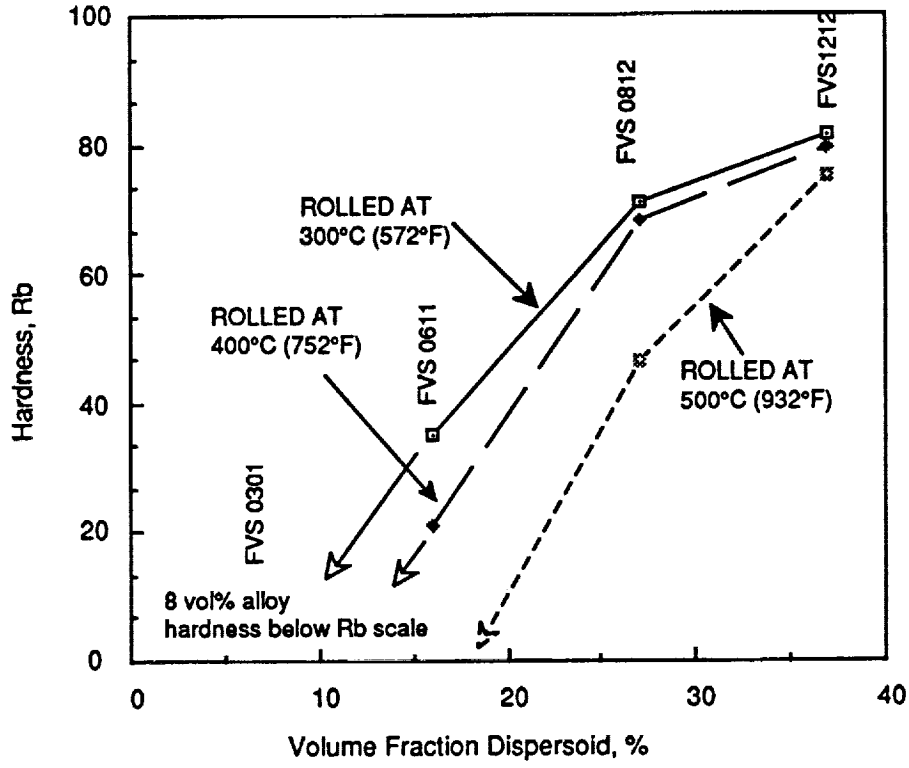

Fig. 44 Effect of Volume Fraction Dispersoid and Rolling Temperature on Al-Fe-V-Si Sheet Hardness

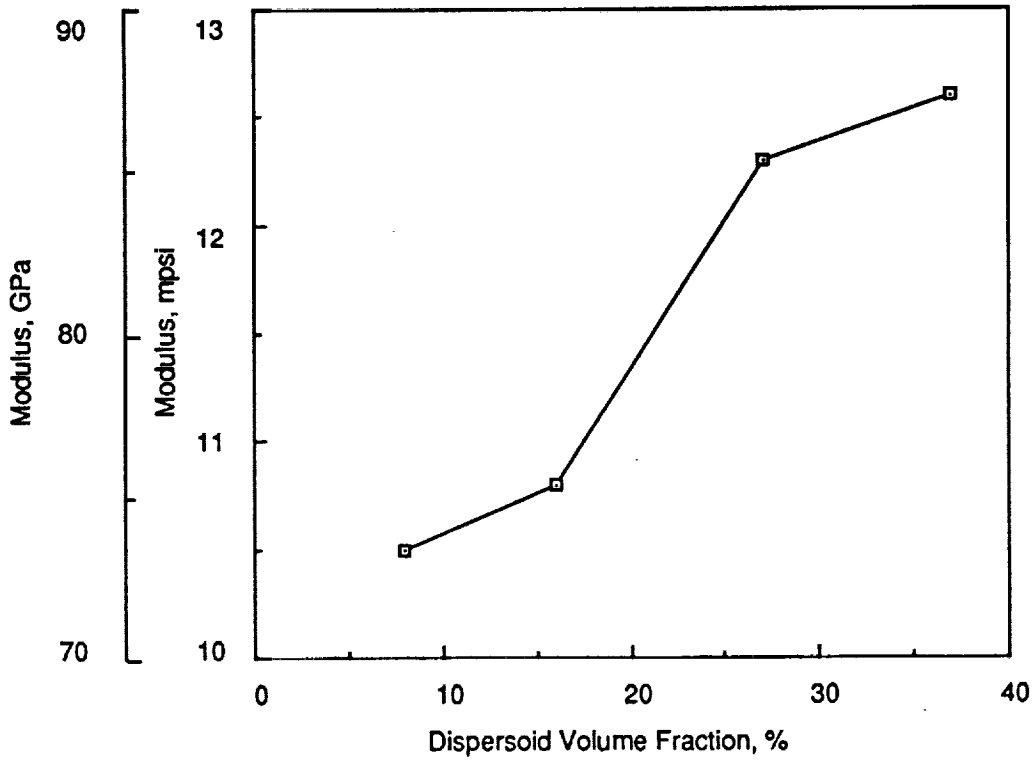

Fig. 45 Effect of Volume Fraction Dispersoid on Tensile Modulus of Al-Fe-V-Si Sheet

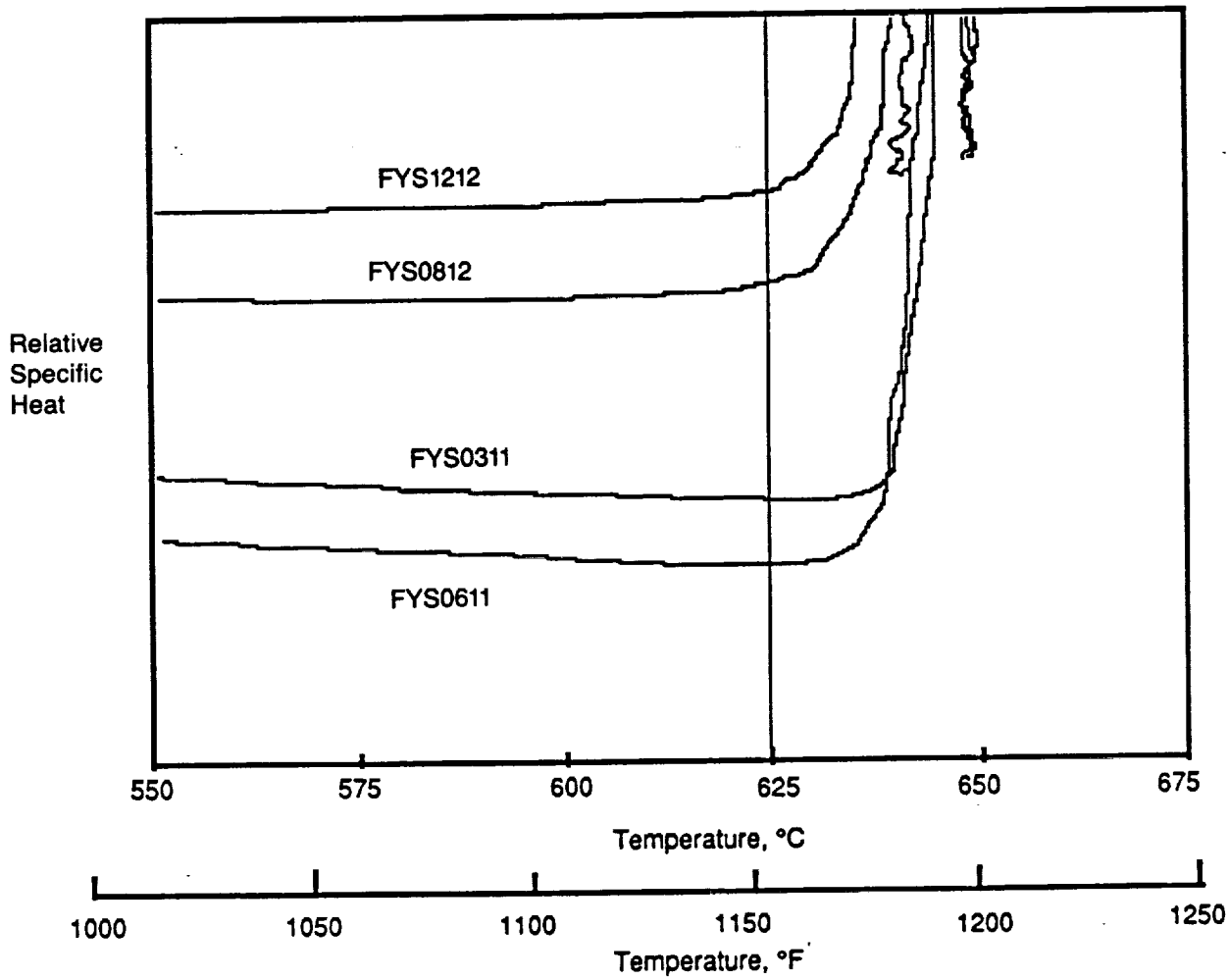

Fig. 46 Differential Scanning Calorimetry (DSC) Analysis of Al-Fe-V-Si Alloys

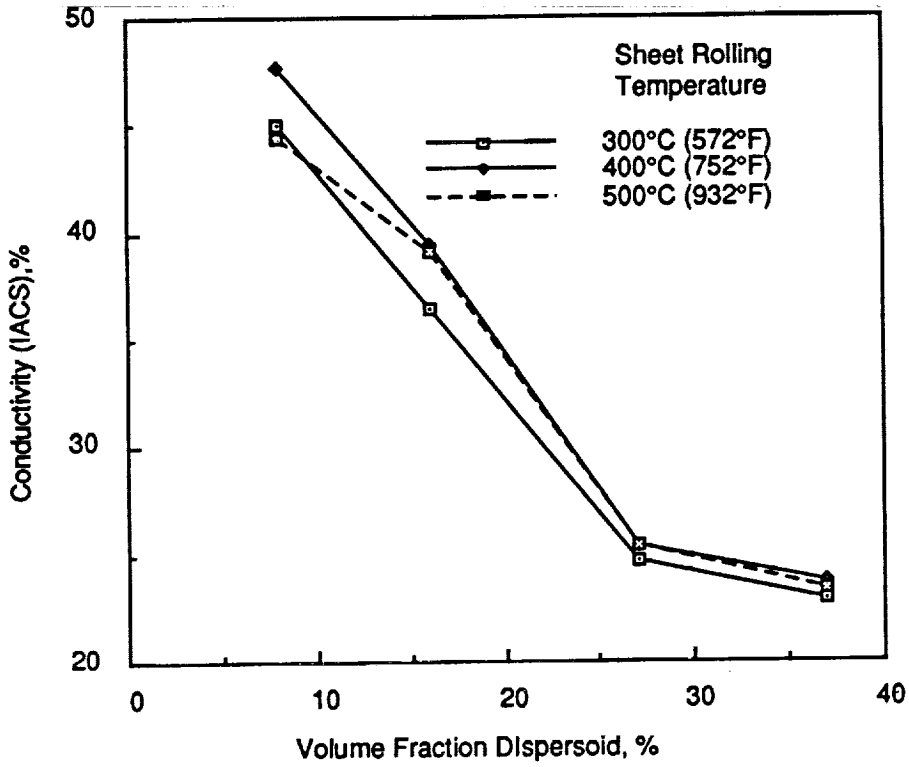

Fig. 47 Effect of Volume Fraction Dispersoid on Electrical Conductivity of Al-Fe-V-Si Sheets

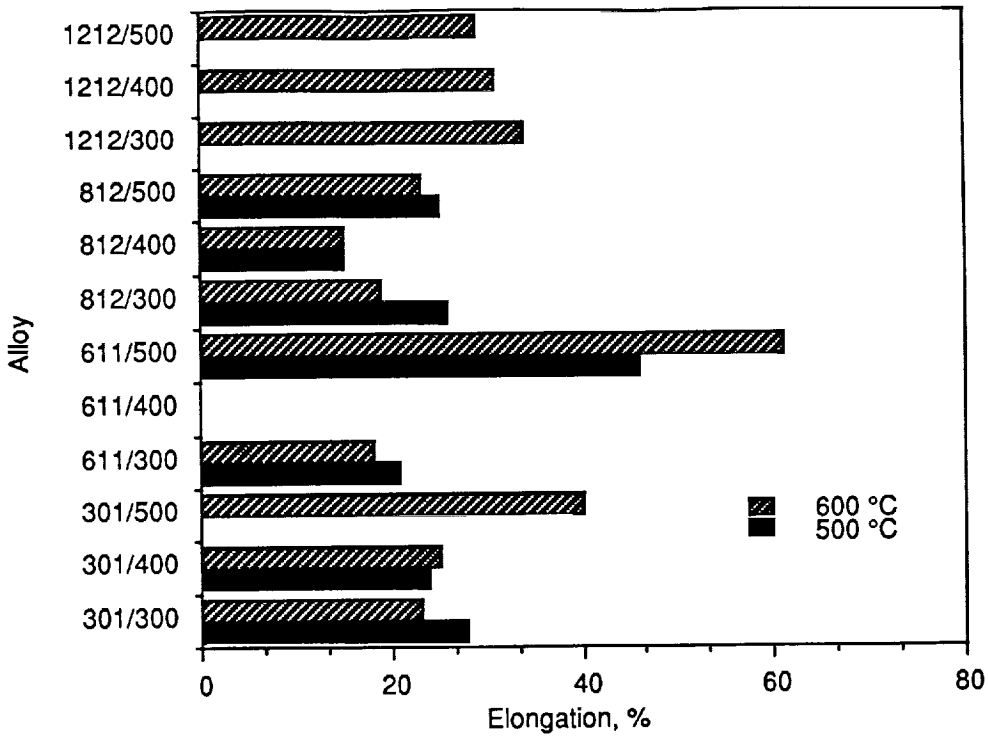

Fig. 48 Alloy Elongation at 500°C and 600°C (932 and 1112°F) at a Strain Rate of $1x10^{-4}$ s^{-1}

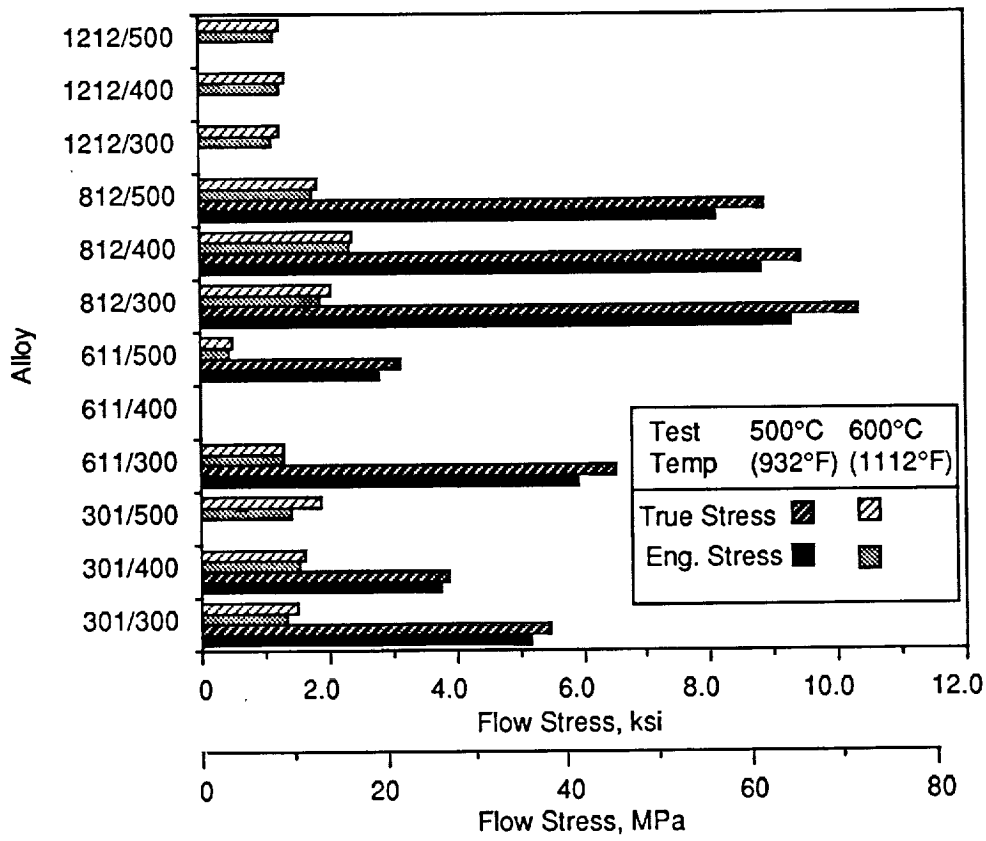

Fig. 49 Maximum Flow Stress at 500°C and 600°C (932 and 1112°F) at a Strain Rate of $1x10^{-1}$ s^{-1}

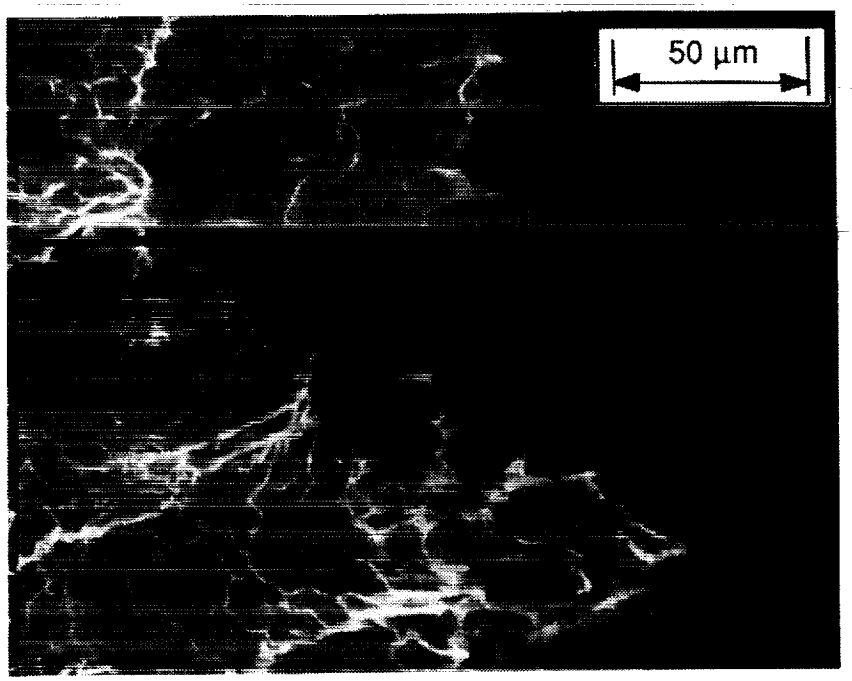

Fig. 50 Ligaments at Fracture Surface of Al-Fe-V-Si Alloys Tested at a Strain Rate of $1x10^{-4}$ s^{-1}

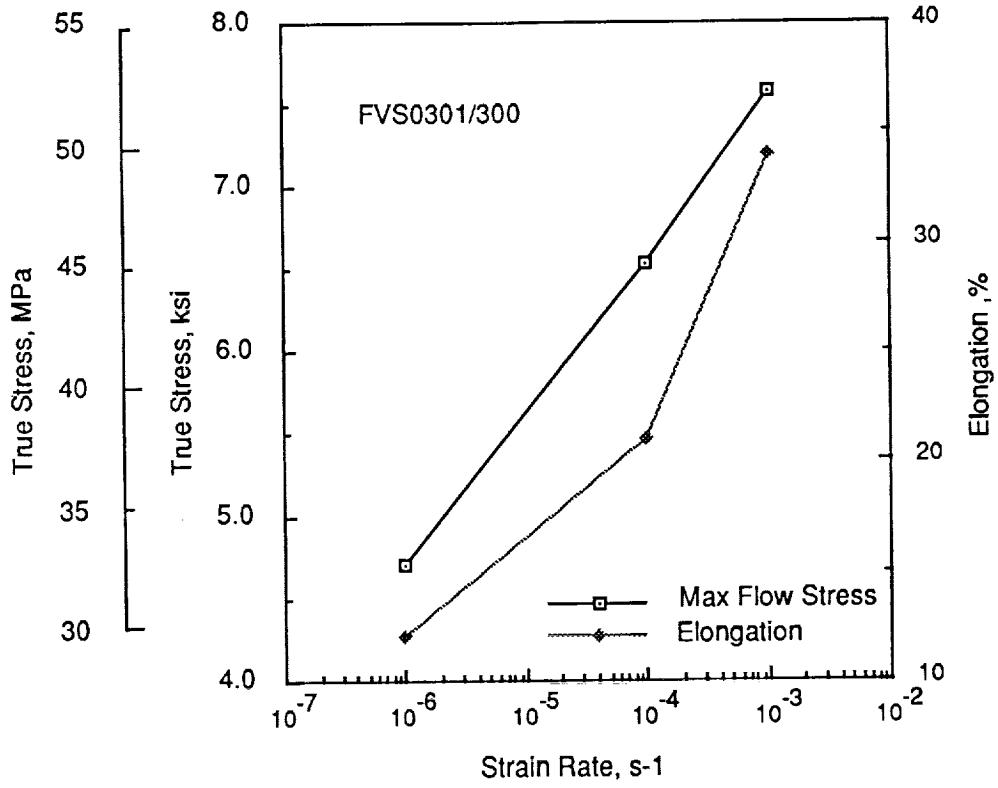

Fig. 51 Flow Stress and Elongation at a Strain Rate of $2.5 X 10^{-4}$ s^{-1} and 500°C (932°F)

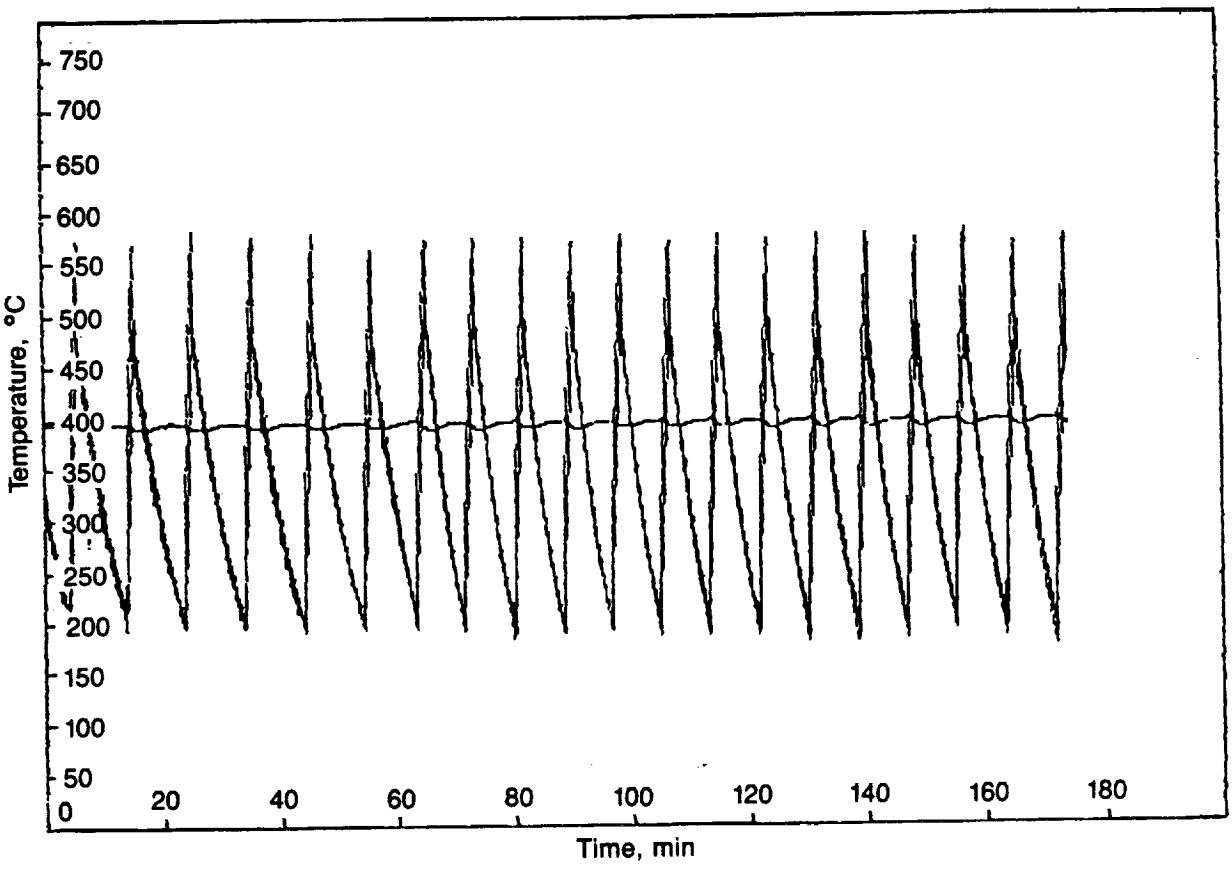

Fig. 52 Temperature Cycling To Evaluate Internal Stress Superplasticity

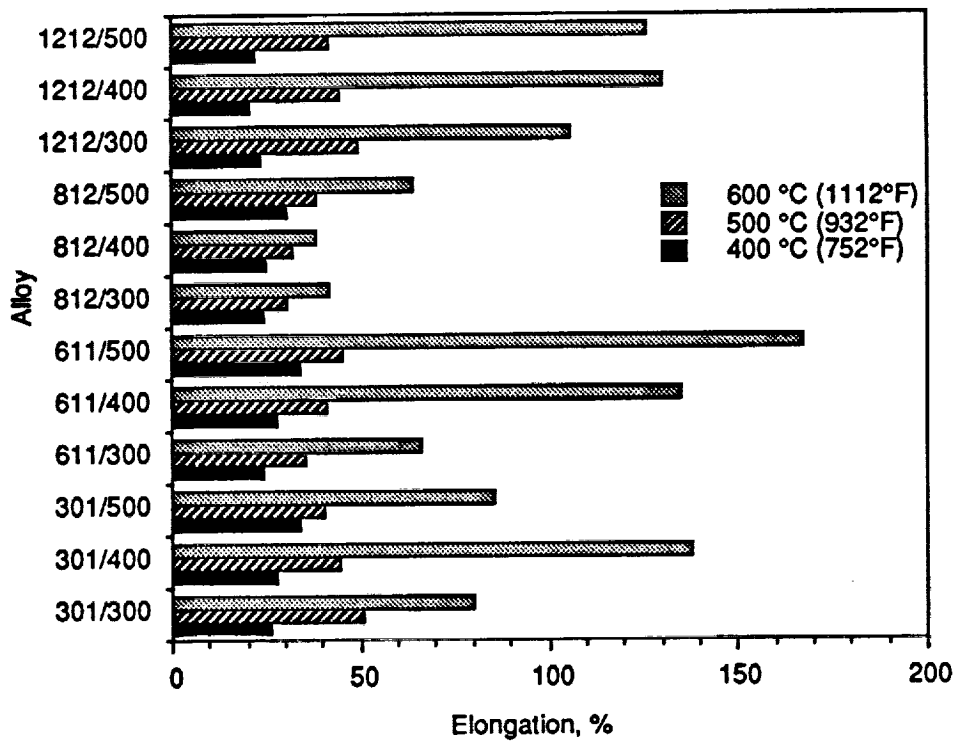

Fig. 53 Effect of High Strain Rate (0.1 s^{-1}) on Elongation at 400, 500 and 600°C (752, 932 and 1112°F)

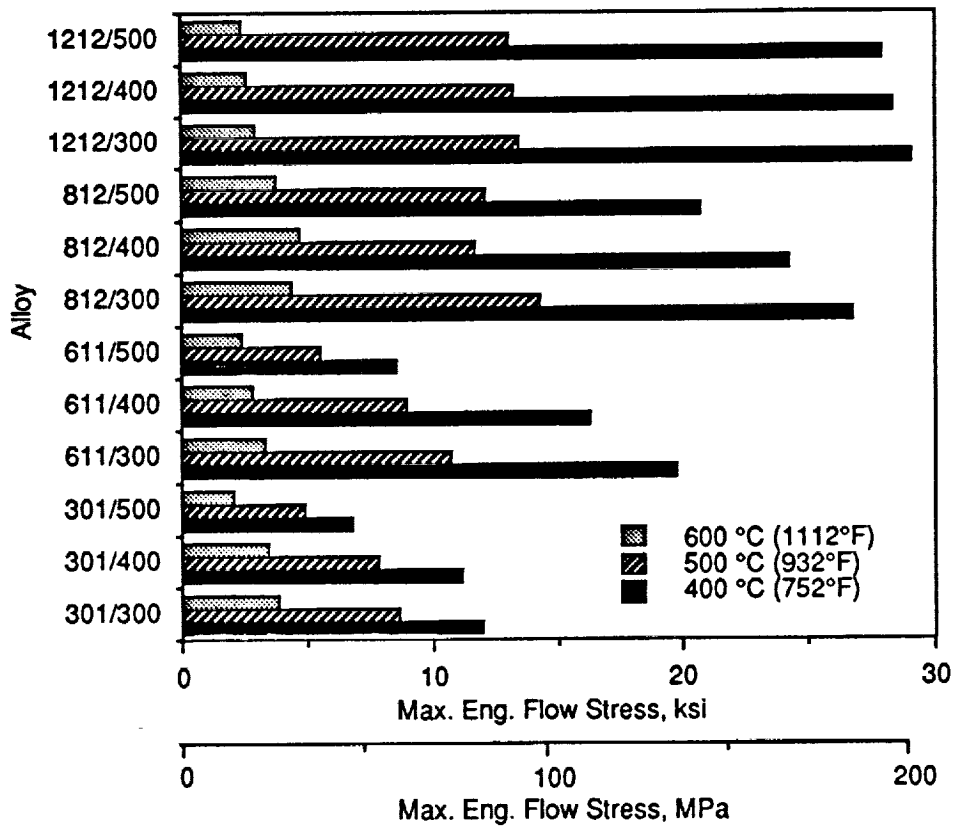

Fig. 54 Effect of High Strain Rate (0.1 s^{-1}) on Flow Stress at 400, 500 and 600°C (752, 932 and 1112°F)

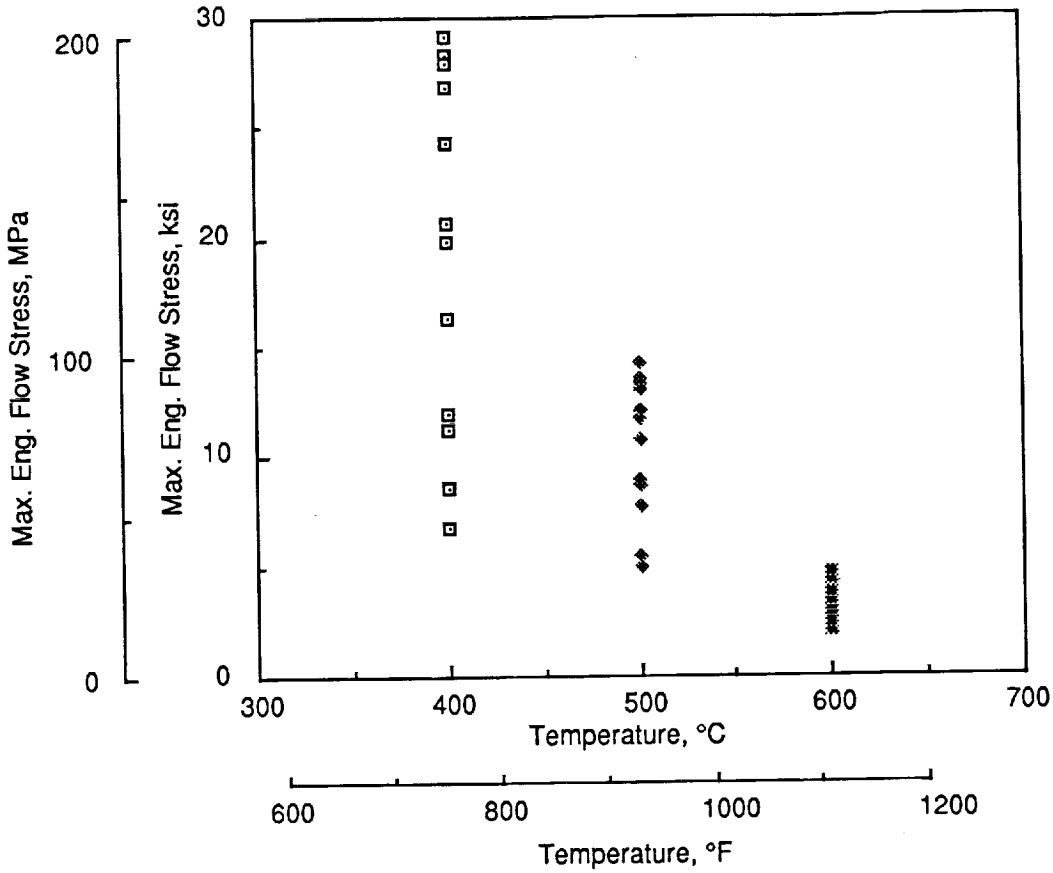

Fig. 55 Effect of Elevated Temperature on Flow Stress of Al-Fe-V-Si Alloy Sheets at a Strain Rate of 0.1 s^{-1}

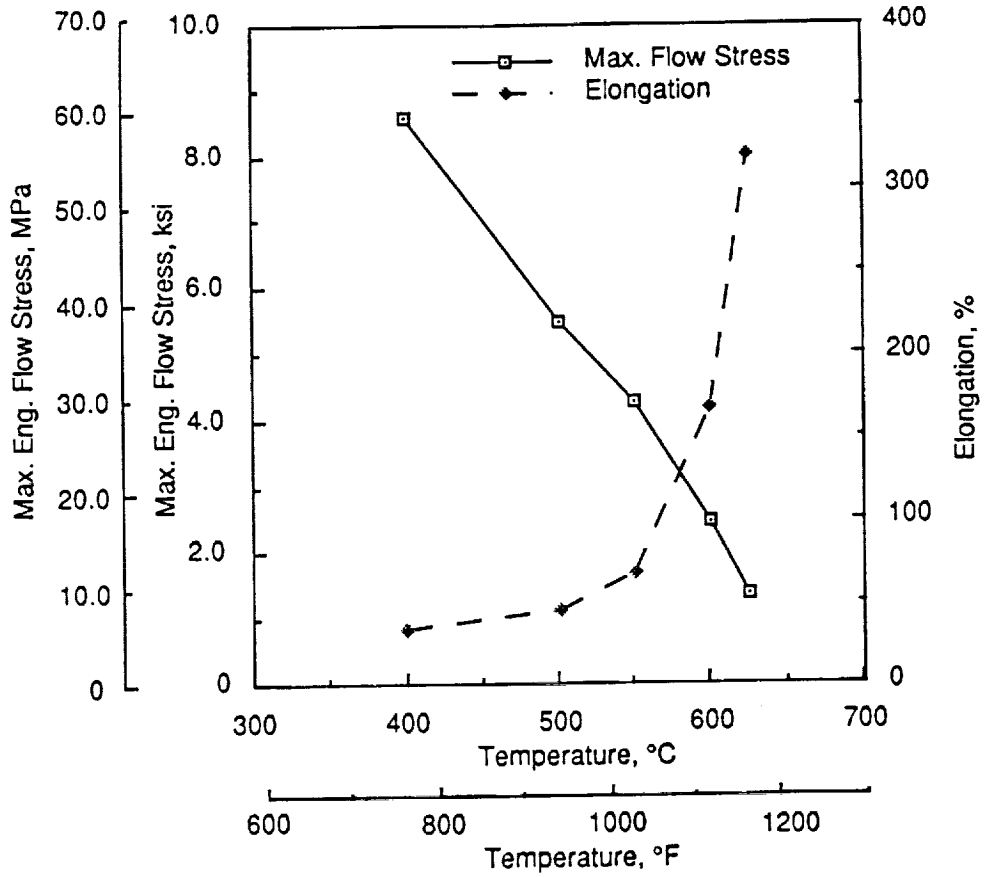

Fig. 56 Effect of Deformation Temperature on Elongation for FVS0611/500 at a Strain Rate of $0.1s^{-1}$. (Data Point at 625°C (1157°F) is from a Test at 0.05 s^{-1})

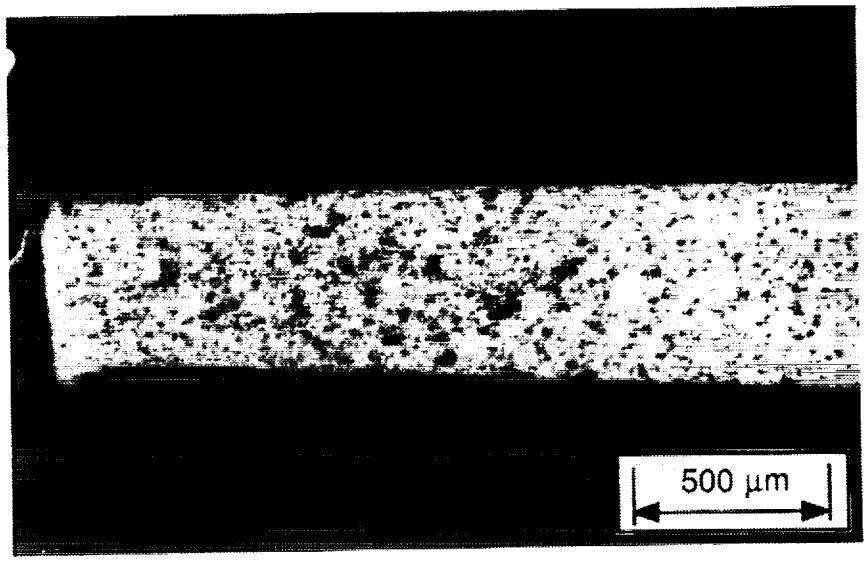

Fig. 57 Cavitation in FVS0611/500 Deformed at 625°C (1157°F) and 0.05 s^{-1}

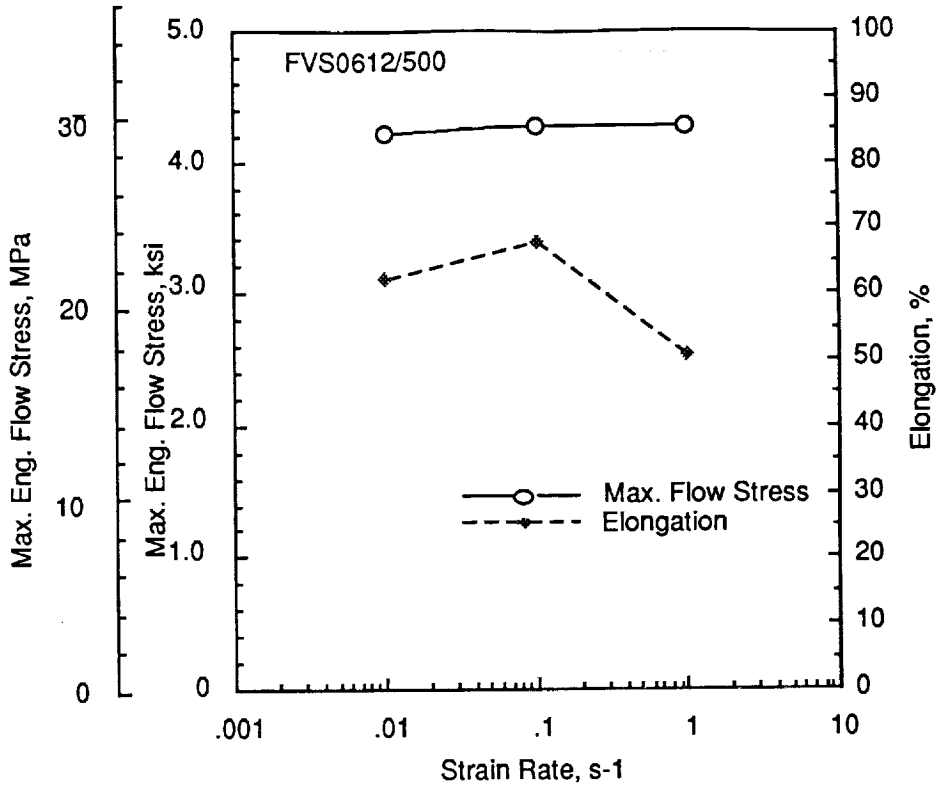

Fig. 58 Effect of Strain Rate on Strength and Elongation at 550°C (1022°F)

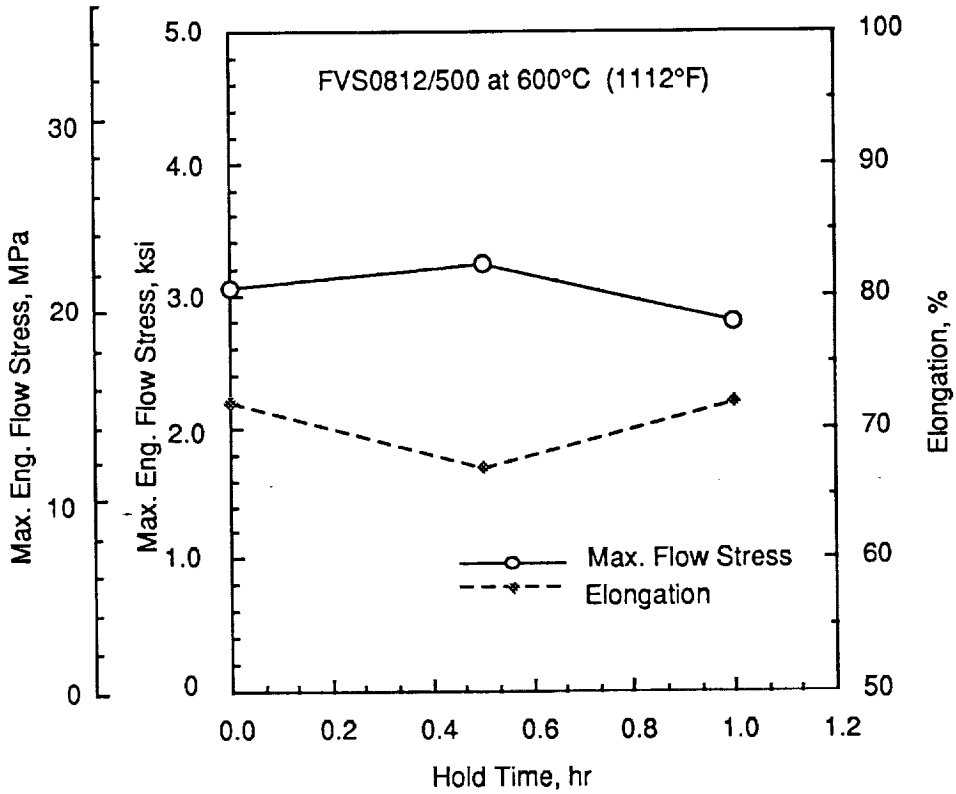

Fig. 59 Effect of Hold Time Prior to Testing on Flow Stress and Elongation of FVS0812/500

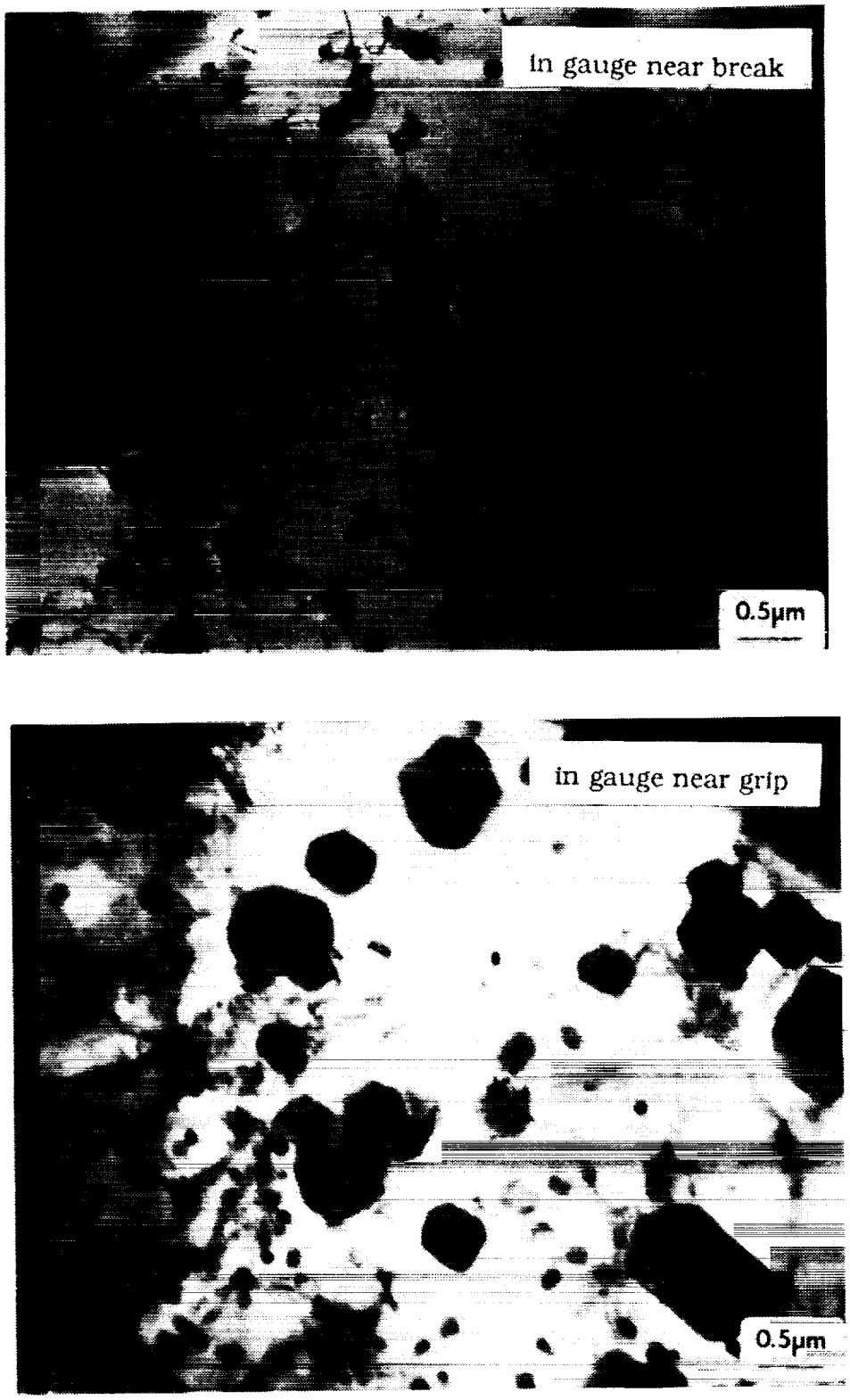

Fig. 60 TEM Micrographs of FVS0301/500 Specimen Deformed at 500°C (932°F) and 0.1 s^{-1}

Fig. 61 TEM Micrographs of FVS0611/500 Specimen Deformed at 600°C (1112°F) and 0.01 s^{-1}

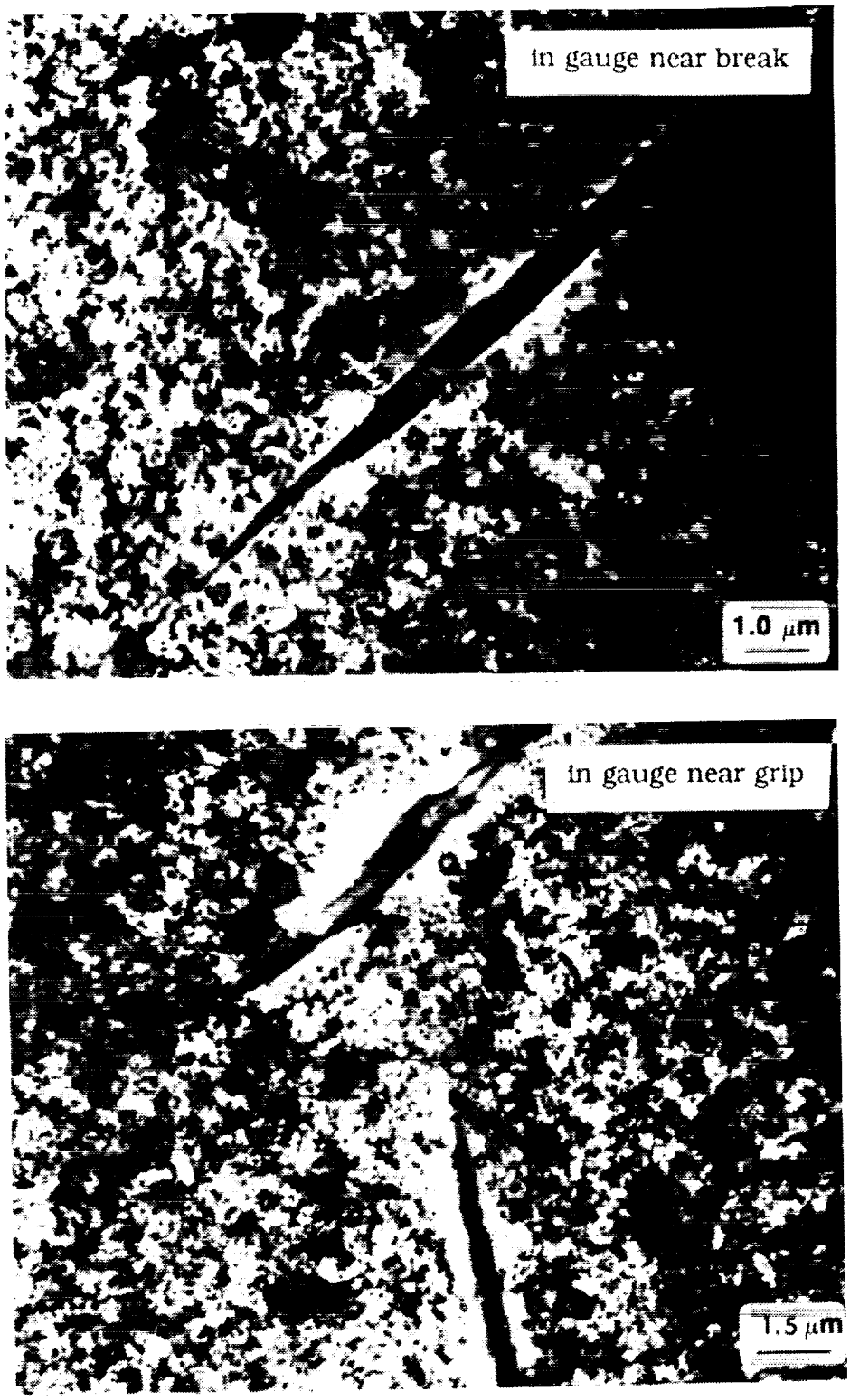

Fig. 62 TEM Micrographs of FVS0812/300 Specimen Deformed at 600°C (1112°F) and 2.2 s^{-1}

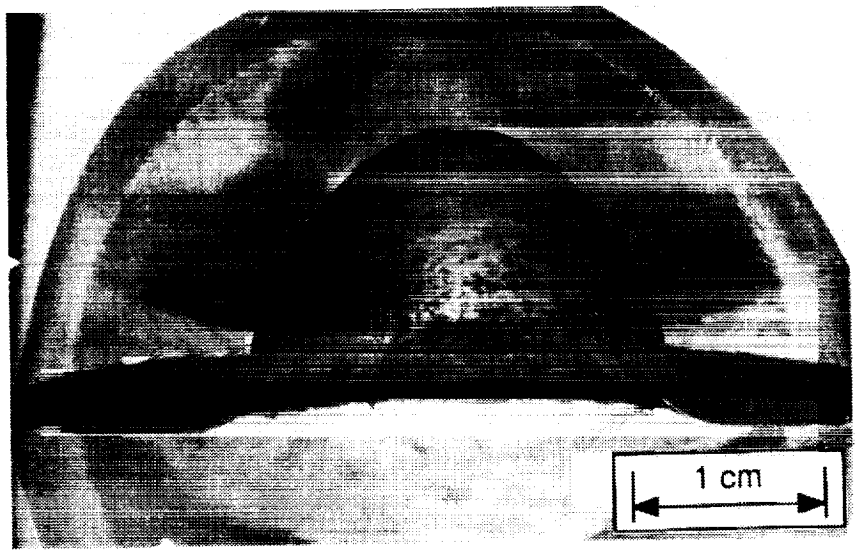

Fig. 63 **FVS0611/500 Dome Formed Using Gas Pressure at 600°C (1112°F)**

ORIGINAL PAGE
BLACK AND WHITE PHOTOGRAPH

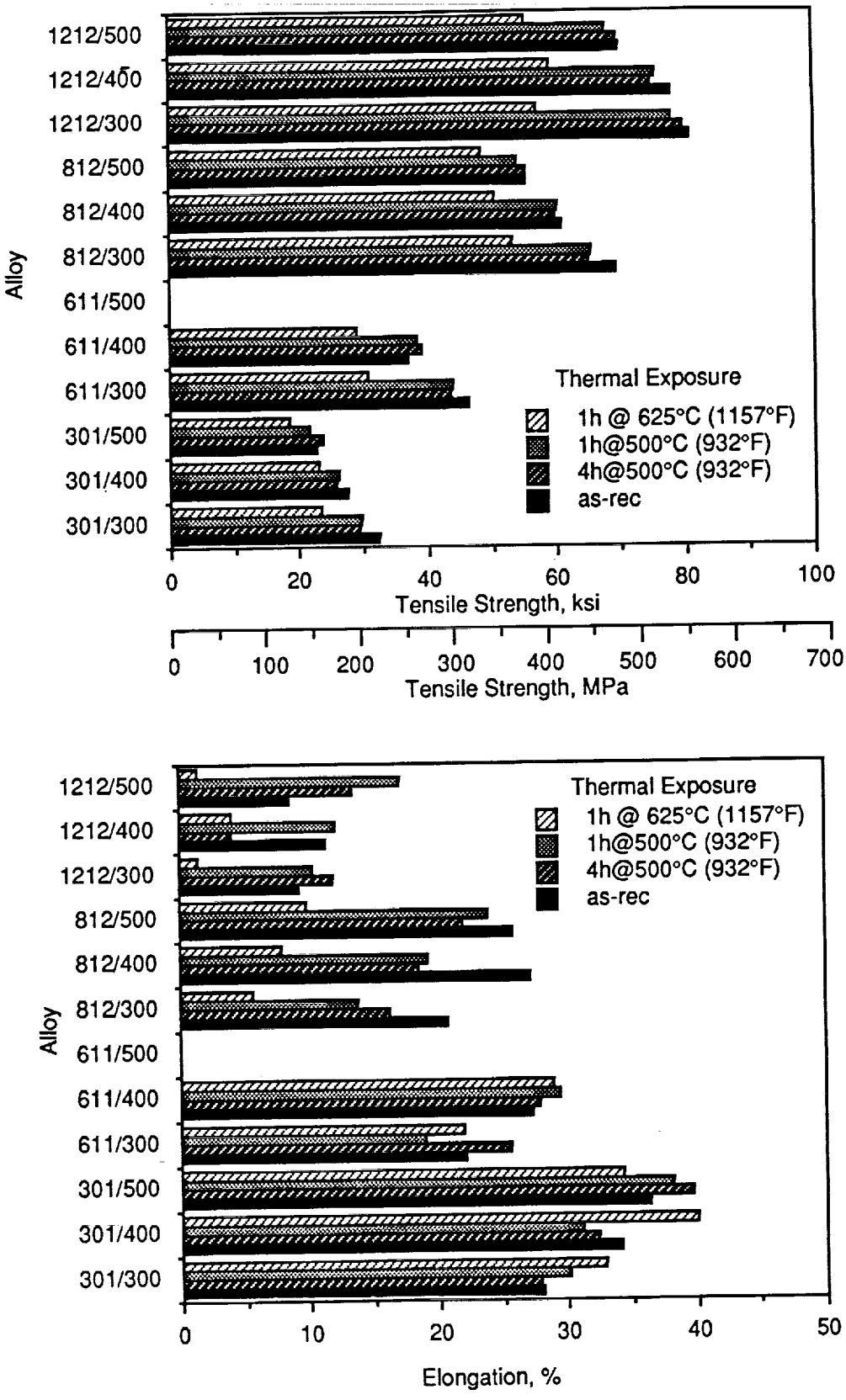

Fig. 64 Elongation and Tensile Strength of Sheet After Elevated Temperature Exposure

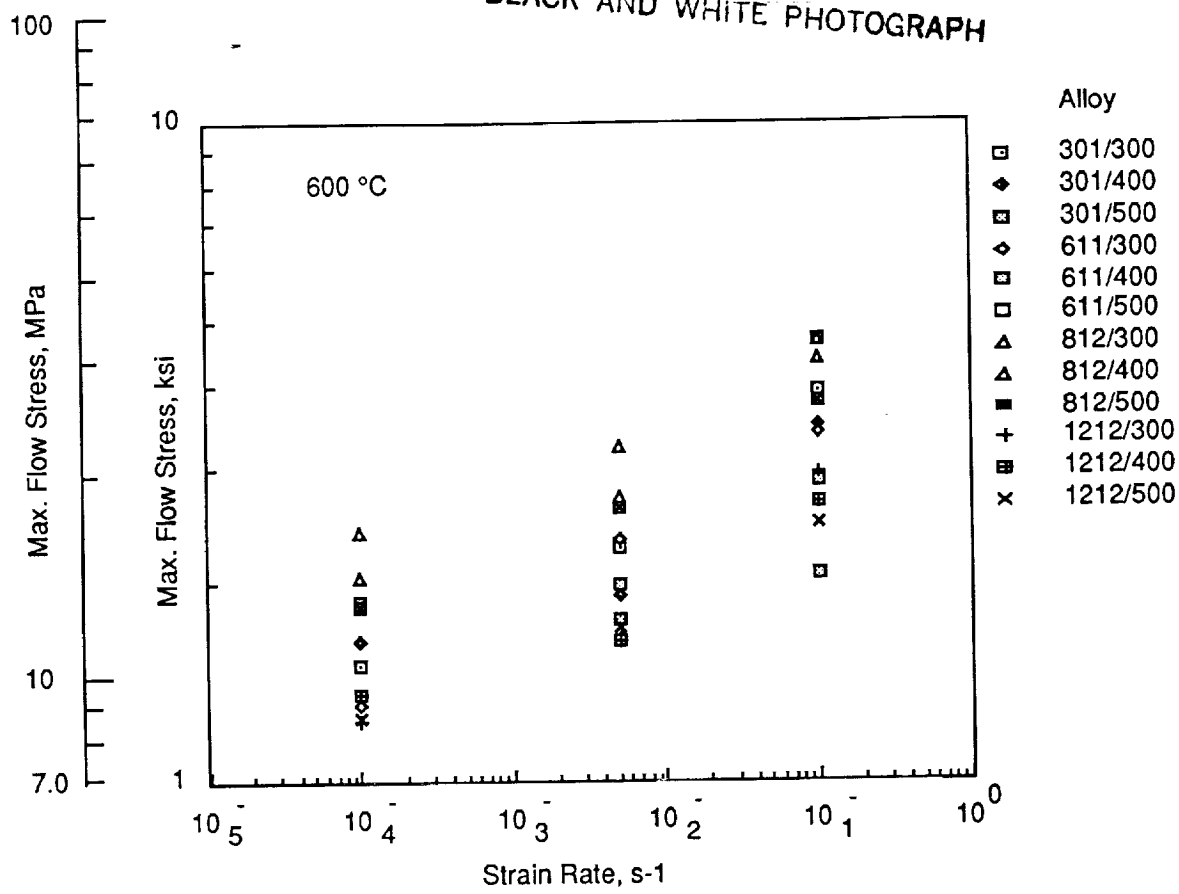

Fig. 65 Effect of Strain Rate on Flow Stress at 600°C (1112°F)

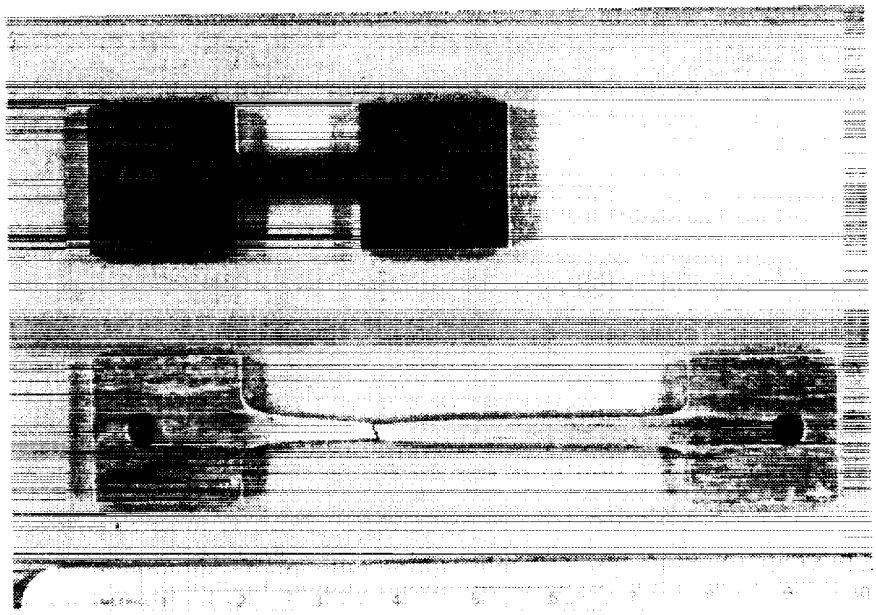

Fig. 66 Enhanced Ductility in FVS0611/500 Alloy

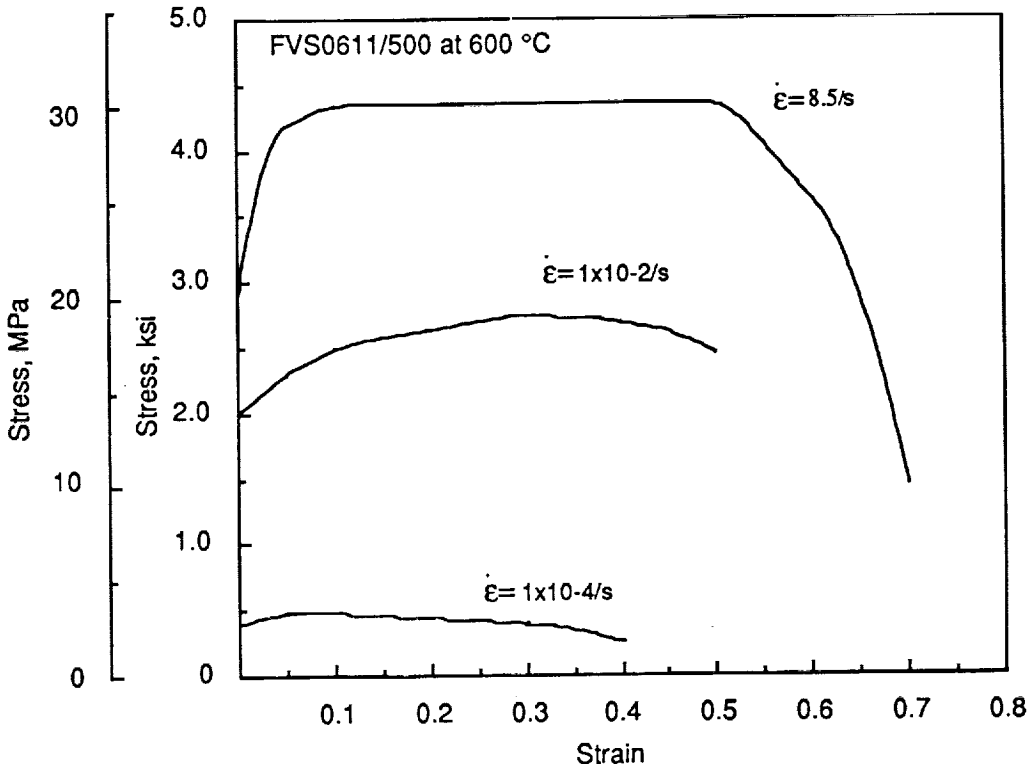

Fig. 67 Stress Strain Curves of Maximum Ductility Alloy Condition

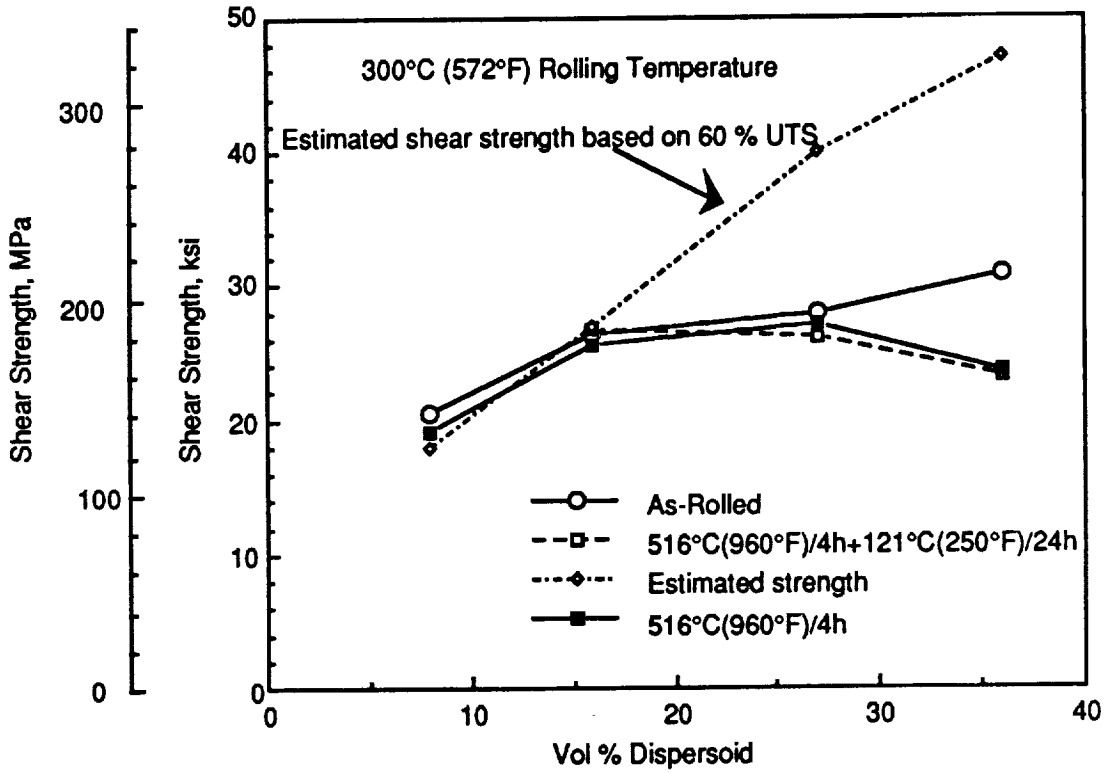

Fig. 68 Effect of Dispersoid Volume Percent and Thermal Exposure on Base Metal Shear Strength

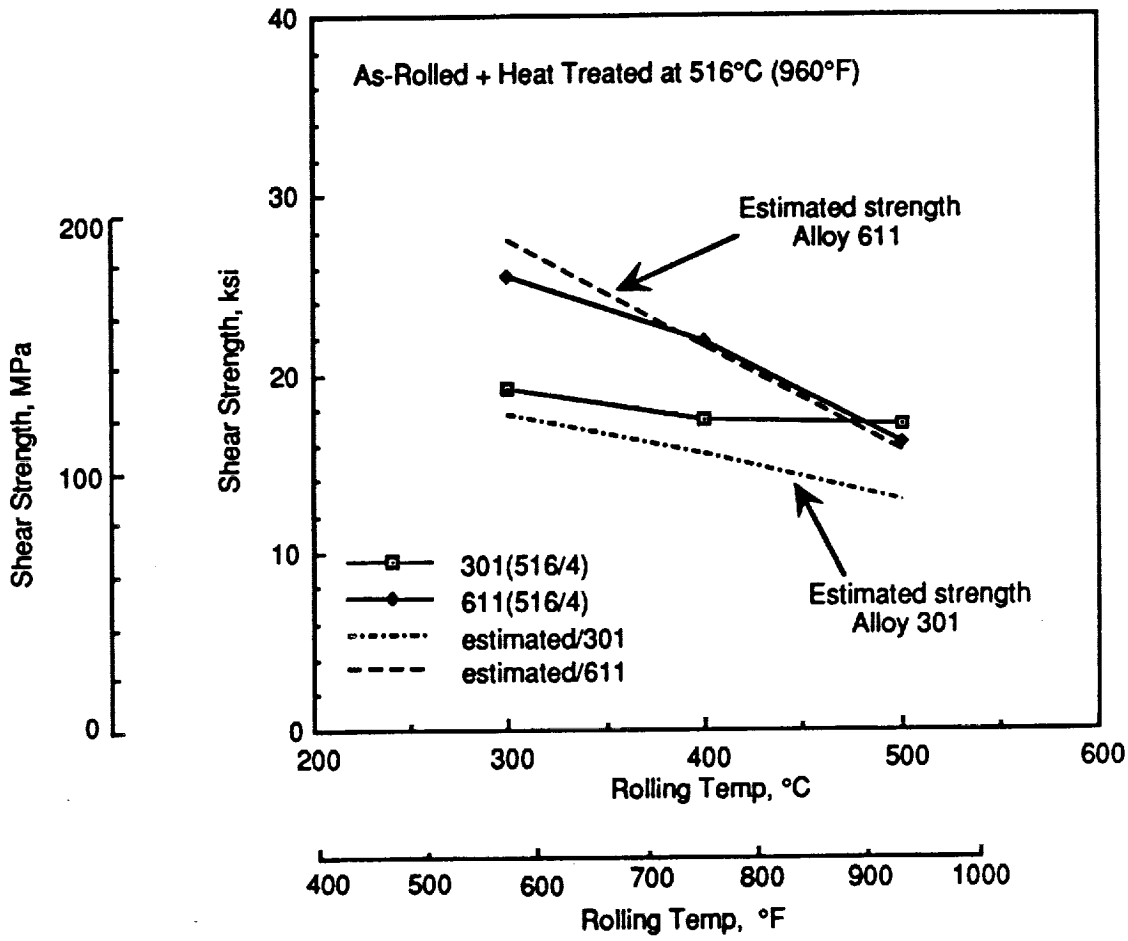

Fig. 69 Effect of Rolling Temperature and Thermal Exposure on Base Metal Shear Strength

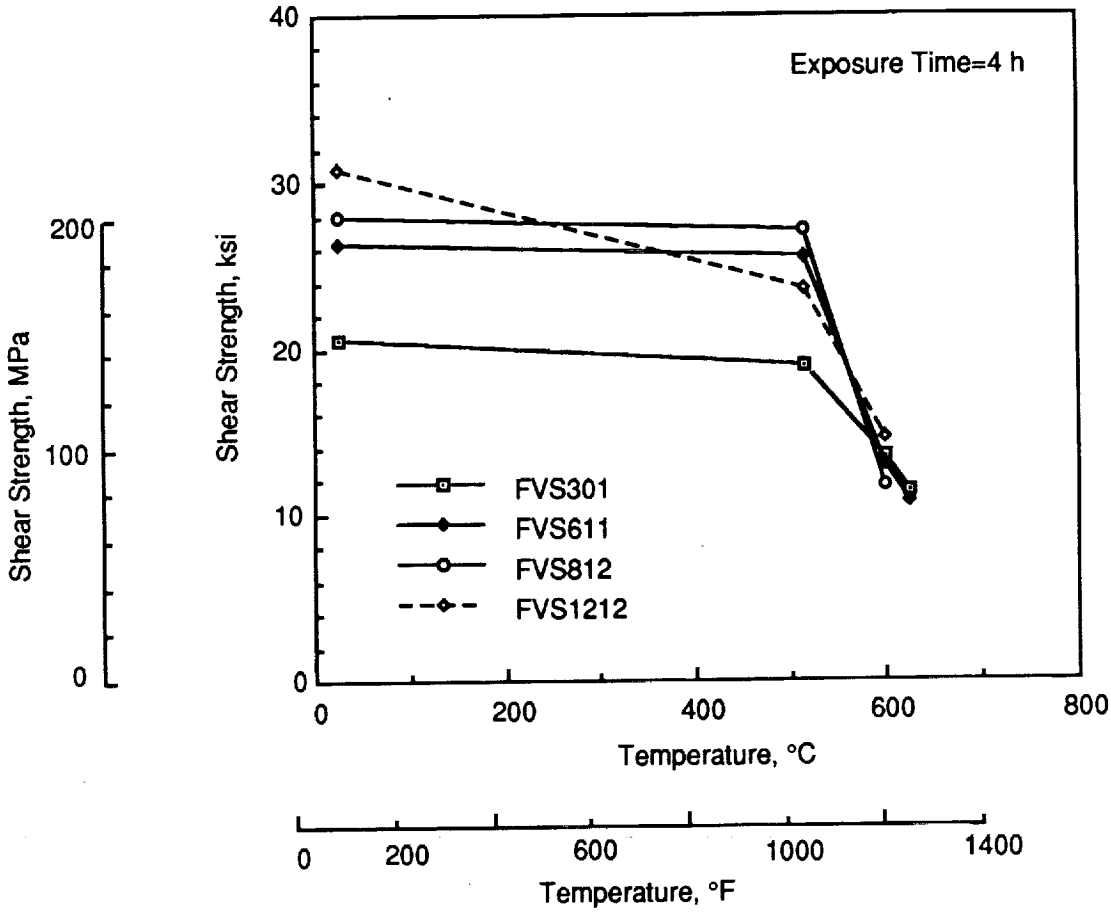

Fig. 70 Effect of Temperature on Base Metal Shear Strength

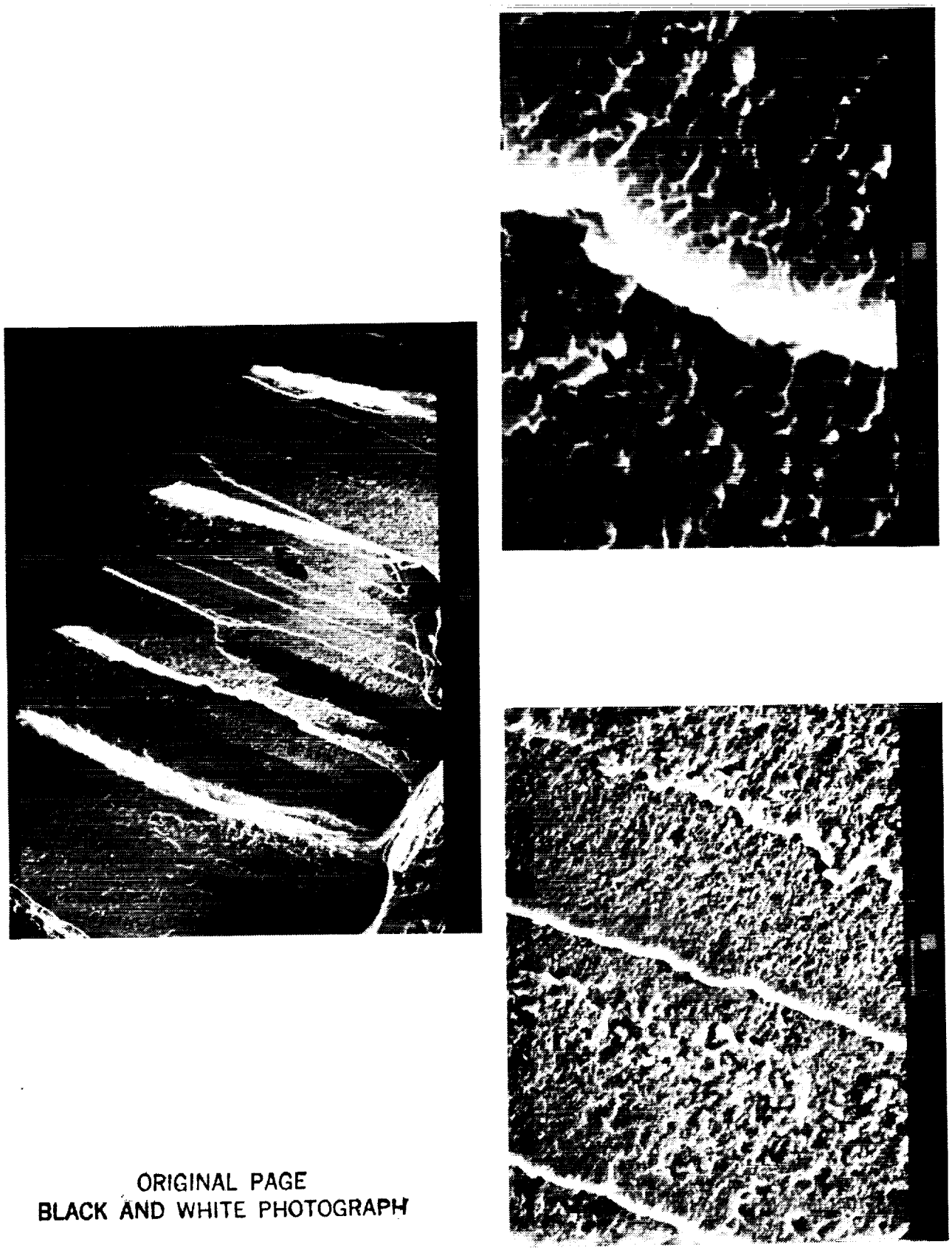

Fig. 71 Fracture Surface of Unbonded, As-Rolled FVS0812/300

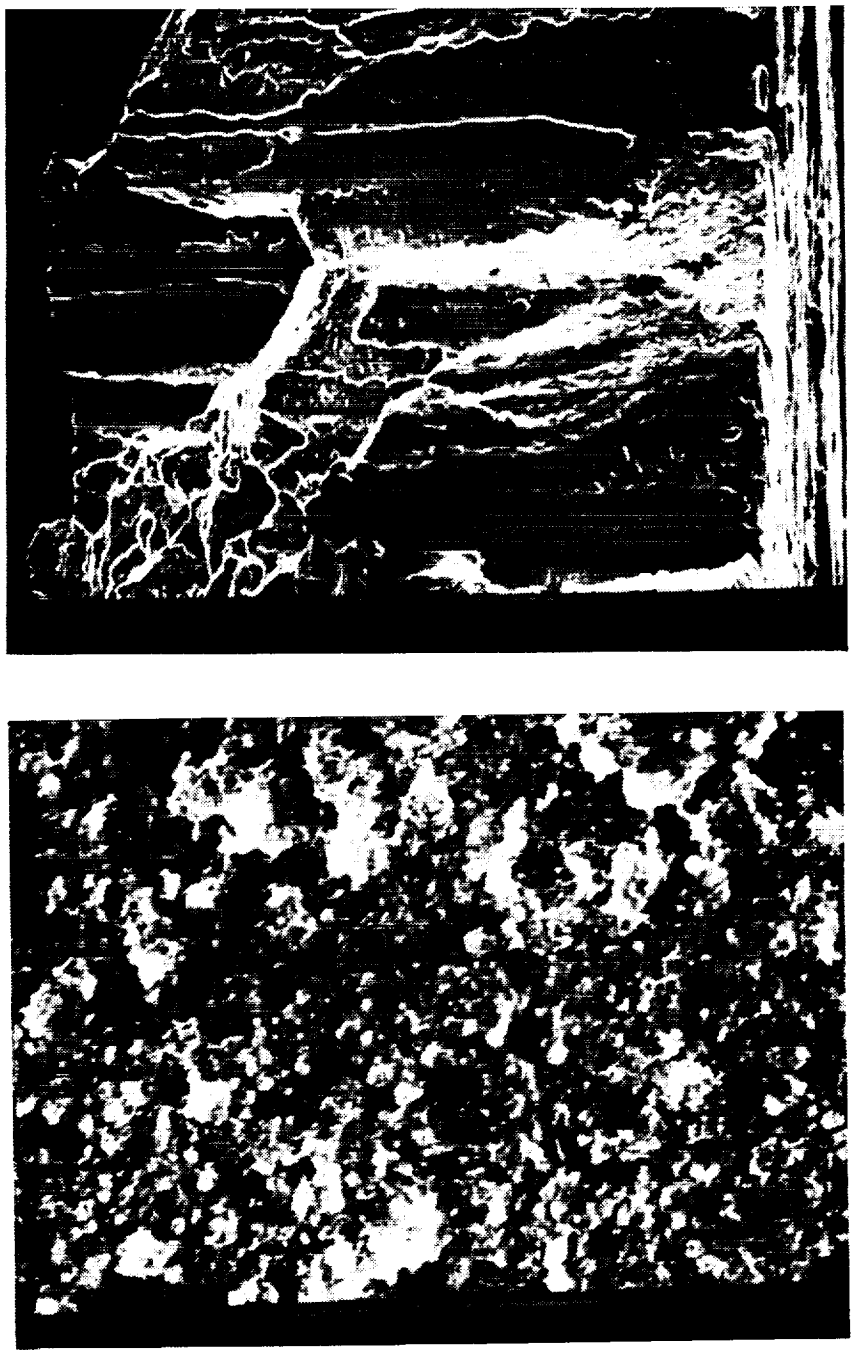

Fig. 72 Fracture Surface of Unbonded, As-Rolled FVS1212/300

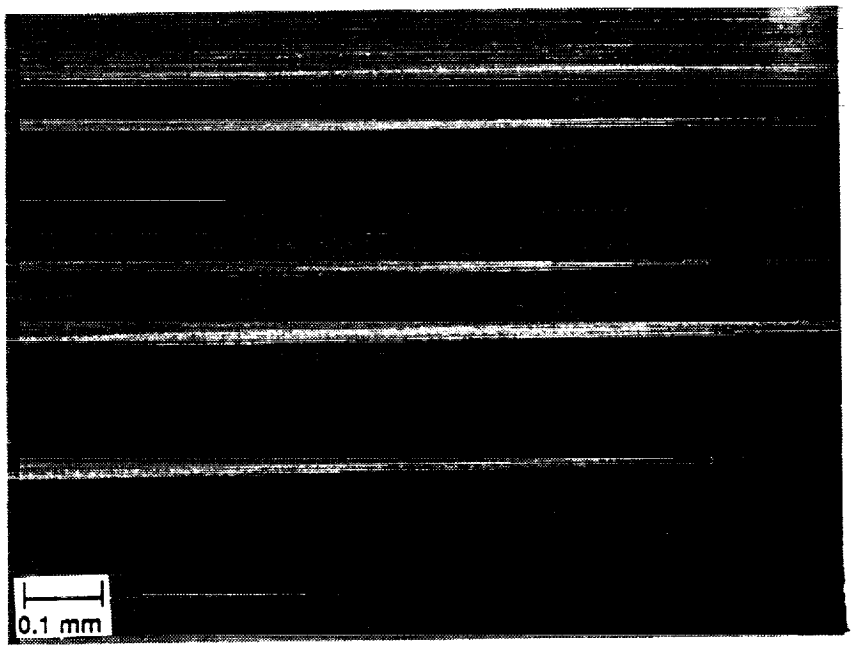

Fig. 73 Microstructural Non-Uniformities (Layers Or Laminations) In Rolled Alloy FVS0812/300

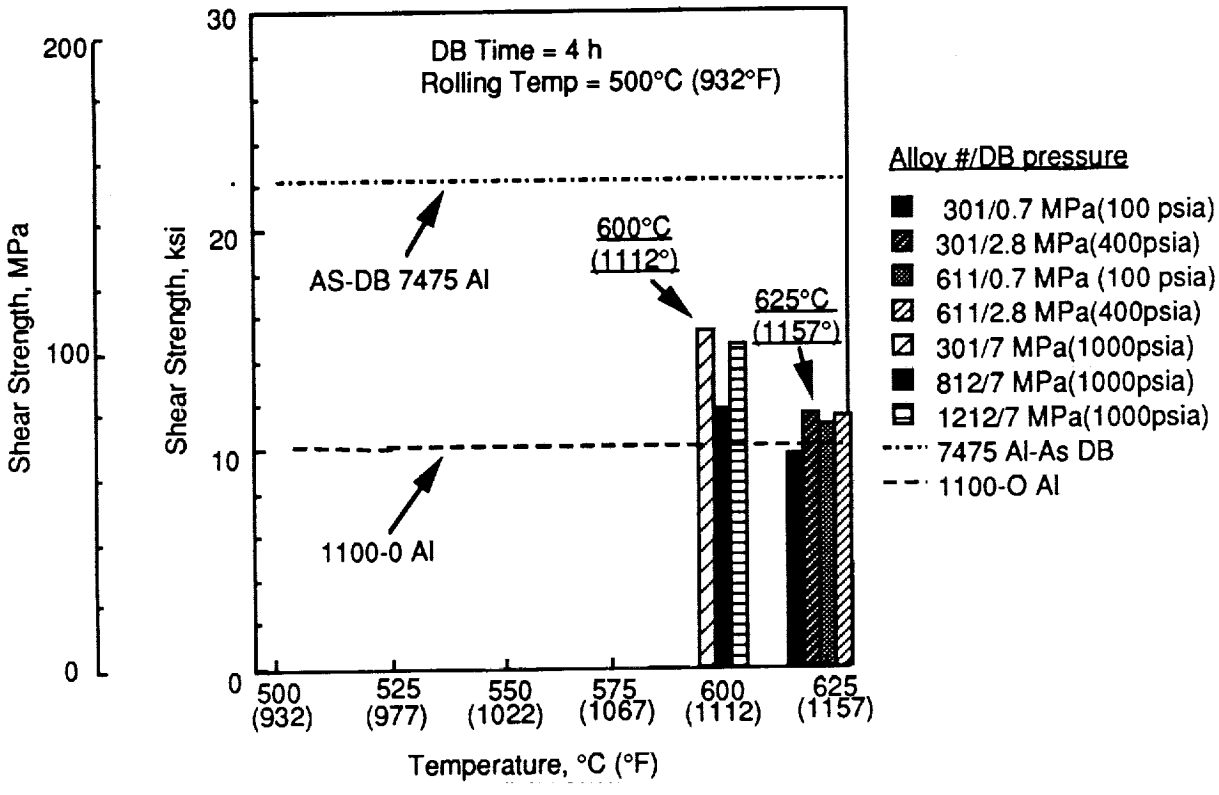

Fig. 74 Effect of Diffusion Bonding Pressure and Time on Shear Strength of Al-Fe-V-Si Alloys

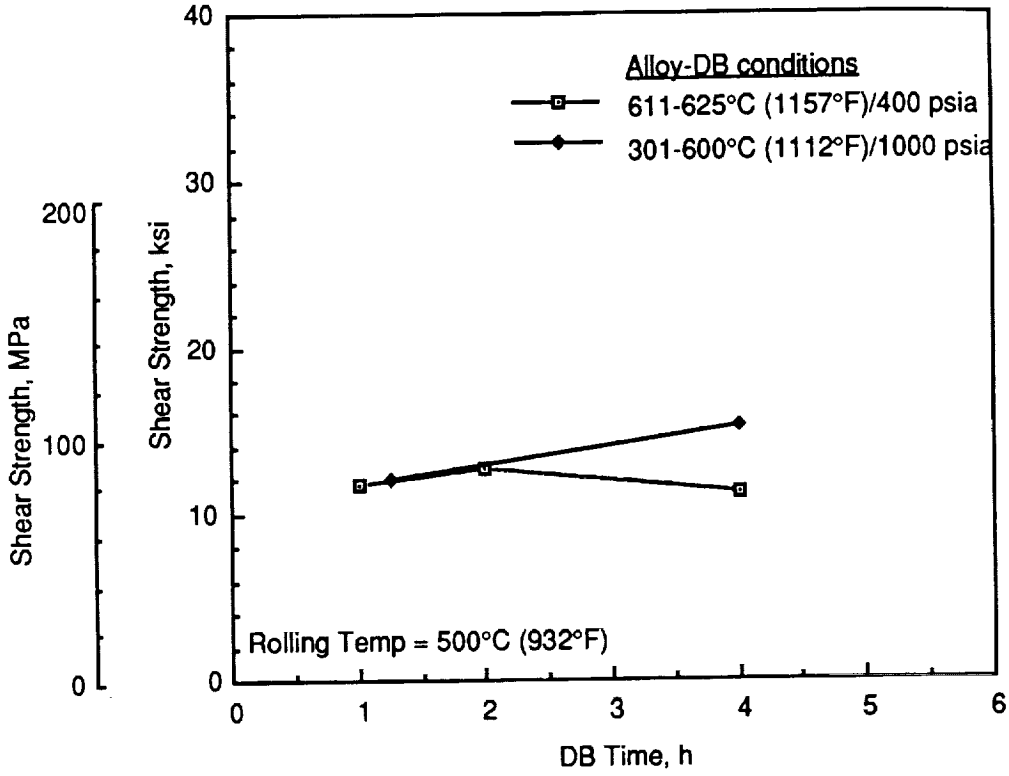

Fig. 75 Effect of Pressure and Temperature on Bond Shear Strength

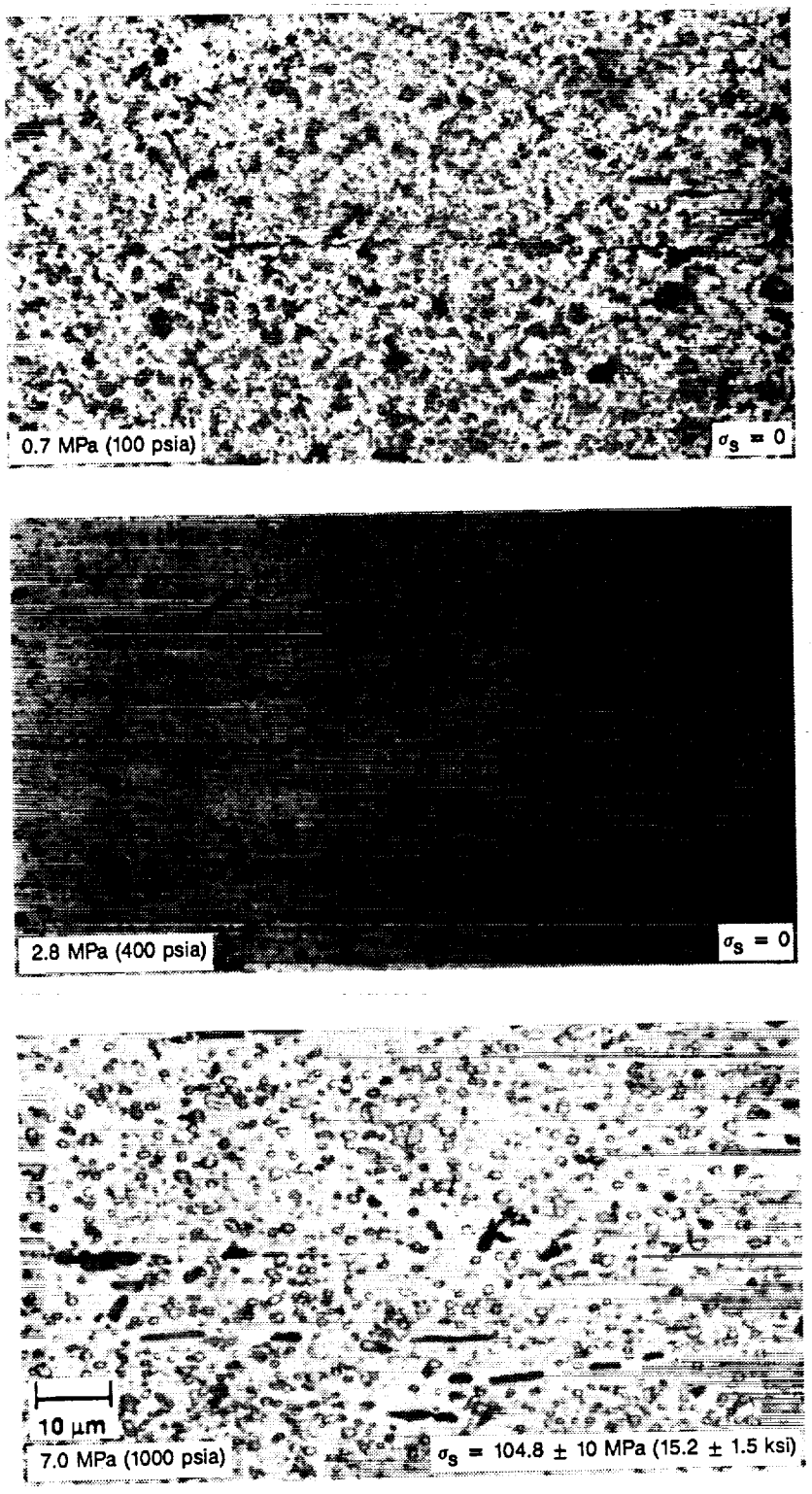

Fig. 76 Effect of Diffusion Bonding Pressure on Bond Shear Strength After Bonding at 600 °C (1112°F) /4 h

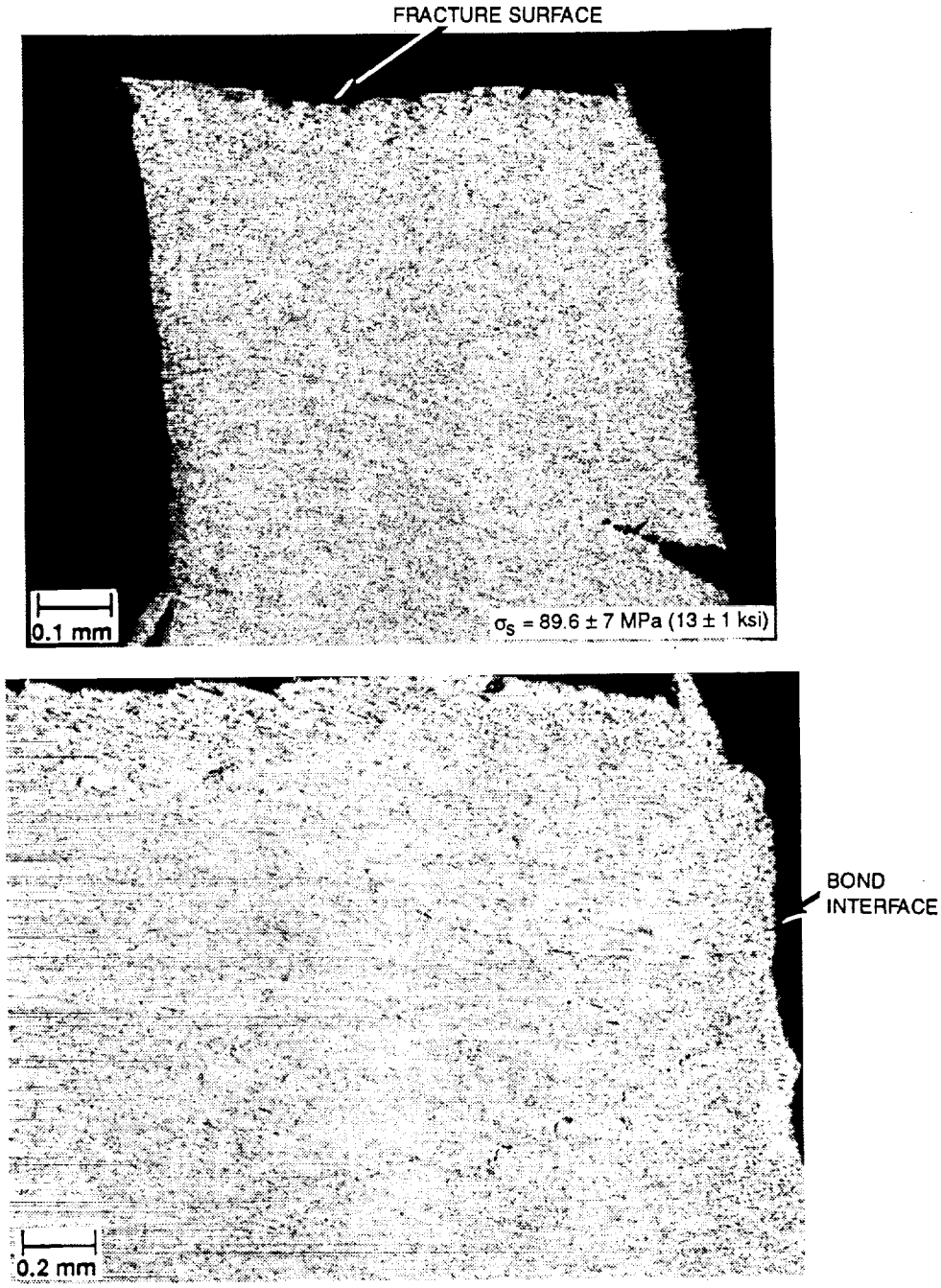

Fig. 77 Shear Failure in FVS0611/500, Bonded at 600°C (1112°F)/ 6.90 MPa (1000 psia)/ 1.25 h

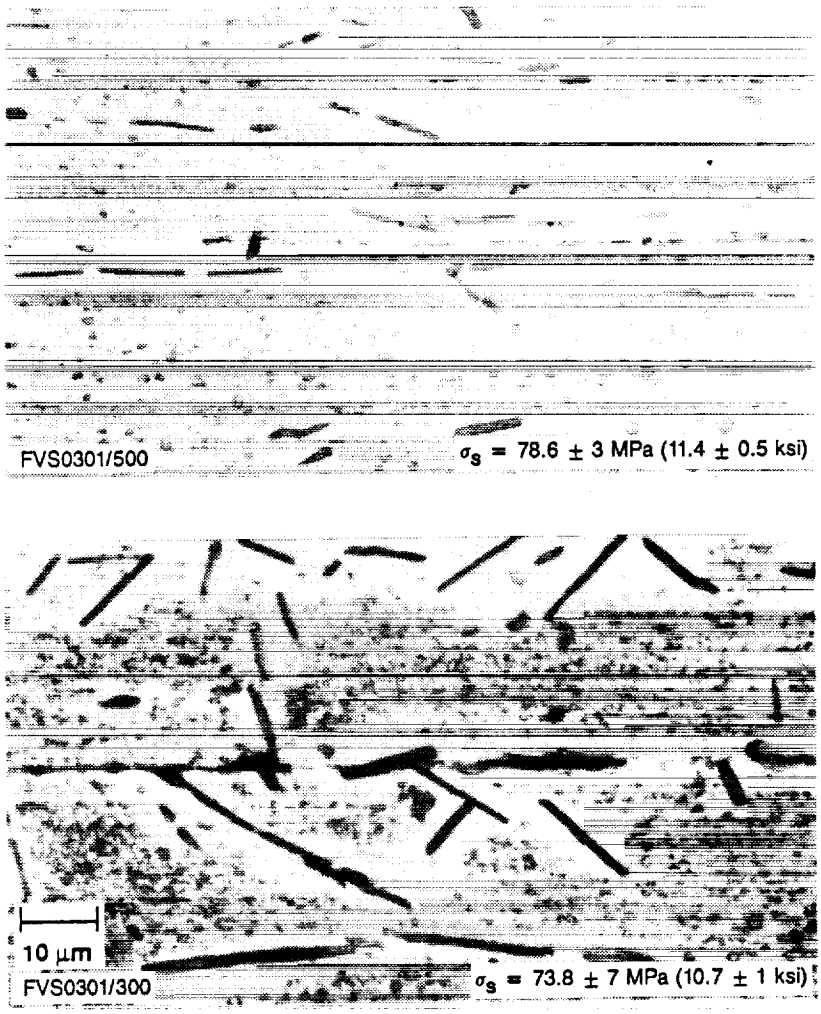

Fig. 78 Microstructure of FVS0301 Bond Regions After DB at 625°C (1157°F) /2.8 MPa (400 psia)/4 h

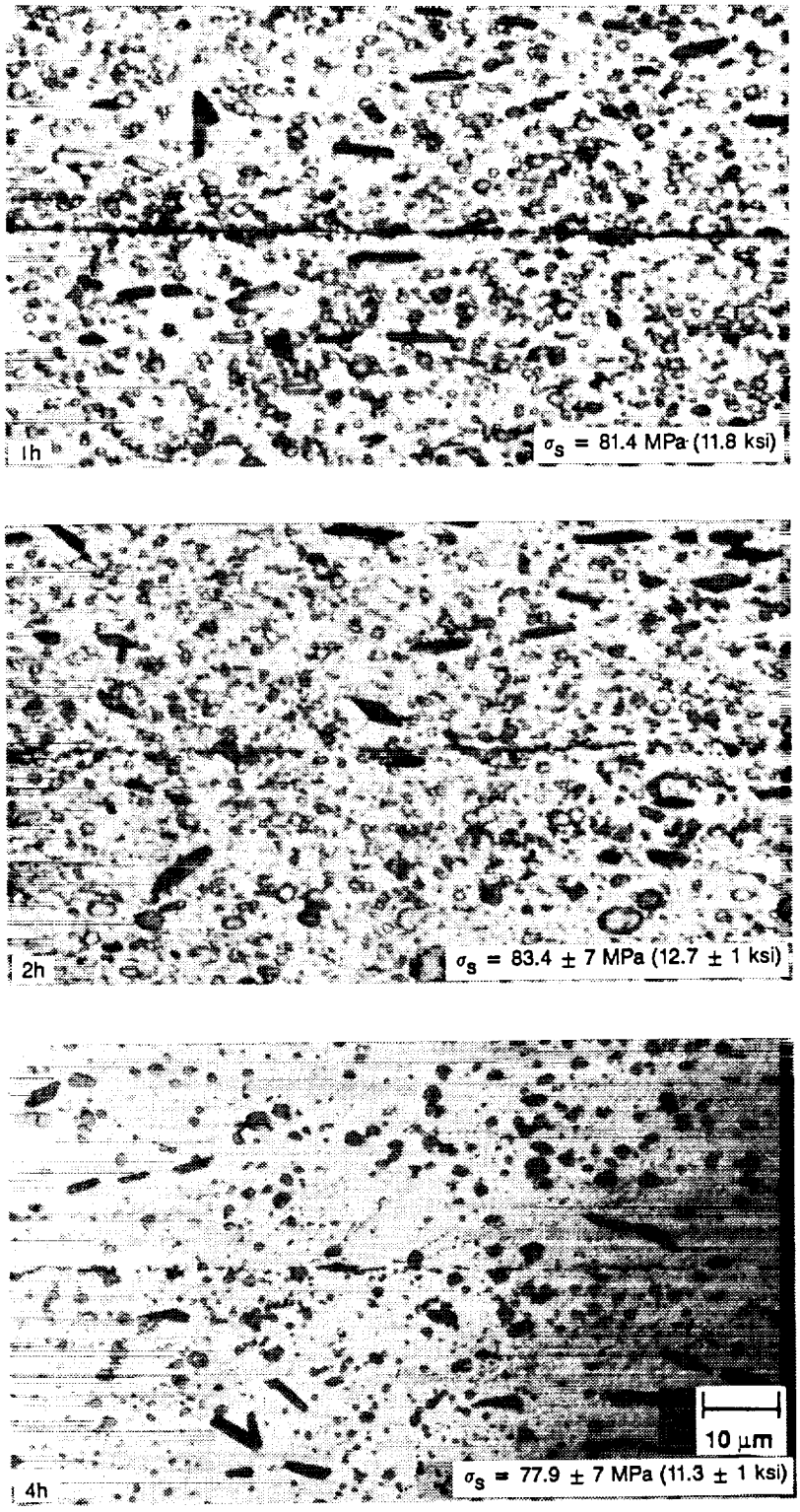

Fig. 79 **Effect of Bonding Time and Temperature on Bond Interface Microstructure and Strength of FVS0611/500**

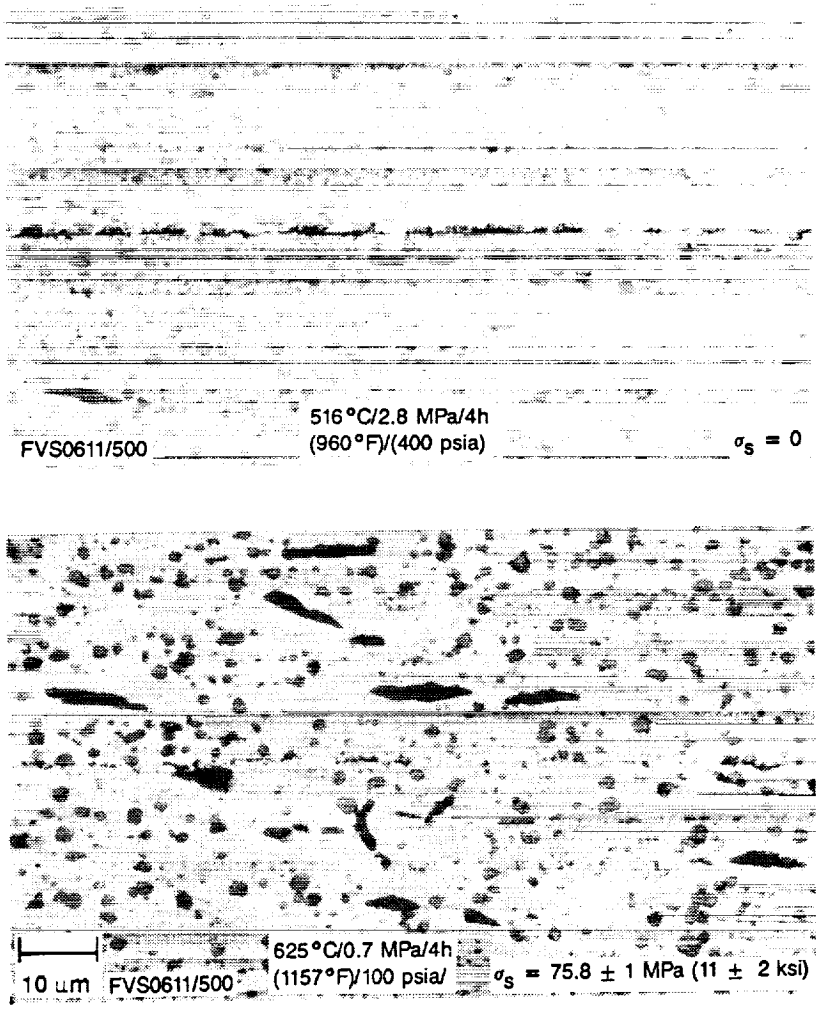

Fig. 80 Effect of Temperature on Microstructure of Bondline in FVS0611/500 Diffusion Bonds

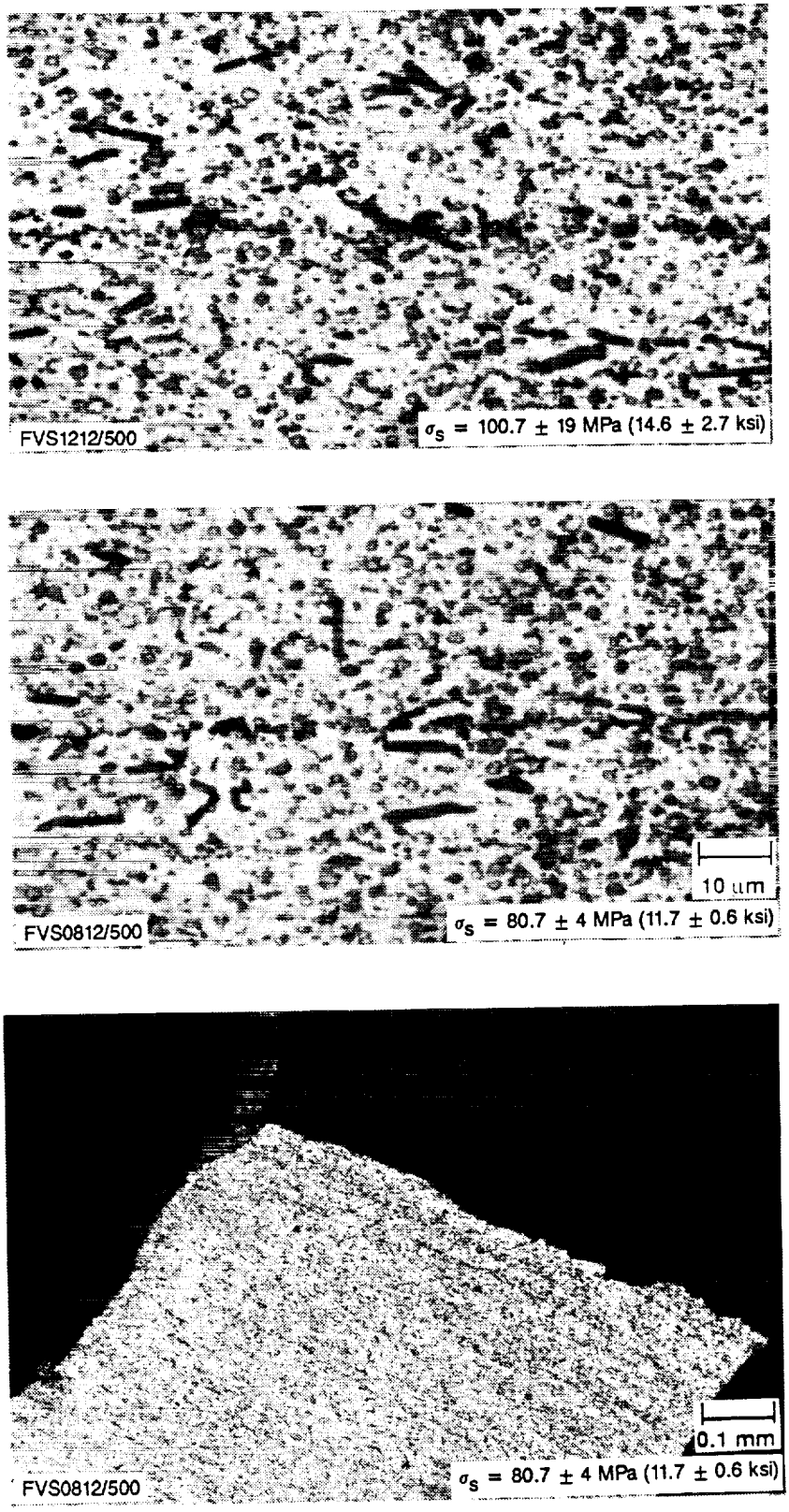

Fig. 81 **Bond Interface Microstructure of High Volume Fraction Alloy Conditions After Bonding at 600°C (1112°F) for 4 h Under 6.90 MPa (1000 psia)**

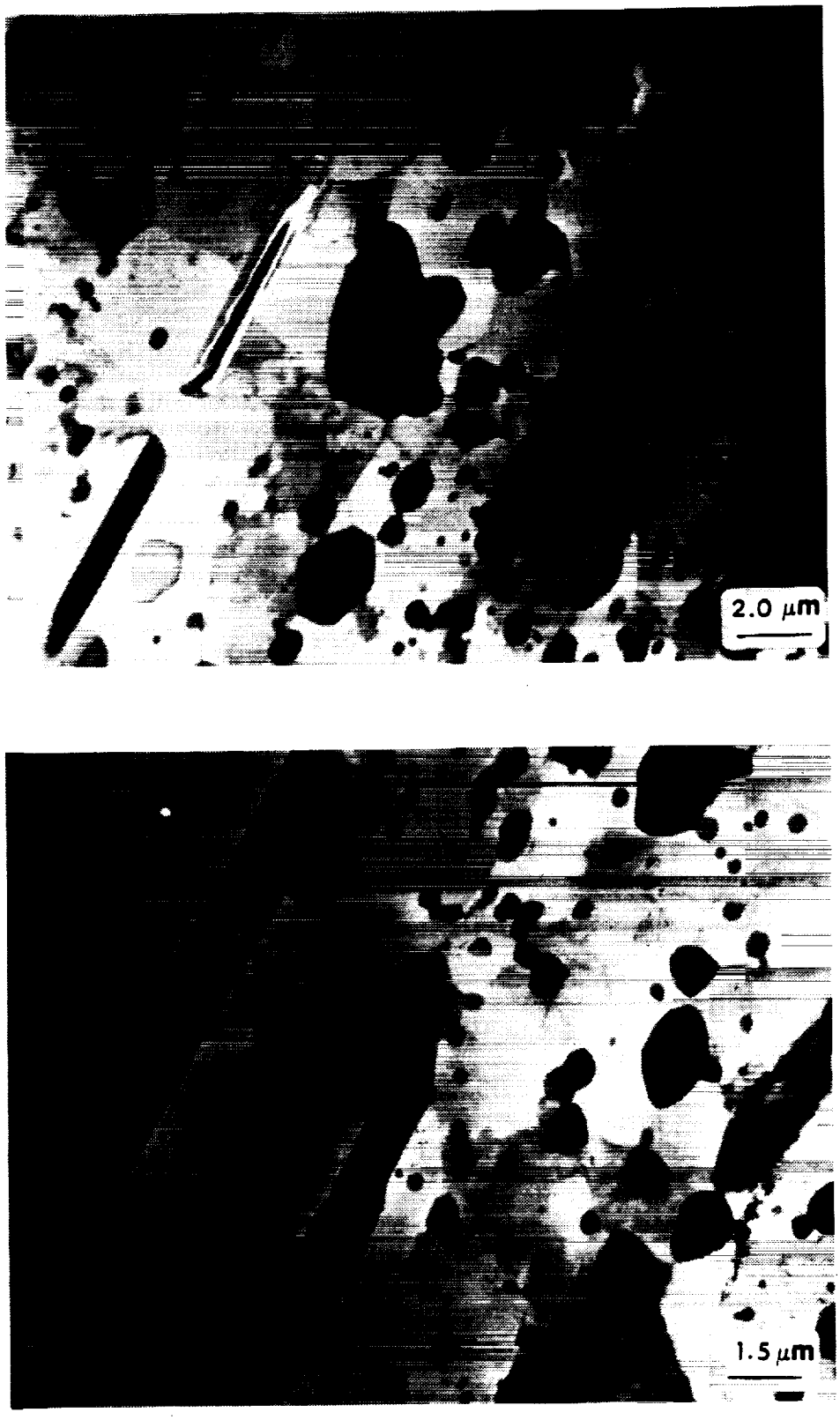

Fig. 82 TEM Micrographs of FVS0812 Bonded at 600°C (1112°F)/ 4 h/ 1000 psia

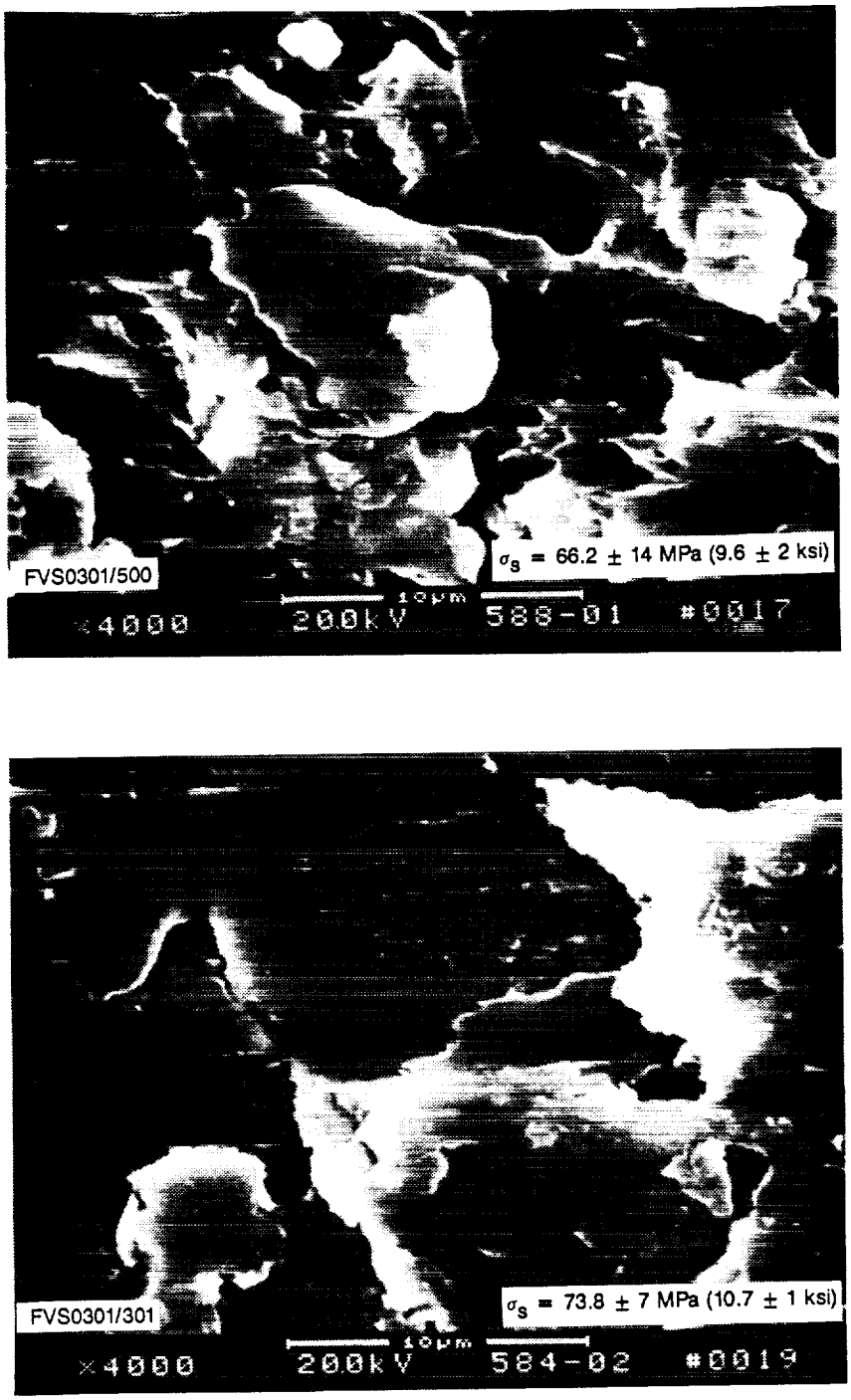

Fig. 83 SEM Fractographs of Shear Fracture Surfaces of FVS0301/300 Bonds and FVS0301/500 Bonds, Bonded at 625°C (1157°F) for 4 h

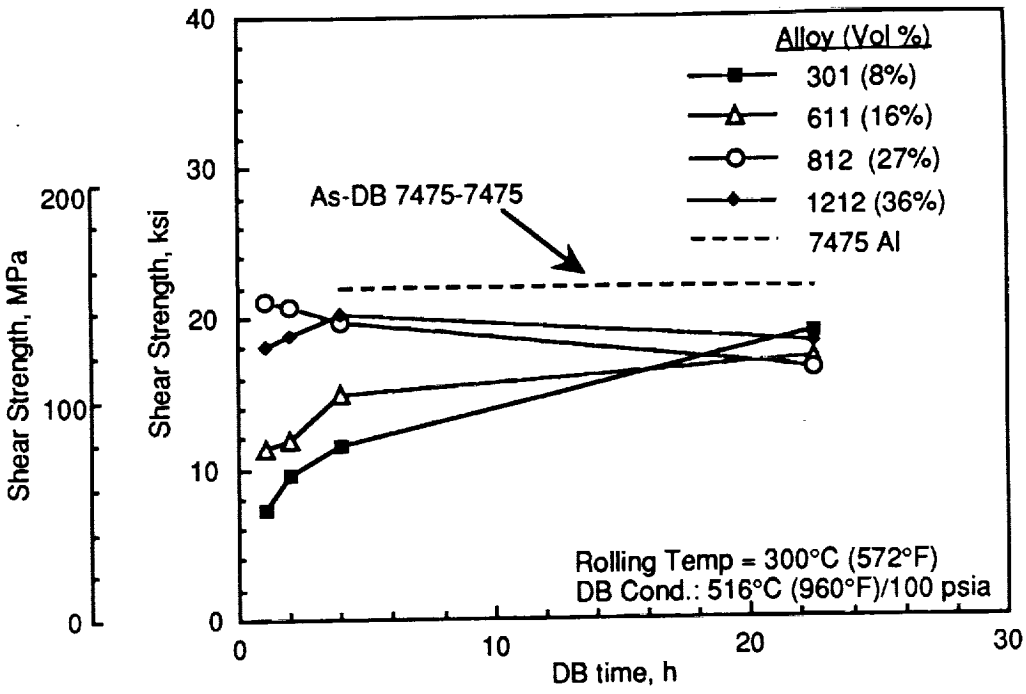

Fig. 84 Effect of Diffusion Bonding Time on Shear Strength of Dissimilar Bonds

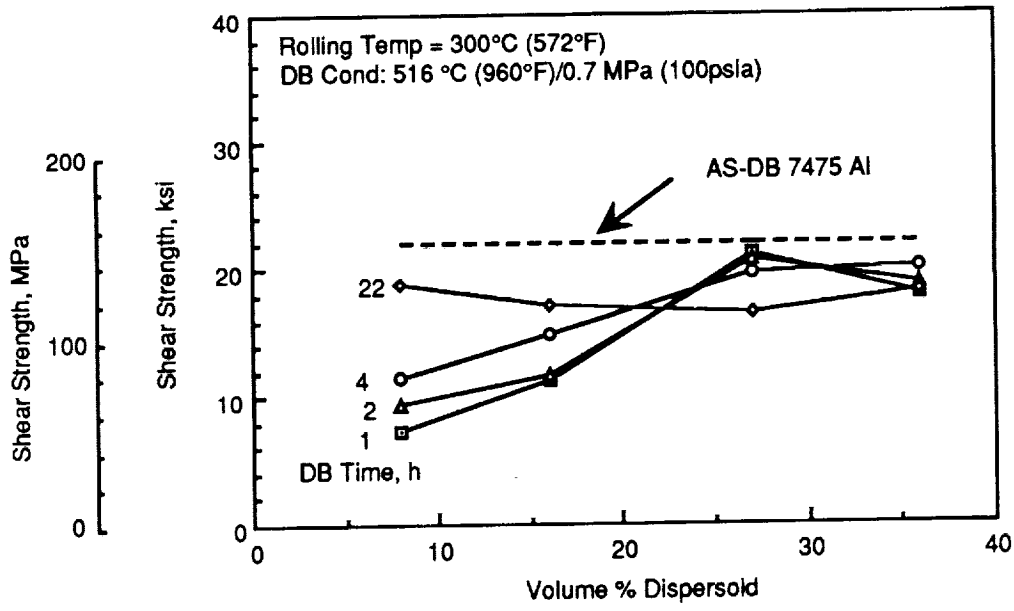

Fig. 85 Effect of Dispersoid Content on Shear Strength of Dissimilar Bonds

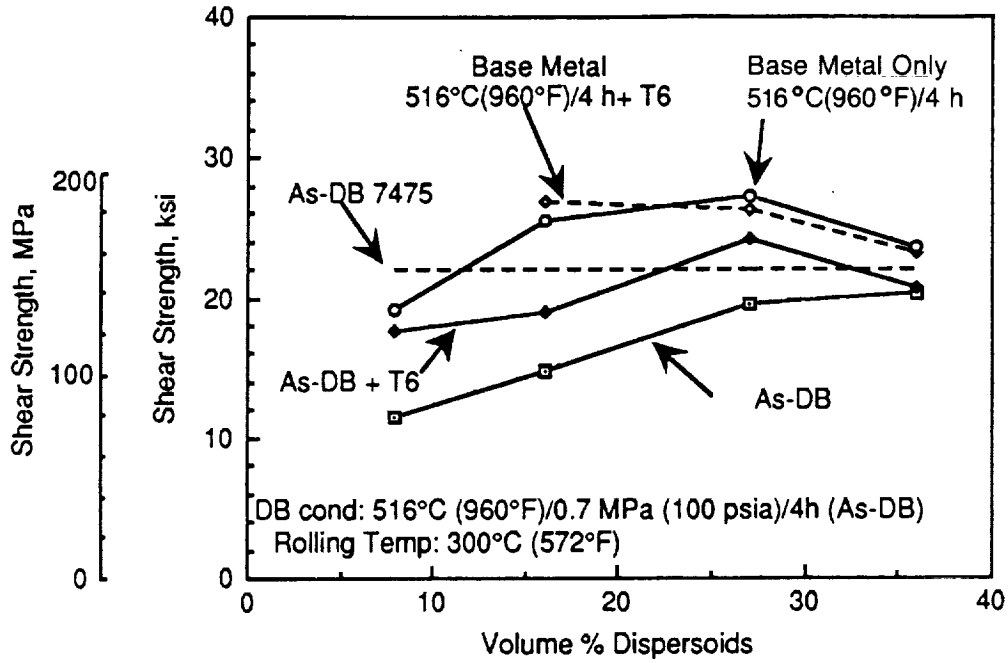

Fig. 86 Effect of Heat Treatment on Shear Strength of Dissimilar Al-Fe-V-Si Bonds with 7475 Al Alloy

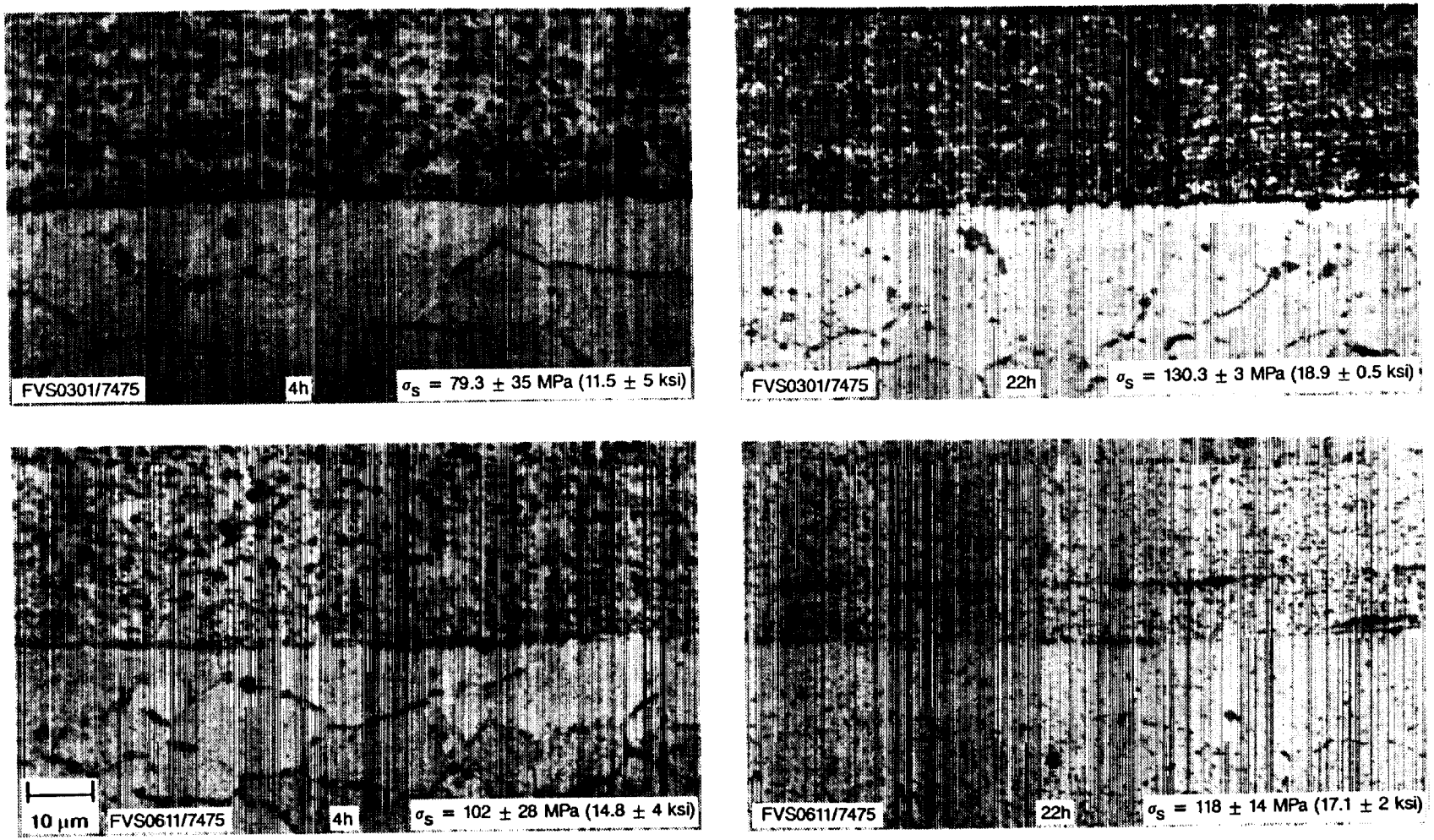

Fig. 87 Interface Microstructure of Bond Region Between FVS0301 and FVS0611 Alloys and 7475 Aluminum Alloy After Diffusion Bonding at 516°C (960°F) at 0.7 MPa (100 psia)

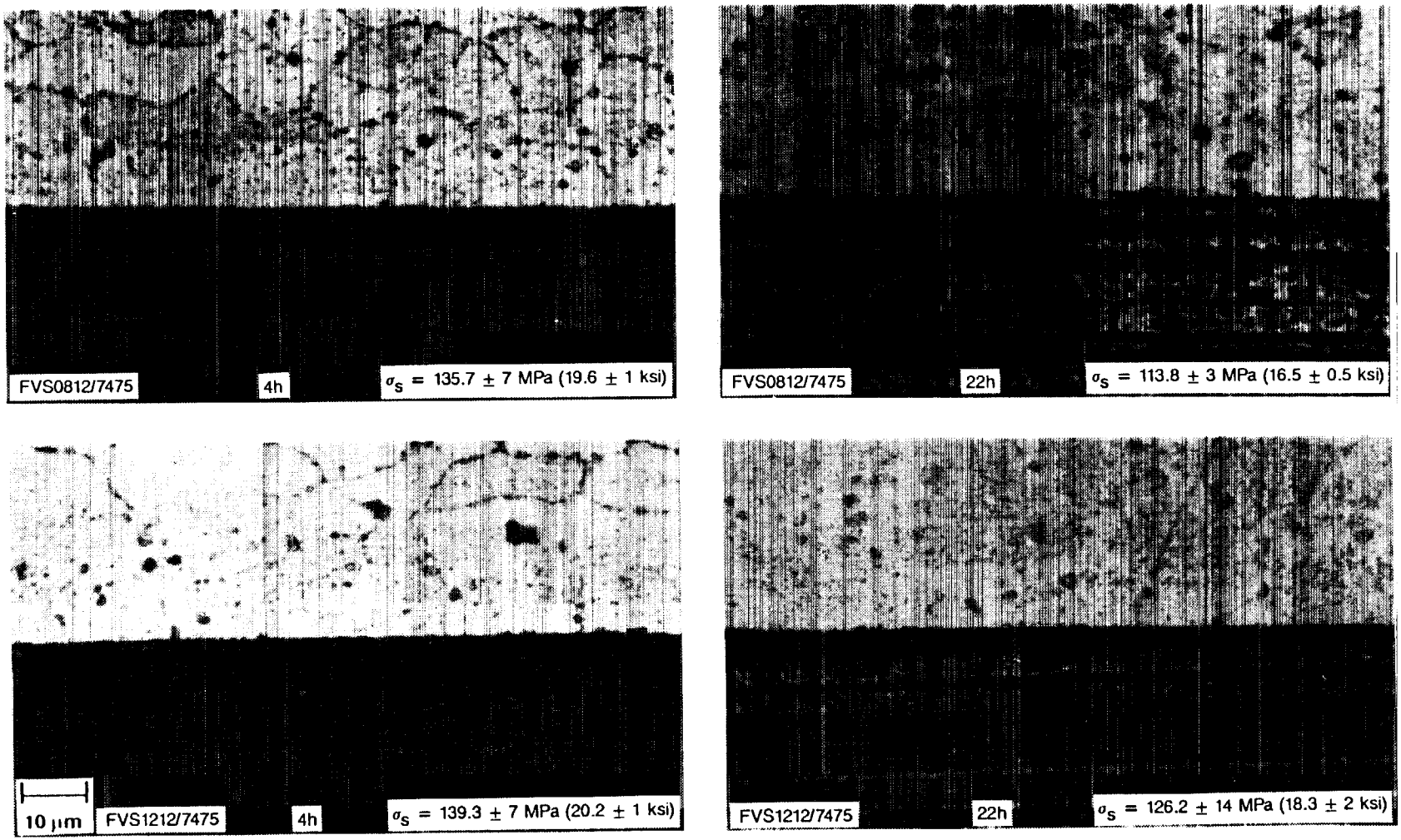

Fig. 88 Interface Microstructure of Bond Region Between FVS0812 and FVS1212 Alloys and 7475 Aluminum Alloy After Diffusion Bonding at 516°C (960°F) at 0.7 MPa (100 psia)

Fig. 89 TEM Micrographs of Dissimilar Bonds Between FVS0812 and 7475 Aluminum Alloy in the As-Bonded Condition After Bonding at 516°C (960°F) for 2 h at 0.7 MPa (100 psia)

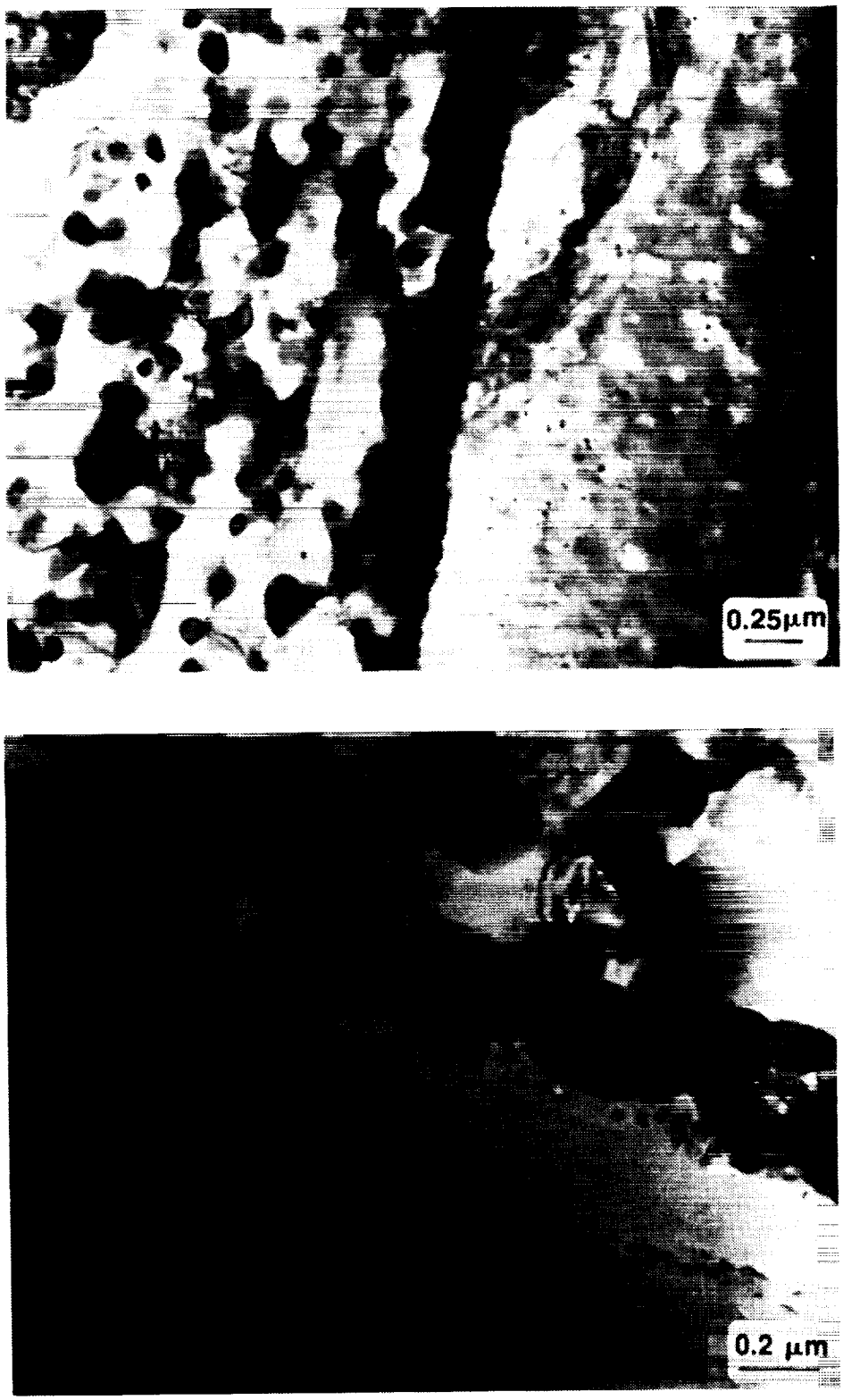

Fig. 90 TEM Micrographs of Dissimilar Bonds Between FVS0812 and 7475 Aluminum Alloy in the Heat Treated Condition (T6) After Bonding at 516°C (960°F) for 2 h at 0.7 MPa (100 psia)

Fig. 91 The Effect of Bonding Time on Interface Diffusion Between FVS0812 and 7475 Aluminum Alloy After Bonding at 516°C (960°F) and 0.7 MPa (100 psia)

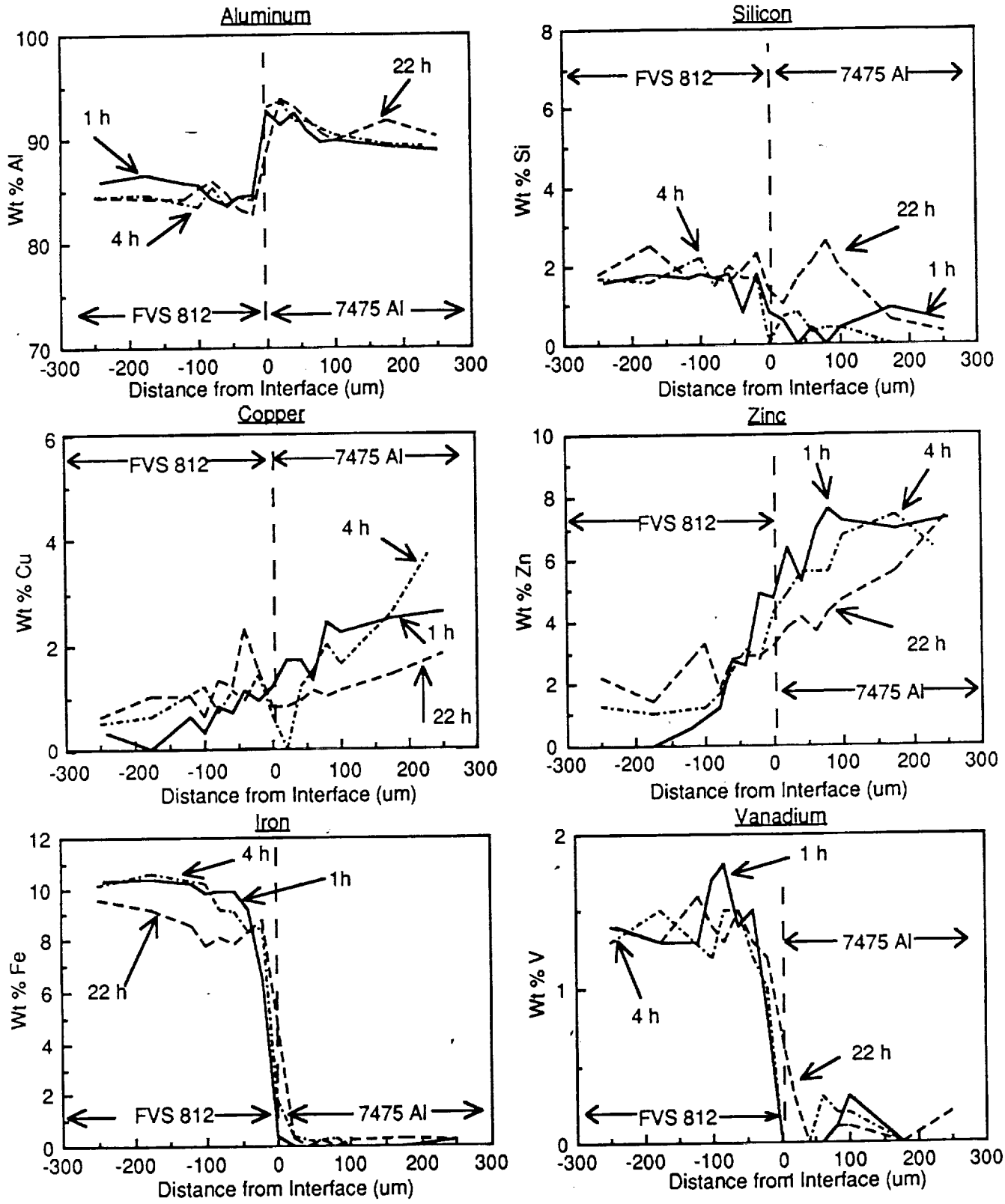

Fig. 92 **Interdiffusion Between Dissimilar Couples of Alloying Elements Between FVS0812 and 7475 Aluminum Alloy After Bonding at 516°C and 0.7 Mpa (100 Psia) for 1, 4 and 22 h As Measured By EDS**

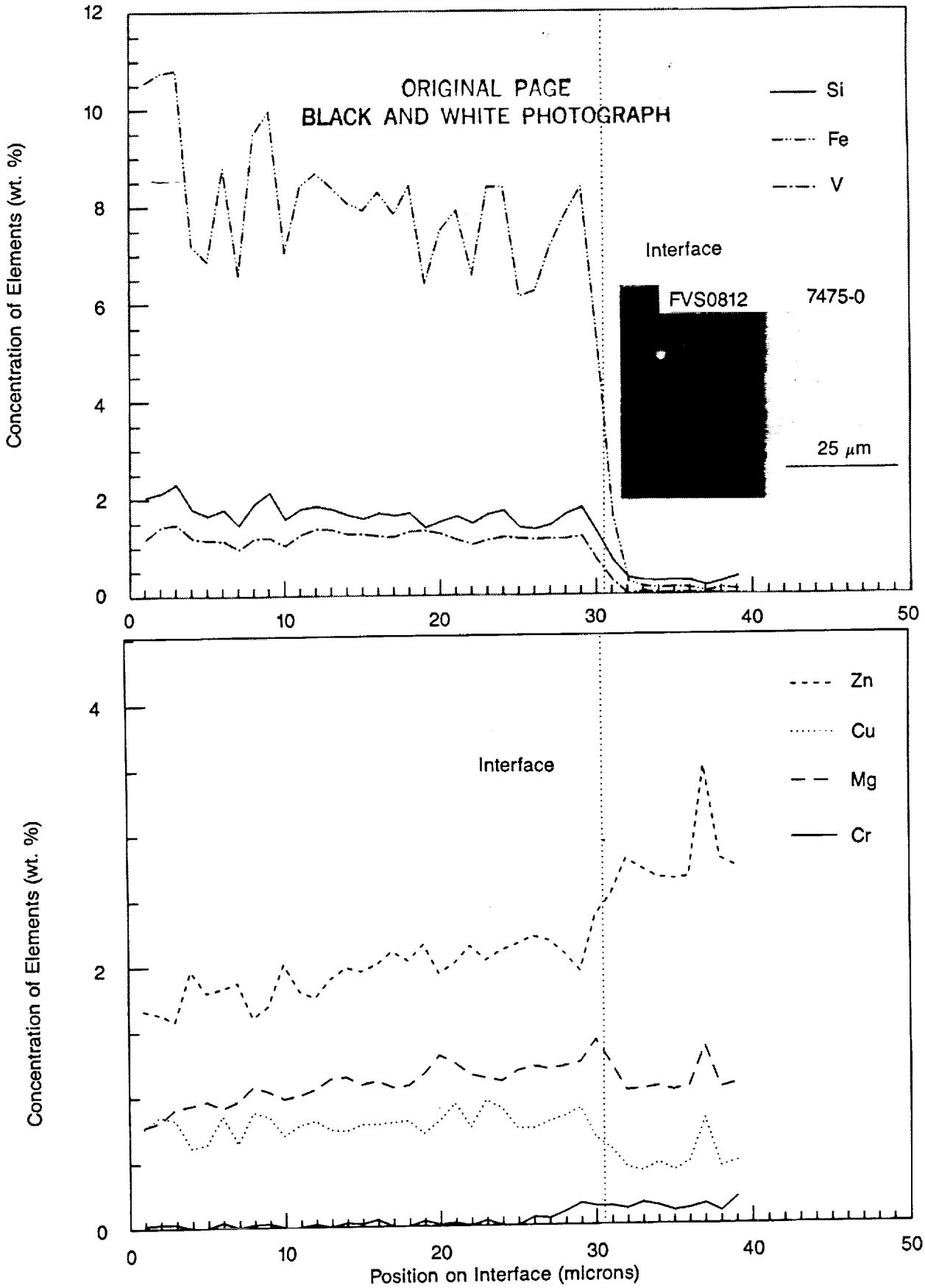

Fig. 93 **Wave Length Dispersive Spectroscopy (WLDS) Showing Diffusion of 7475 Al Alloy Performed on a Dissimilar Couple After a 2 h Bonding Cycle**

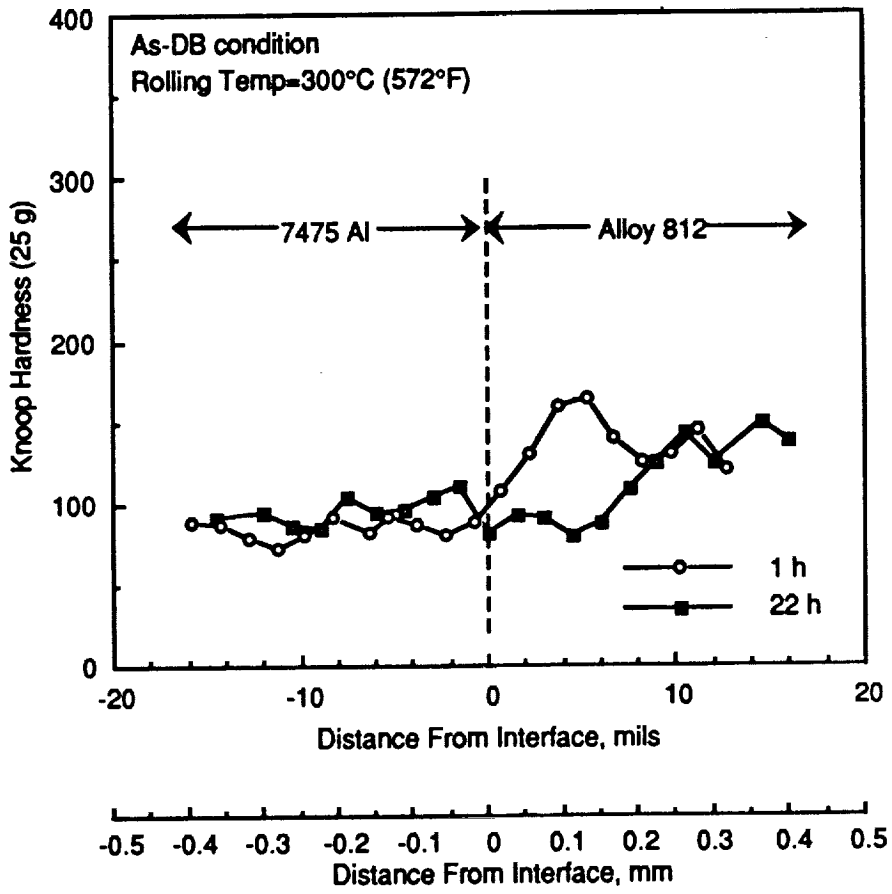

Fig. 94 Effect of Bonding Time on Hardness Profile of As-Bonded Specimens Between FVS0812 and 7475 Aluminum Alloy

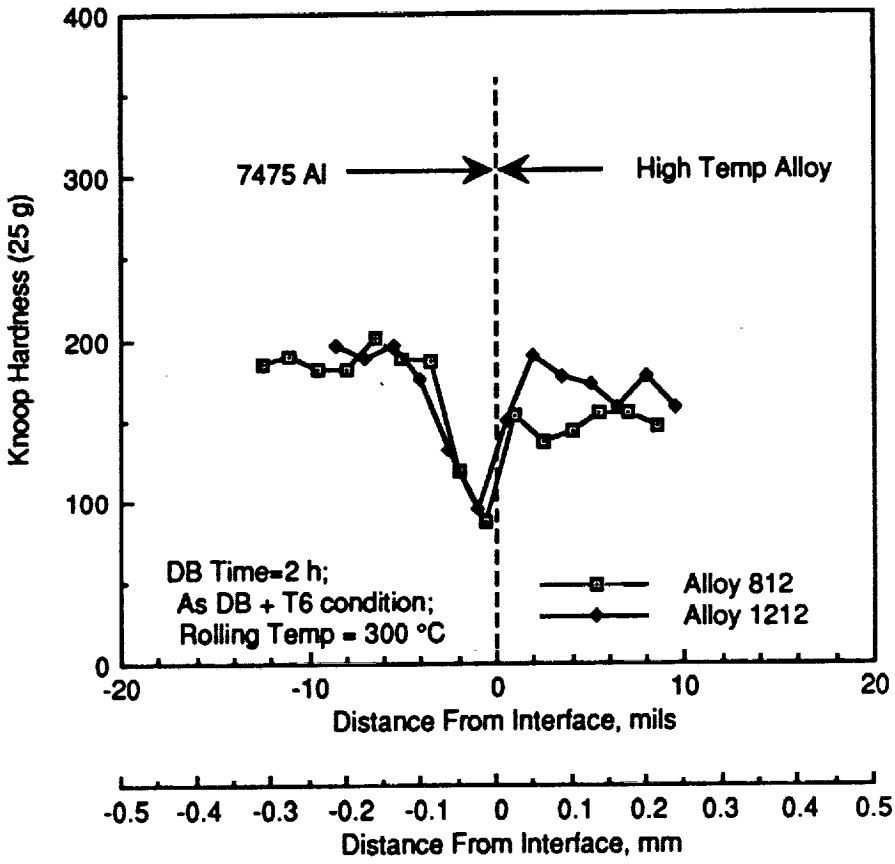

Fig. 95 Effect of Post-Bond (T6) Heat Treatment on Hardness of Dissimilar Bonds Between FVS0812/7475 and FVS1212/7475 Bonded at 516°C (960°F) for 2 h at 0.7 MPa (100 psia)

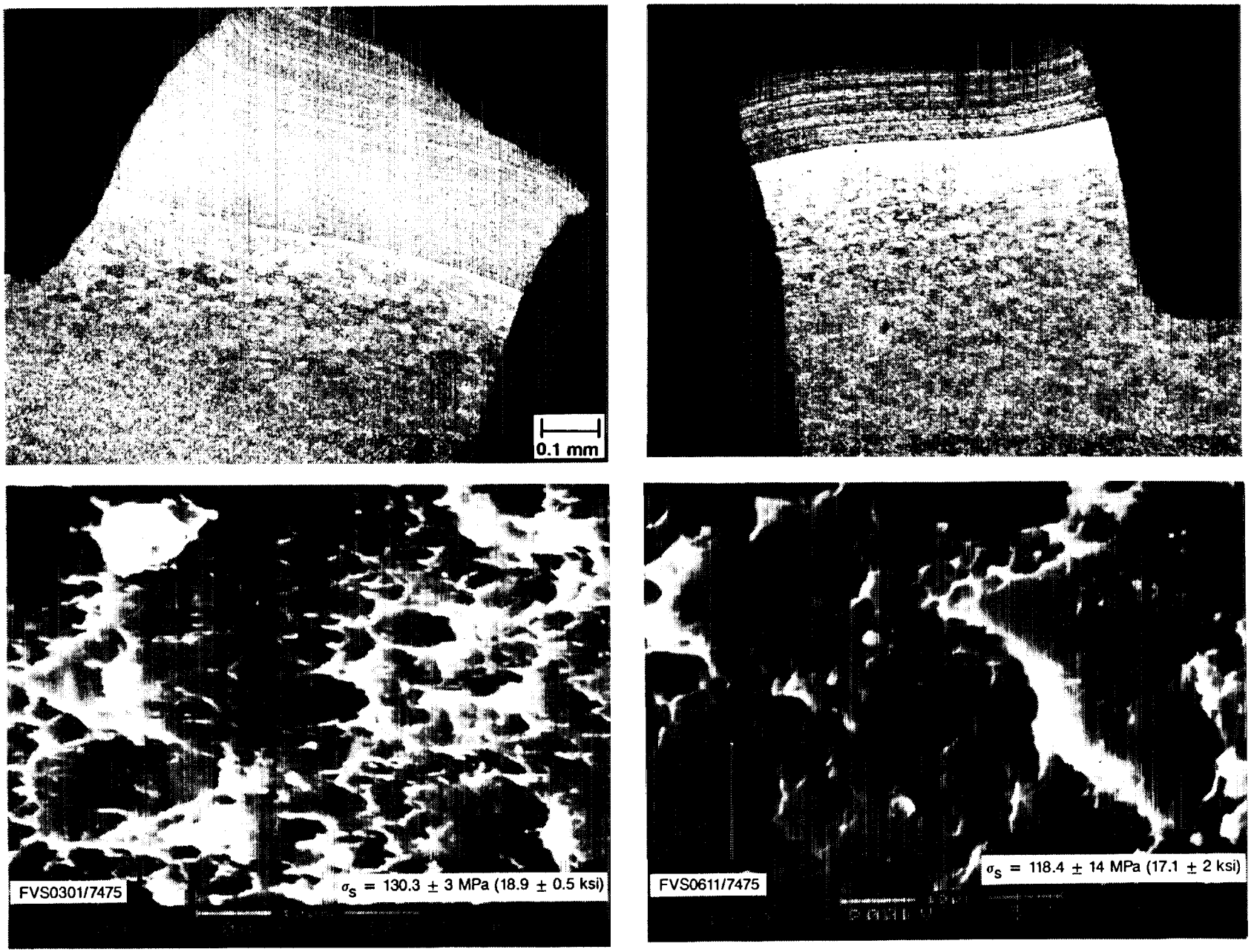

Fig. 96 Dissimilar Bond Fracture Appearance After Bonding at 516°C (960°F) for 22 h at 0.7 MPa (100 psia)

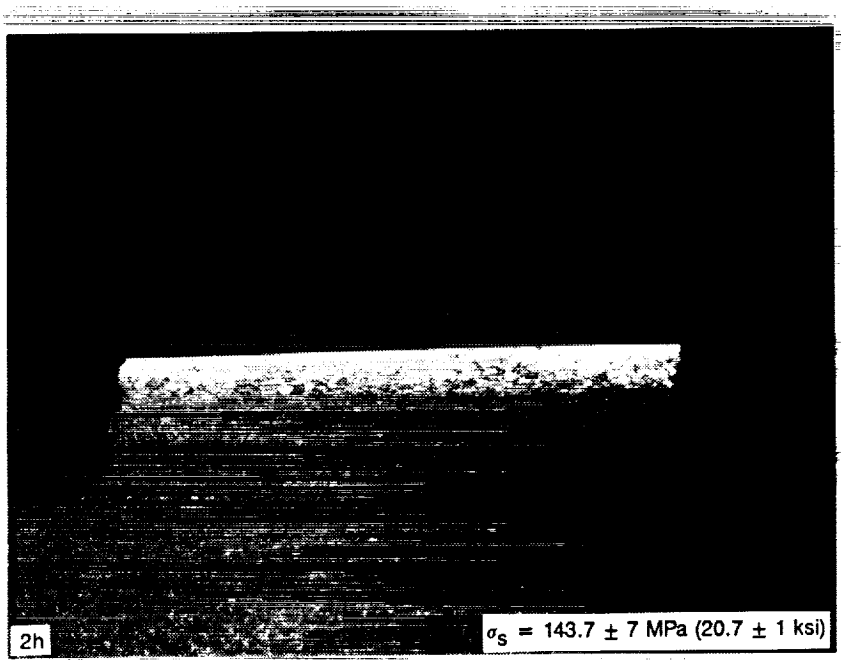

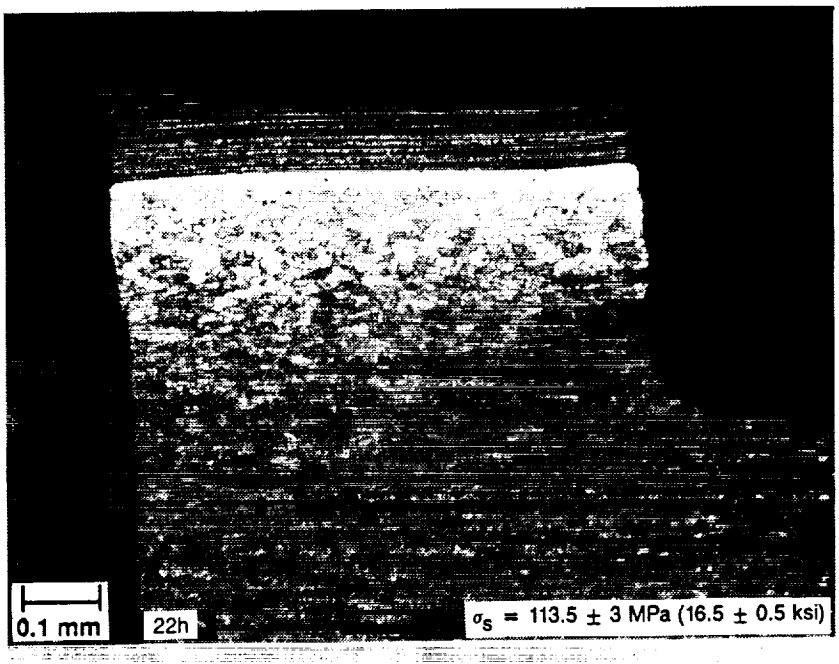

Fig. 97 **Fractured Specimens of FVS0812/7475 After Bonding at 516°C (960°F) under 0.7 MPa (100 psia) for 2 and 22 h**

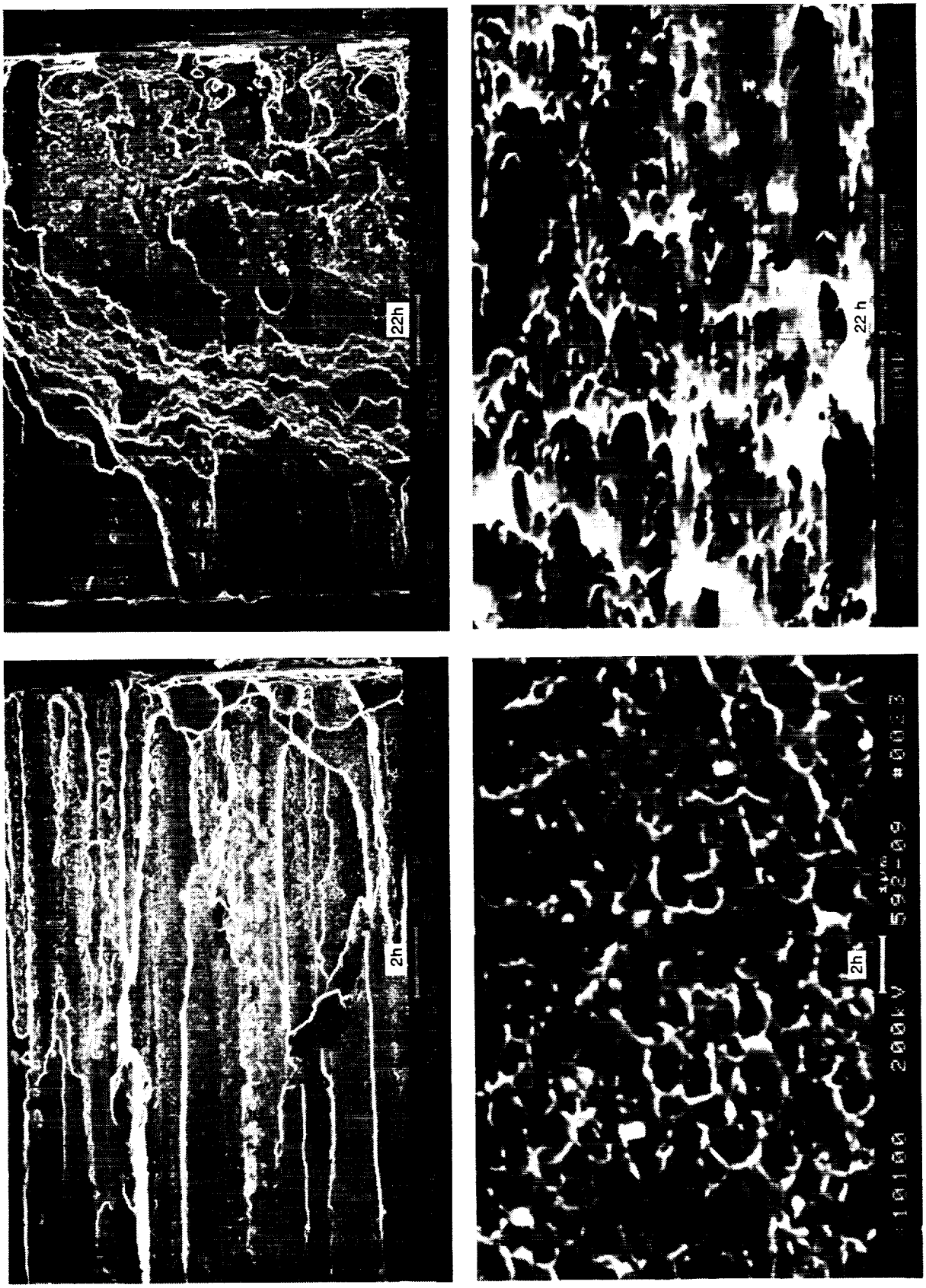

Fig. 98 Fracture Surfaces for 2 and 22 h Dissimilar Bonds at 516°C (960°F) under 0.7 MPa (100 psia)

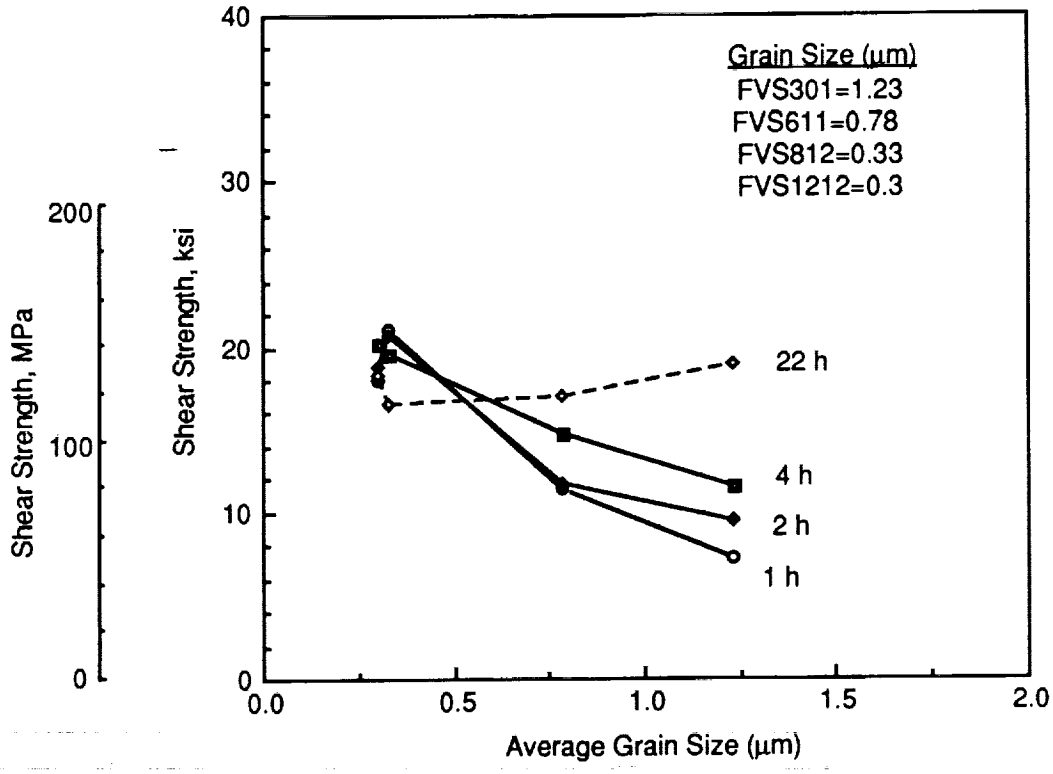

Fig. 99 Effect of Al-Fe-V-Si Alloy Grain Size on Dissimilar DB Shear Strength

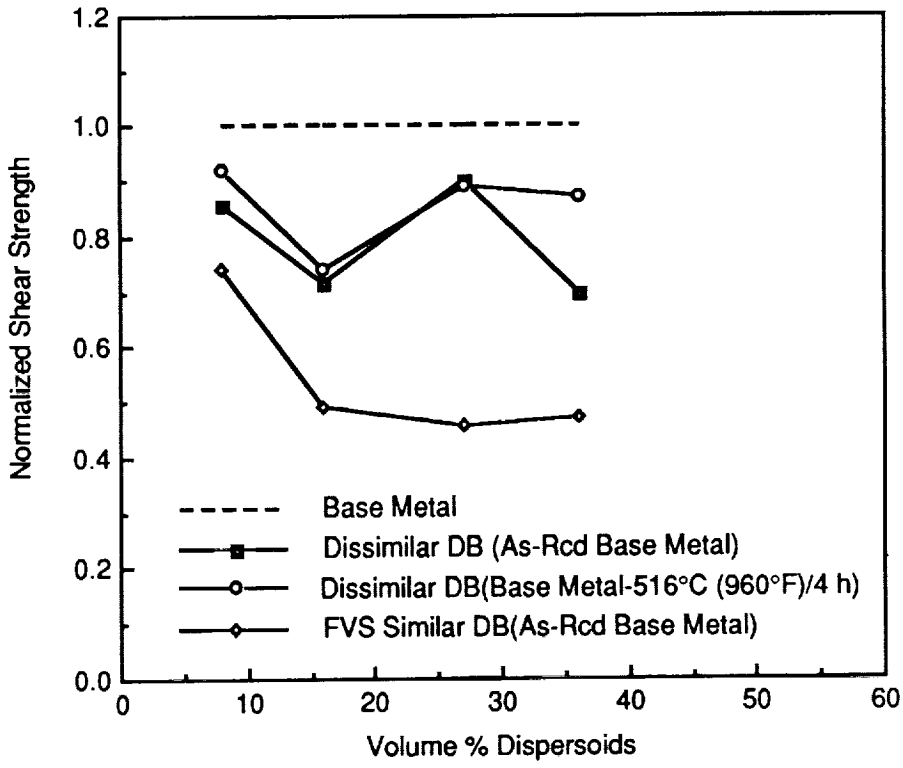

Fig. 100 Normalized Shear Strength of Diffusion Bonds

THIS PAGE INTENTIONALLY LEFT BLANK

Report Documentation Page

1. Report No.	2. Government Accession No.	3. Recipient's Catalog No.
NASA CR-181849		

4. Title and Subtitle

Superplastic Forming and Diffusion Bonding of Rapidly Solidified, Dispersion Strengthened Aluminum Alloys for Elevated Temperature Structural Applications

5. Report Date
September 1989

6. Performing Organization Code

7. Author(s)
E.Y. Ting and J. R. Kennedy

8. Performing Organization Report No.
RE-772

10. Work Unit No.
505-63-01-02

9. Performing Organization Name and Address
Grumman Corporate Research Center
A02-26
Bethpage, NY, 11714

11. Contract or Grant No.
NAS1-18533

13. Type of Report and Period Covered
Contractor Report

12. Sponsoring Agency Name and Address
National Aeronautics and Space Administration
Langley Research Center
Hampton, VA 23665-5225

14. Sponsoring Agency Code

15. Supplementary Notes

Langley Technical Monitor: Dick Royster

Final Report Assistant Technical Monitor: John Wagner

16. Abstract

Rapidly solidified alloys, based upon the Al-Fe-V-Si system and designed for elevated temperature applications, were evaluated for superplasticity and diffusion bonding behavior. Alloys with 8, 16, 27, and 36 volume percent silicide dispersoids were produced; dispersoid condition was varied by rolling at 300, 400, and 500°C (572, 752, and 932°F). Superplastic behavior was evaluated at strain rates from $1x10^{-6}$ to 8.5 s^{-1} at elevated temperatures. The results indicated that there was a significant increase in elongation at higher strain rates and at temperatures above 600°C (1112°F). However, the exposure of the alloys to temperatures > 600°C (1112°F) resulted in the coarsening of the strengthening dispersoid and the degradation of mechanical properties. Diffusion bonding was possible using low gas pressure at temperatures > 600°C (1112°F) which also resulted in degraded properties. The bonding of Al-Fe-V-Si alloys to 7475 aluminum alloy was performed at 516°C (960°F) without significant degradation in microstructure. Bond strengths equal to 90% that of the base metal shear strength were achieved. The mechanical properties and microstructural characteristics of the alloys were investigated.

17. Key Words (suggested by Author(s))	18. Distribution Statement
Dispersion Strengthened Alloys, Superplastic, Diffusion Bonding	Unclassified- Unlimited Subject Category 26

19. Security Classif. (of this report)	20. Security Classif. (of this page)	21. No. of pages	22. Price
Unclassified	Unclassified	138	